

TEMPERATURE TRANSITIONS AS A QUALITY GAGE
FOR NON-IDEAL SUPERCONDUCTORS

by

JOHN DOUGLAS BANNISTER

B.A.Sc., University of Toronto
(1959)

M.S., Northwestern University
(1961)

Submitted in Partial Fulfillment
of the requirements for the
Degree of Doctor of Science
at the

MASSACHUSETTS INSTITUTE OF TECHNOLOGY

September, 1964

Signature of Author Signature redacted
Department of Mechanical Engineering
September 8, 1964

Certified by Signature redacted
Thesis Supervisor

Accepted by Signature redacted
Chairman, Departmental Committee
on Graduate Students



77 Massachusetts Avenue
Cambridge, MA 02139
<http://libraries.mit.edu/ask>

DISCLAIMER NOTICE

Due to the condition of the original material, there are unavoidable flaws in this reproduction. We have made every effort possible to provide you with the best copy available.

Thank you.

Despite pagination irregularities, this is the most complete copy available.

TEMPERATURE TRANSITIONS AS A QUALITY GAGE
FOR NON-IDEAL SUPERCONDUCTORS

by

John Douglas Bannister

Submitted to the Department of Mechanical Engineering
on September 8, 1964 in partial fulfillment of the
requirement for the degree of Doctor of Science.

ABSTRACT

A correlation between observable quantities in the high magnetic field-low temperature and low magnetic field-high temperature regions of superconductor performance was found. This correlation provides a basis for the indirect test of high field critical currents. The correlation is empirical because of the present inadequacy of the theory when applied to commercial materials.

Based on a threshold criterion of lowest detectable voltage (in this case 10^{-6} volts) the critical current density data for commercial niobium-tin ribbon was formulated in terms of the impressed transverse magnetic field through the equation $\alpha/J = H + H^*$. The α parameter is a merit factor which was found to be an exponential function of the temperature span of the resistive transition in the earth's magnetic field and at low current density near the critical temperature. A major qualification was that a temperature span in excess of 0.65°K indicated mechanical damage to the ribbon and a reduced value of α .

The applicability of the above equation confirms previous work (28, 29, 30, 31, 32) that attributed high critical current densities at high magnetic fields in non-ideal superconductors to the ability of microstructure defects to stabilize the currents against the Lorentz force. The factor α is apparently related to the density and/or intensity of these defects.

The correlation of α with the high temperature resistive transitions provides the empirical link which will allow an indirect test for non-ideal superconductors.

Thesis Supervisor: S. C. Collins

Title: Professor of Mechanical
Engineering

ACKNOWLEDGEMENTS

The author is grateful to Drs. Wayne Keller and D. F. Fairbanks of the National Research Corporation for supplying the superconducting ribbon used in these experiments and for the use of the superconducting solenoids. Karl Benner and Jerry O'Callahan of the Cryogenic Engineering Laboratory were always helpful in the machine shop but more particularly on one occasion their quick action helped to save the author's eyes from permanent damage by acid flux. Bob Cavileer was of essential and continual assistance by maintaining a supply of liquid helium for the experiments. Richard Cummings merits special mention as a vigorous partner in discussion and a prolific source of constructive criticism. To the many other persons who contributed in various ways to this research and who may have been inadvertently omitted from explicit mention the author is very grateful.

Over the period of time in which this research was conducted, the author was associated with a man who is truly described by the expression that he is a scholar and a gentleman. This association with Professor Collins has been one of the fine things in the author's life and will always be treasured.

TABLE OF CONTENTS

	<u>Page</u>
Abstract	ii
Acknowledgements	iv
Tables	vi
Figures	vii
Plates	ix
Nomenclature	x
I. Introduction	1
II. Literature	10
III. Theory	14
Thermodynamics of the Phase Transition	14
Electrodynamics of the Super- conducting State	17
The Intermediate State	19
Non-Ideal Superconductors	23
Summary	40
IV. Experimental Method	45
The Superconductor	45
Apparatus	46
Instrumentation and Calibrations	59
Procedure	63
V. Experimental Results	70
Preliminary Tests	70

TABLE OF CONTENTS (Continued)

	<u>Page</u>
Temperature Transitions	78
Magnetic Field Transitions	82
VI. Correlation and Discussion	111
Critical Current Formulation	111
Correlation with Temperature Transitions	114
Conclusions	119
VII. Future Work	121
VIII. References	122
 Appendices	
A Copper Plating Process	125
B Current Control Circuit Diagram	127
C Superconducting Solenoid Calibrations	128
D Tabulation of Temperatures for Normal Liquid Hydrogen Vapor Pressures	129
E Wheatstone Bridge Circuit	130
 Biographical Note	 131

TABLES

	<u>Page</u>
I. Preliminary Test Comparison	75
II. Corrélation Results	115

FIGURES

<u>Number</u>		<u>Page</u>
1.	I_c - H_c - T surface for an ideal superconductor in a parallel magnetic field.	6
2.	I_c - H_c - T surface for a non-ideal superconductor.	8
3.	Critical currents against magnetic field for Kunzler Nb ₃ Sn wire. Extracted from reference 11.	12
4a.	Cylindrical ideal superconductor in a transverse magnetic field.	21
4b.	Maximum surface field against applied magnetic field for a cylindrical ideal superconductor in a transverse magnetic field.	22
5.	Zero temperature thermodynamic critical magnetic field against critical temperature for various superconductors.	24
6a.	Graphical illustration of the penetration depth and coherence length.	29
6b.	Magnetization curve for a negative surface energy superconductor.	32
7a.	Results of Kamper for persistent currents in a non-ideal superconducting ring. Extracted from reference 28.	34
7b.	Results of Heaton and Rose-Innes for non-ideal superconductors. Extracted from reference 29.	35
8.	Temperature dependence of the defect density factor α of Kim, Hempstead and Strnad. Extracted from reference 31.	39
9.	Supercurrent capacity dependence on annealing time by Heaton and Rose-Innes. Extracted from reference 29.	43
10.	Schematic of the high temperature test apparatus.	50
11.	Schematic of the high magnetic field test apparatus.	57
12.	Typical carbon resistor temperature calibrations.	64

FIGURES (Continued)

<u>Number</u>		<u>Page</u>
13.	Critical current data by two experimental procedures.	68
14.	Critical current against temperature in the earth's magnetic field.	71
15.	Transition band of resistance on a current against temperature plot.	73
16.	Critical currents by two threshold criteria.	74
17.	Comparative critical current data for three samples.	76
18.	Comparative magnetic field data for three samples.	77
19.	Effect of test current on temperature transitions.	79
20.	Voltage against temperature for a typical resistive transition.	81
21-40.	Temperature transitions.	83-102
41.	Magnetic field transition 4BA9D-T10	103
42.	Critical current density against magnetic field. Threshold criterion; 1.0 microvolt. Sample bend radius 0.48 cm.	106
43.	Critical current density against magnetic field. Threshold criterion; P/w = 40 milliwatt/cm. Sample bend radius 0.48 cm.	107
44.	Critical current density against magnetic field. Threshold criterion; 1.0 microvolt. Sample bend radius 0.96 cm.	108
45.	Critical current density against magnetic field. Threshold criterion; P/w = 1.0 milliwatt/cm. Sample bend radius 0.96 cm.	109
46.	Critical current density against magnetic field. Threshold criterion; full quench. Sample bend radius 0.96 cm.	110
47.	Formulation of critical current data	112
48.	Defect density parameters against temperature transition width.	116

PLATES

	<u>Page</u>
1. Temperature test apparatus	48
2. Magnetic field test apparatus	49
3. Sample holder for temperature test	54
4. Sample holder for magnet test	58

NOMENCLATURE

a	linear dimension
B	magnetic induction
c	speed of light in a vacuum
D	demagnetization coefficient
e	electronic charge
e	base of natural logarithms
E	electric field intensity
F(T)	temperature function defined by equation III-3
g	specific Gibbs free energy
H	magnetic field intensity
H _b	magnetic field of highest intensity on the surface of a superconductor with a finite demagnetization coefficient
H _c	thermodynamic critical field
H _{c1}	upper critical magnetic field for a non-ideal superconductor
H _{c2}	magnetic field of first penetration for a negative-surface-energy superconductor
H _e	externally applied magnetic field
H _i	current induced magnetic field on the surface of a conductor
H _o	thermodynamic critical magnetic field at zero temperature
H ⁺	parameter of the critical current density equation VI-1
h	connective heat transfer coefficient

NOMENCLATURE (Continued)

\hbar	Planck's constant
I	current
J	current density
K	thermal conductivity
k	parameter of the Ginsburg-Landau phenomenological theory; defined by equation III-31
L	latent heat of transition
M	magnetization
p	pressure
P	electrical power
r	radial measurement
R	resistance
R_0	residual resistance
s	specific entropy
t	thickness dimension
T	temperature
T_c	critical temperature at zero magnetic field
u	specific internal energy
u_s	surface energy per unit area
v	specific volume
w	width dimension
x	concentration of ortho-hydrogen
α	defect density parameter
δ	surface energy parameter

NOMENCLATURE (Continued)

v	coherence length
v'	pseudo coherence length
γ	volume fraction of a conductor which is in the superconducting state
Λ	parameter of the London equations III-8-9
λ	London penetration depth; defined by equation III-18
λ'	psuedo penetration depth
ρ	electric charge density
ρ_0	residual resistivity
σ	electrical conductivity
μ	magnetic permeability

Subscripts

c	critical state
n	normal state
o	zero temperature (except R_0 and ρ_0)
s	superconducting state

As an engineer, the author apologizes for the units used in this thesis but since the literature in the field is dominated by physicists he concluded that readability would not be improved by bucking the trend.

I. INTRODUCTION

It is fitting to introduce a thesis involving superconductors with reference to Kamerlingh Onnes⁽¹⁾ who discovered the phenomenon of superconductivity in 1911. While measuring the electrical resistance of mercury as a function of temperature he found that the resistance dropped to an undetectable quantity at about 4°K. Kamerlingh Onnes discovery led to a series of attempts to measure the resistance of superconductors by various investigators including Professor Collins. Professor Collins maintained a persistent current in a lead ring for approximately two and one half years and in the absence of any detectable decay in the current estimated the maximum resistivity of the superconductor at 10^{-21} ohm-cm. Quinn and Ittner⁽²⁾ have since lowered this maximum to 10^{-23} ohm-cm.

The discovery of superconductivity naturally led to enthusiasm for the use of superconductors as engineering tools. This enthusiasm was damped however, when it was found, again by Kamerlingh Onnes⁽³⁾, that the property of superconductivity could be destroyed by rather modest magnetic fields. Silsbee⁽⁴⁾ postulated and was later confirmed experimentally that a superconductor could carry an increasing

supercurrent only to that value which produced at its surface the critical magnetic field. According to current understanding of the phenomenon the situation is not quite this simple but it is sufficiently valid that workers in the field were dissuaded from attempting to produce high magnetic fields by means of superconducting coils.

The recent resurgence in applying superconductors to engineering problems was prefaced in 1954 by Matthias, Geballe, Geller and Corenzwit⁽⁵⁾ who reported the high critical temperature of 18.05°K for the compound Nb₃Sn. In 1961 Kunzler, Buehler, Hsu and Wernick⁽⁶⁾ reported that Nb₃Sn wires could carry current densities in excess of 10⁵ amp/cm² while subjected to a magnetic field of 88 kilogauss. Almost simultaneously Berlincourt, Hake and Leslie⁽⁷⁾ reported similar high current densities at high magnetic fields for some niobium-zirconium alloys. These results gave substantial impetus to those who were endeavouring to produce high magnetic fields by using superconducting coils. Indeed, Autler^(8,9) had already produced a field of 4300 gauss with a superconducting niobium wire solenoid and was early in reporting fields in excess of 28 kilogauss produced by superconducting Nb₃Sn coils. This brief history by no means does justice to all the workers who contributed to the development of high field superconductors but rather serves as an indication of the highlights.

In the past five years the number of workers and the effort expended towards the use of superconductors for producing high magnetic fields have mushroomed considerably. A report on all the results would comprise a thesis in itself. Therefore it will suffice to state that magnetic fields in excess of 100 kilogauss have been achieved by Nb_3Sn coils while niobium zirconium coils consistently produce in excess of 50 kilogauss and occasionally more than 70 kilogauss.

Two major problems confront the engineer who wishes to design a superconducting coil. One of these problems is the so-called coil effect whereby a superconductor proves incapable of carrying the same current in the presence of an equivalent magnetic field when wound in a coil as it can when tested as a short sample. This problem has received much attention but has not yet been solved to the point where this effect is computable.

The other problem consists of a lack of a quality test applicable to long lengths of superconductor. It is relatively simple to test ten to twenty feet of superconducting ribbon or wire in a conventional Bitter magnet or superconducting solenoid but high magnetic fields of sufficient volume to test thousands of feet of superconductor are not available. Further, the preparations necessary for such a test are comparable to those for winding a solenoid so that one might rather wind the solenoid and see how well it performs. Unfortunately, this latter procedure just about

describes the state of the art of winding superconducting solenoids. It is difficult to isolate the factor which limits the performance of any given solenoid. Invariably, a solenoid will not fulfill the promise of tests on short lengths of wire or ribbon which have been taken from the ends of the length used to wind the solenoid. This result may be attributed to non-homogeneity of quality, local stressing, short circuits in the winding or the so-called coil effect. Apparently, a valid quality test could eliminate some of the guesswork. Since a direct quality test is not practicable a means of indirect testing needs to be found. If a correlation were available between the behaviour of superconductors when subjected to high temperature and that when subjected to high magnetic fields then an indirect quality test might be possible. It is to this end that this thesis was directed.

As there can be some confusion in terms when one discusses superconductor it is appropriate to clarify the terms which will be used later by way of further introduction. The terms "ideal, soft" "first kind or Type I," superconductors vis-a-vis "non-ideal, hard" or "second kind or Type II" are commonly used to describe the two types of superconductors which will henceforth be referred to as ideal and non-ideal.

An ideal superconductor is characterized by perfect electrical conductivity and perfect diamagnetism when in the

superconducting state. The threshold magnetic field has been found to follow approximately the following relation with respect to temperature.

$$H_e \approx H_0 \left[1 - \left(\frac{T}{T_c} \right)^2 \right] \quad \text{I-1}$$

where H_c = threshold magnetic field at $T^{\circ}\text{K}$.

If we combine equation I-1 with the Silsbee Rule for a wire

$$I_c = 5r H_i \quad \text{I-2}$$

and add the current induced field to an external field parallel to the wire

$$H_c^2 = H_i^2 + H_e^2 \quad \text{I-3}$$

we get an equation for a threshold surface for an ideal superconducting wire carrying a current in a parallel magnetic field

$$\left\{ 1 - \left(\frac{T}{T_c} \right)^2 \right\}^2 = \left(\frac{I_c}{5r H_0} \right)^2 + \left(\frac{H_e}{H_0} \right)^2 \quad \text{I-4}$$

This surface is sketched in Figure 1. It is apparent that indirect testing would be possible for an ideal superconductor simply by measuring I_c at two temperatures near T_c to

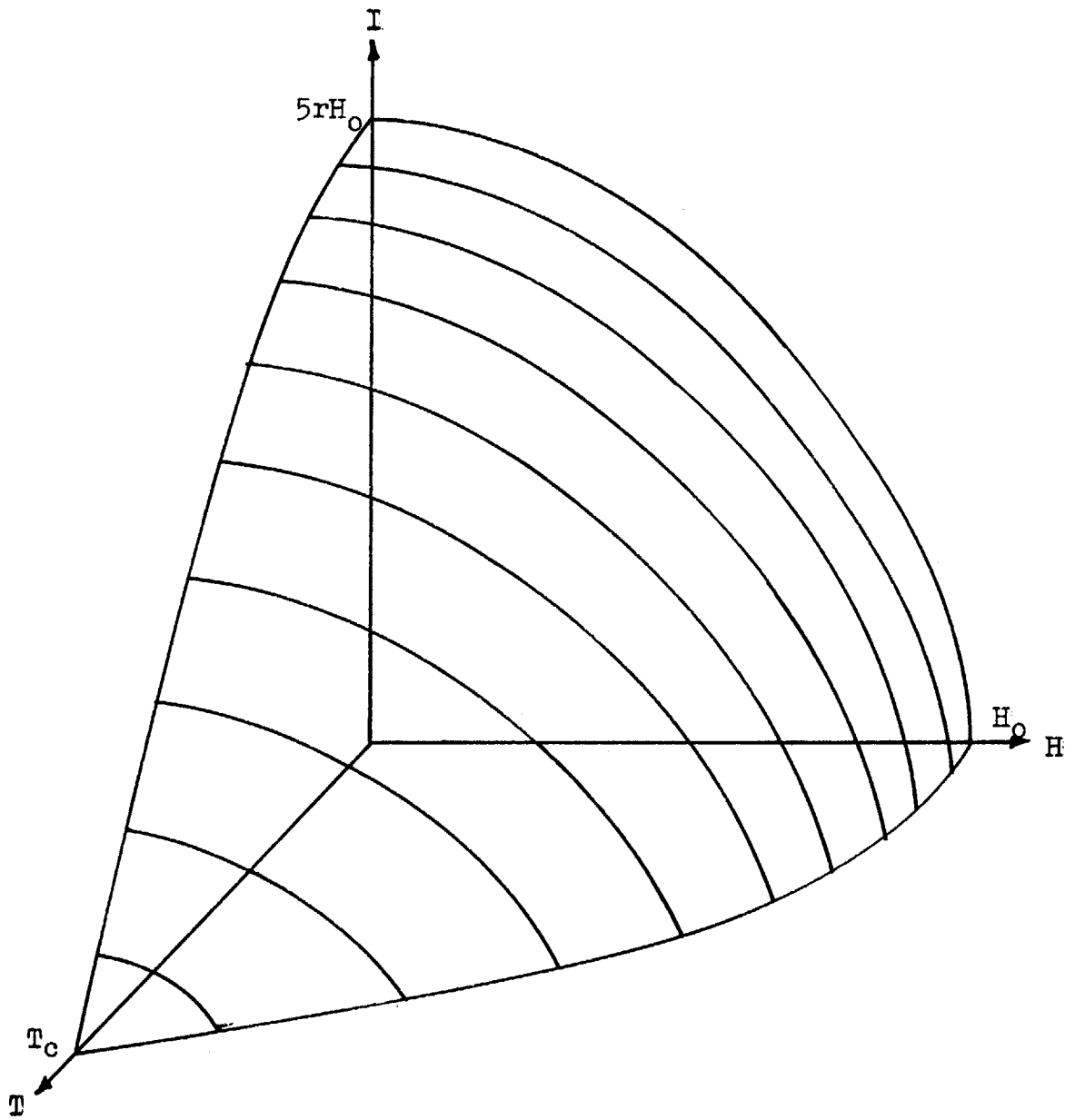


Figure 1.

I-H-T Surface for an ideal superconductor in a parallel magnetic field

establish the surface parameters T_c and H_0 .

Unfortunately, the superconductors of engineering interest are of the non-ideal type. Aside from the fact that they can carry high current densities in the presence of high magnetic fields, non-ideal superconductors differ from ideal superconductors by admitting magnetic flux into their interiors while still maintaining zero electrical resistance. This is known as an incomplete or partial Meissner Effect, so called because Meissner and Ochsenfeld⁽¹⁰⁾ in 1933 first discovered that the diamagnetism of ideal superconductors was independent of the order of cooling and application of the magnetic field. Detailed discussion of non-ideal superconductors is more properly done in Chapter III. However, it should be noted that even "ideal" superconductors as found in practice only approach the concept of an ideal superconductor.

With the help of some data on Nb_3Sn by Kunzler⁽¹¹⁾ and Logue⁽¹²⁾ the author has sketched in Figure 2 his conception of the I-H-T surface for a non-ideal superconductor. The purpose of this thesis is to find a correlation between the behaviour in the area marked I and that in the area marked II of various samples of a non-ideal superconductor which have undergone differing manufacturing conditions. The superconductor chosen for study is Nb_3Sn ribbon manufactured by rolling tin on niobium and heat treating to produce Nb_3Sn on a niobium strata. The predominant manufacturing

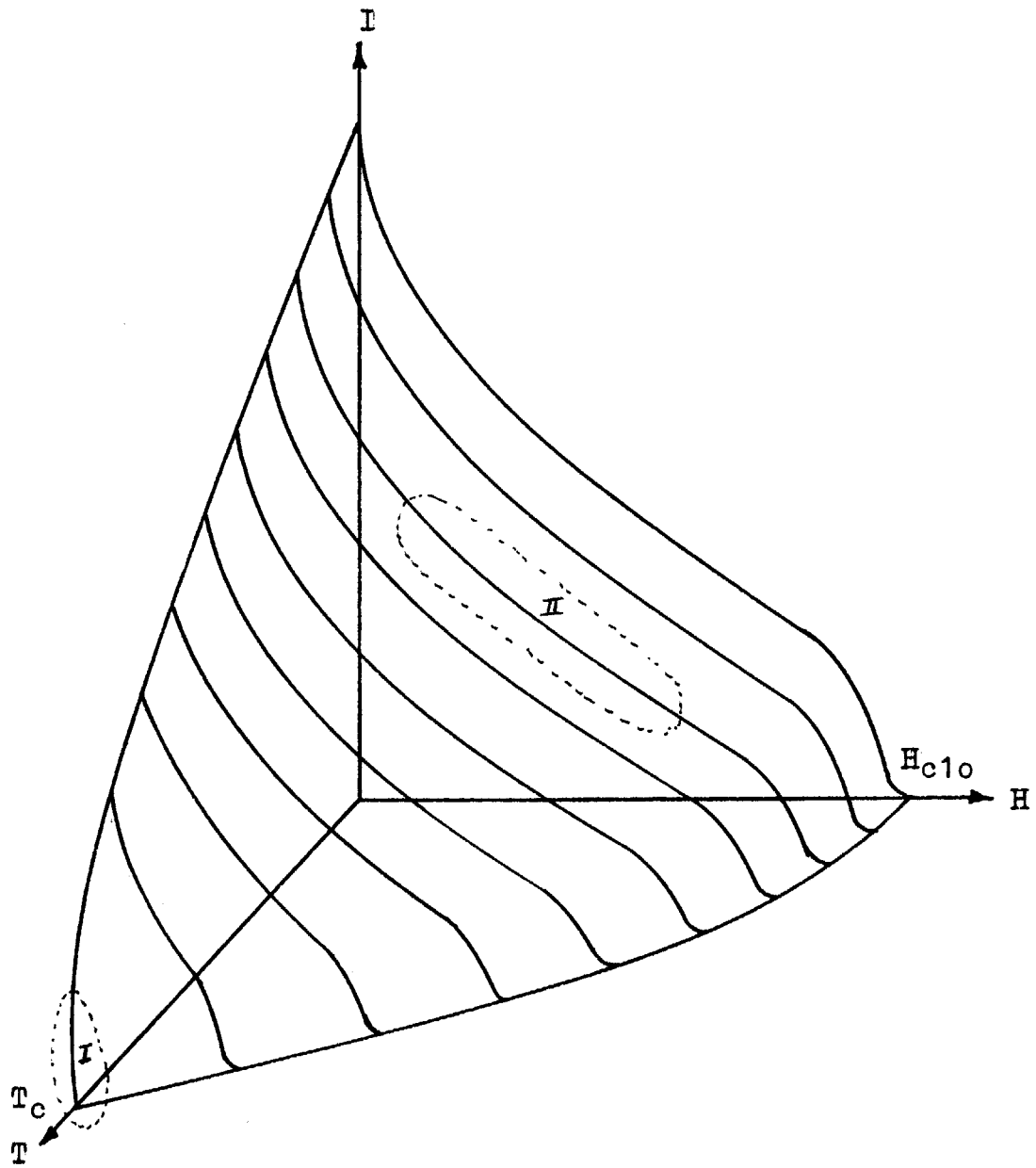


Figure 2.

I-H-T Surface for a non-ideal superconductor

factors are purity of constituents and heat treatment time and temperature. The expected variation in result is that of effective cross-section of Nb_3Sn available to carry supercurrents.

As is apparent from the brief discussion of ideal superconductors there is some reason to expect a correlation between the two areas in question. Unfortunately, the theory of non-ideal superconductors has not been developed to the degree that one can formulate the surface sketched in Figure 2 mathematically. Additional reasons for suspecting a correlation will be discussed in Chapter III.

II. LITERATURE

An extensive literature survey has revealed no previous work which could be applied directly to the problem outlined in Chapter I. Research into superconductivity has been motivated mostly by a need for understanding the phenomenon rather than by a desire to use superconductors as tools. An exception to this statement is probably the work by computer engineers on the use of cryotrons as memory elements. Further, the correlation which we seek will be special in nature and somewhat difficult to generalize because the measurements of transport current capacity in a magnetic field depend greatly on the geometry of the superconductor and its attitude in the magnetic field. Hence, persons seeking a generalized understanding of superconductivity are not motivated to experiments of this kind.

There are many data available on the transport current capacity of non-ideal superconductors (6, 7, 11, 13, 14, 15). The references here indicated are not all-encompassing but rather indicative of the type of data. These data do not lend themselves to generalization because the performance of the superconductors is strongly dependent on the manufacturing process and the experimental set-up. This type of data is generally reported by metallurgical researchers

who wish to indicate the quality of a particular set of alloys or compounds. A typical set of this type of data as extracted from reference 6 is shown in Figure 3. Although many of the data on superconductors taken in this form were presented as families of curves representing various manufacturing parameters, the author was unable to find instances where corresponding data were taken near the critical temperature which case would have allowed a test for the correlation sought in this thesis.

The work of previous workers can be of qualitative assistance in anticipating the effects of various perturbations on the performance of superconductors. While studying resistive transitions in tantalum wire Fink⁽¹⁶⁾ found that samples of various purities exhibited linear I_c vs T curves of slopes increasing with purity and converging on a common critical temperature. On the other hand Rinderer⁽¹⁷⁾ was able to displace the critical temperature for tin over the range 3.27°K to 3.72°K by adding impurities. The discrepancy between these results may stem from the fact that tantalum behaves as a non-ideal superconductor while tin approximates an ideal superconductor. Desorbo⁽¹⁸⁾ and Seriphim, Novick and Budnick⁽¹⁹⁾ report that dissolved gases lower the critical temperature of niobium and tantalum respectively, and Desorbo also reports a decrease in the magnetic field of first penetration into the superconductor with increased quantities of dissolved gas.

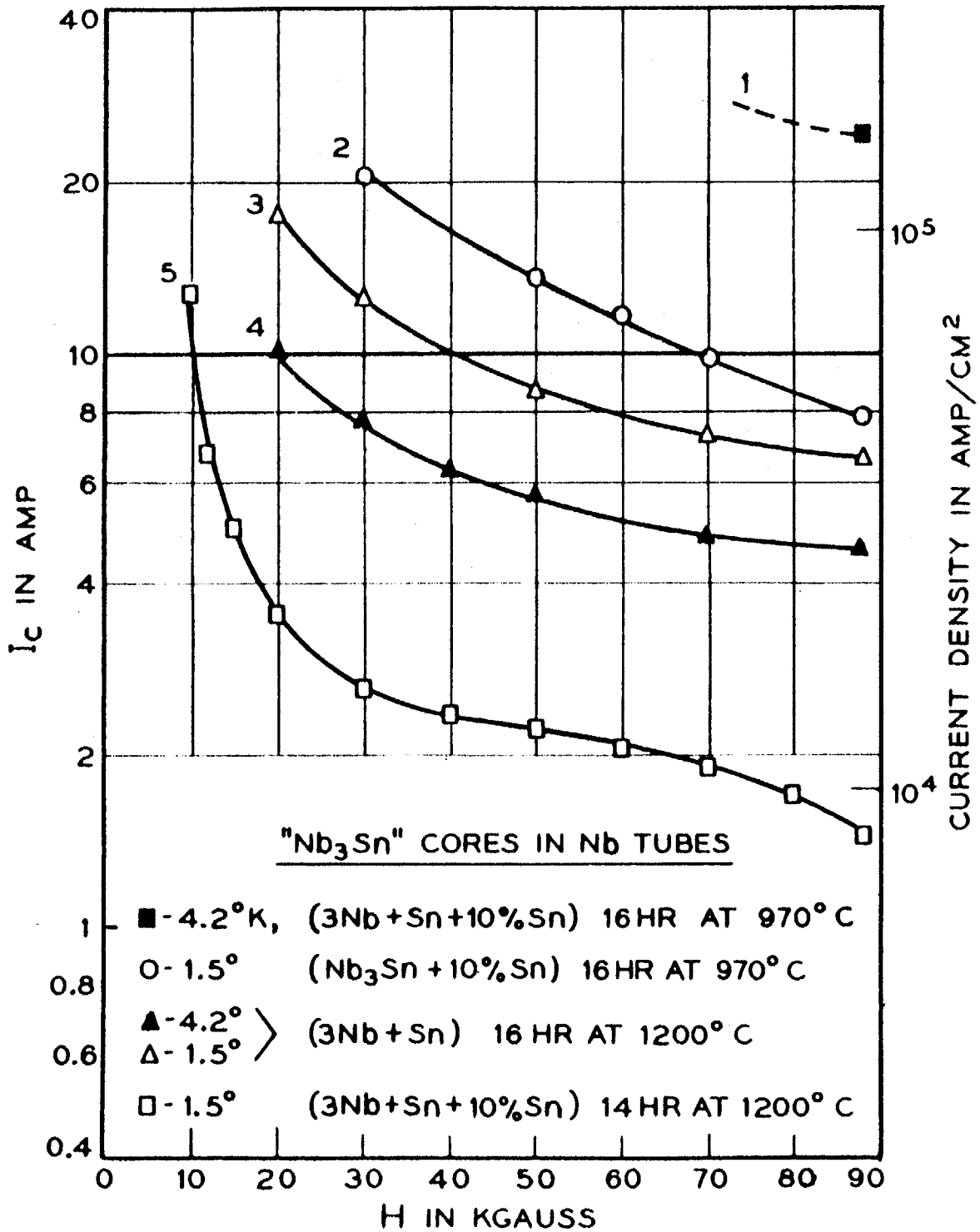


Figure 3.

Critical currents against magnetic field for Kunzler wire. Extracted from reference 11.

Simmons and Douglass⁽²⁰⁾ found that a superconducting tin film had a lowered critical temperature when in intimate contact with a normal conductor.

Muller and Saur⁽²¹⁾ were able to lower the temperature of resistance transitions in Nb_3Sn films on Nb wires by as much as 2°K by applying suitable stresses to the wires.

Kunzler⁽¹¹⁾ reported that an increased dislocation density achieved by cold work greatly enhanced the supercurrent capacity of the niobium-zirconium alloy in high magnetic fields. Kneip, Betterton, Easton and Scarbrough⁽²²⁾ showed that essentially the same results could be achieved by precipitation induced defects.

In summary, reports of previous workers indicate that many factors associated with a commercial manufacturing process can cause variations in the supercurrent capacity at high magnetic fields and also variations in the behaviour near the critical temperature at zero magnetic field. Unfortunately, these workers have concentrated on one or the other area and give no indication as to the possible correlation between variations in the two areas.

III. THEORY

As mentioned in Chapter I the theory of non-ideal superconductors has yet to be developed to the state where-
by we could extract a mathematical expression which would
relate observable quantities in the high field-low tempera-
ture region to those in the high temperature-low field
region. About the most we can hope for is that a review
of the current theories will give us additional basis for
expecting the correlation which we seek and serve as a guide
for experimental work. The theory given below was extracted
largely from three books by London⁽²³⁾, Shoenberg⁽²⁴⁾ and
Lynton⁽²⁵⁾ and is supplemented as indicated by later papers.
It will be necessary to develop the macroscopic theory in
an orderly manner but with as much abbreviation as possible
in order to eventually arrive at a guide to experiment.

Thermodynamics of the Phase Transition

As mentioned previously an ideal superconductor
behaves as follows

<u>Normal State</u>	<u>Superconducting State</u>
$H > H_c(T)$	$H < H_c(T)$
$\underline{B} = \underline{H}, \mu = 1, \underline{M} = 0$	$\underline{B} = 0, \mu = 0, \underline{M} = -\frac{H}{4\pi}$
$\sigma = \sigma_n$	$\sigma = \infty$

It is important to note that both of the properties $\underline{B} = 0$ and $\underline{p} = 0$ are necessary to describe the superconducting state since perfect conduction alone would result in a locked-in magnetic flux if the superconductor were cooled into the superconducting state while an external magnetic field was impressed.

The transition between these states may be treated thermodynamically as a phase transition as follows. We write the Gibbs free energy function

$$g = u - T_s - \frac{1}{4\pi} \underline{B} \cdot \underline{H} + pv \quad \text{III-1}$$

We can neglect volume changes and rewrite III-1 in the form

$$g(H, T) = f(T) - \frac{1}{4\pi} \int_0^H \underline{B}(\underline{H}) \cdot d\underline{H} \quad \text{III-2}$$

If we perform the integration for both the superconducting and normal states we get,

$$g_s(H, T) = f(T)$$

$$g_n(H, T) = f(T) - \frac{1}{8\pi} (H^2 - H_c^2)$$

Further, defining a temperature function

$$F(T) \equiv f(T) + \frac{1}{8\pi} H_c^2(T) \quad \text{III-3}$$

we obtain

$$g_s = F(T) - \frac{H_c^2(T)}{8\pi} \quad \text{III-4}$$

$$g_n = F(T) - \frac{H^2}{8\pi} \quad \text{III-5}$$

It is apparent that the free energies of both states are equal at the phase boundary where $H = H_c$. The specific entropy is given by

$$S = -\left(\frac{\partial g}{\partial T}\right)_H$$

and when applied to III-4 and III-5 proves to be discontinuous at the phase boundary

$$S_n - S_s = -\frac{1}{8\pi} \frac{\partial(H_c^2)}{\partial T} = -\frac{1}{4\pi} H_c \frac{\partial H_c}{\partial T} \quad \text{III-6}$$

This means that there is a latent heat of transition

$$L = T(S_n - S_s) = -\frac{T}{4\pi} H_c \left(\frac{\partial H_c}{\partial T}\right) \quad \text{III-7}$$

which is absorbed by the superconductor as it goes from the superconducting to the normal state because $\partial H_c / \partial T$ is a negative factor. This latent heat increases from zero at $T = 0$ through a maximum to zero at $T = T_c$ where $H_c = 0$ and hence is dependent on the presence of a magnetic field.

This thermodynamic discussion is presented to illustrate that there is a thermodynamically treatable phase transition involved and some of the results will be used later.

Electrodynamics of the Superconducting State

Attributing the diamagnetism to circulating supercurrents London (p 28) made the fundamental assumption that the supercurrent is always determined by the local magnetic field which takes the form

$$c \operatorname{curl} \underline{\Lambda J_s} = - \underline{H} \quad \text{III-8}$$

and

$$\frac{\partial}{\partial t} (\underline{\Lambda J_s}) = \underline{E} \quad \text{III-9}$$

He assumes superconductive and normal components to the current density

$$\underline{\dot{J}} = \underline{J_s} + \underline{J_n} \quad \text{III-10}$$

and that the normal component obeys Ohm's law

$$\underline{J_n} = \sigma \underline{E} \quad \text{III-11}$$

Combining III-8, -9, -10, -11 we obtain

$$-c \operatorname{curl} \underline{\Lambda J} = \underline{H} + \sigma \underline{\Lambda \overset{\circ}{H}} \quad \text{III-12}$$

and

$$\frac{\partial}{\partial t} (\Lambda \underline{J}) = \underline{E} + \sigma \Lambda \underline{E} \quad \text{III-13}$$

Using equations III-12 and 13 and Maxwell's equations we can successively eliminate the variables \underline{H} , \underline{E} , \underline{J} and ρ thus

$$\text{curl curl } \underline{H} + \frac{4\pi}{\Lambda c^2} \underline{H} + \frac{4\pi\sigma}{c^2} \underline{H} + \frac{1}{c^2} \underline{H}^{\circ\circ} = 0 \quad \text{III-14}$$

$$\text{curl curl } \underline{E} + \frac{4\pi}{\Lambda c^2} \underline{E} + \frac{4\pi\sigma}{c^2} \underline{E} + \frac{1}{c^2} \underline{E}^{\circ\circ} = 0 \quad \text{III-15}$$

$$\text{curl curl } \underline{J} + \frac{4\pi}{\Lambda c^2} \underline{J} + \frac{4\pi\sigma}{c^2} \underline{J} + \frac{1}{c^2} \underline{J}^{\circ\circ} = 0 \quad \text{III-16}$$

$$\frac{4\pi}{\Lambda} \rho + 4\pi\sigma \rho + \rho^{\circ\circ} = 0 \quad \text{III-17}$$

For steady fields Faraday's Law gives

$$\text{curl } \underline{E} = - \frac{\underline{H}}{c} = 0$$

Then from III-15 $\underline{E} = 0$

which accounts for perfect conductivity.

In applying the above equations to particular shapes of superconductors London (p 33) found that in all time-independent cases the magnetic field was essentially zero at a depth into the interior of the superconductor which was greater than $c \sqrt{\Lambda/4\pi}$. Hence the bodies of dimensions

much greater than $c \sqrt{\Lambda/4\pi}$ London's equations account for perfect diamagnetism. The quantity

$$\lambda \equiv c \sqrt{\Lambda/4\pi} \quad \text{III-18}$$

has become known as the London penetration depth and is of the order of 10^{-5} cm.

London (p 41-47) describes several experiments designed to measure the penetration depth which has been found to be temperature dependent approximately as follows

$$\lambda = \lambda_0 \left\{ 1 - \left(\frac{T}{T_c} \right)^4 \right\}^{-\frac{1}{2}} \quad \text{III-19}$$

The Intermediate State

In the section on the thermodynamics of phase transition it was assumed that all points on the surface of the superconductor were exposed to the same magnetic field intensity. Such a condition is possible for a cylindrical superconductor in a parallel magnetic field. However, in a transverse field a superconductor of dimensions greater than the penetration depth, has a finite demagnetization coefficient. That is, the superconductor distorts the externally applied field in a manner such that the field intensity at some point on its surface is greater than the applied field as given by

$$H_e = H_b(1 - D) \quad \text{III-20}$$

Then in a transverse magnetic field a circularly cylindrical superconductor has a demagnetization coefficient, $D = 1/2$ and will feel the critical field at its transverse diameter when the external field is only $1/2 H_c$. This configuration is illustrated in Figure 4a.

The initial explanation of this type of transition was that the flux penetrated the superconductor relieving the flux concentration at the diameter. This explanation led to a situation where the flux had been admitted to the interior of the superconductor and remained there with the superconductor being nowhere subjected to a critical field.

Such an explanation was unacceptable to London (p 98) who postulated that when a superconductor felt a critical magnetic field at any point on its surface, it immediately broke up into a laminar structure of superconducting and normal phases parallel to the magnetic field. This laminar structure London called the intermediate state. In the intermediate state the relative thicknesses of the superconducting and normal lamina are such as to maintain the field intensity inside the normal lamina at H_c . The situation is illustrated by plotting the midpoint field intensity against the external field as shown in Figure 4b.

The laminar structure of the intermediate state has been verified experimentally as is indicated by London (p 109) and the lamina have been found to have thicknesses large with respect to the penetration depth. London (p 111)

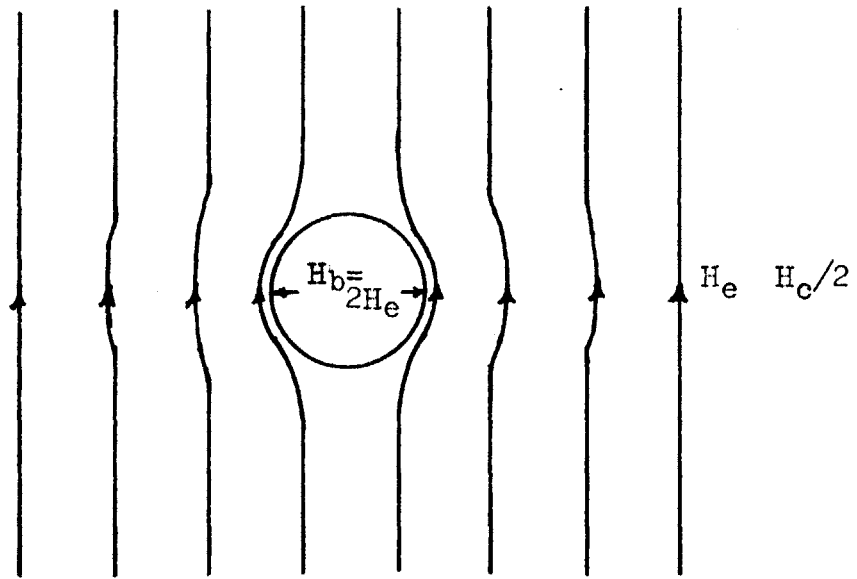


Figure 4a. Cylindrical ideal superconductor in a transverse magnetic field.

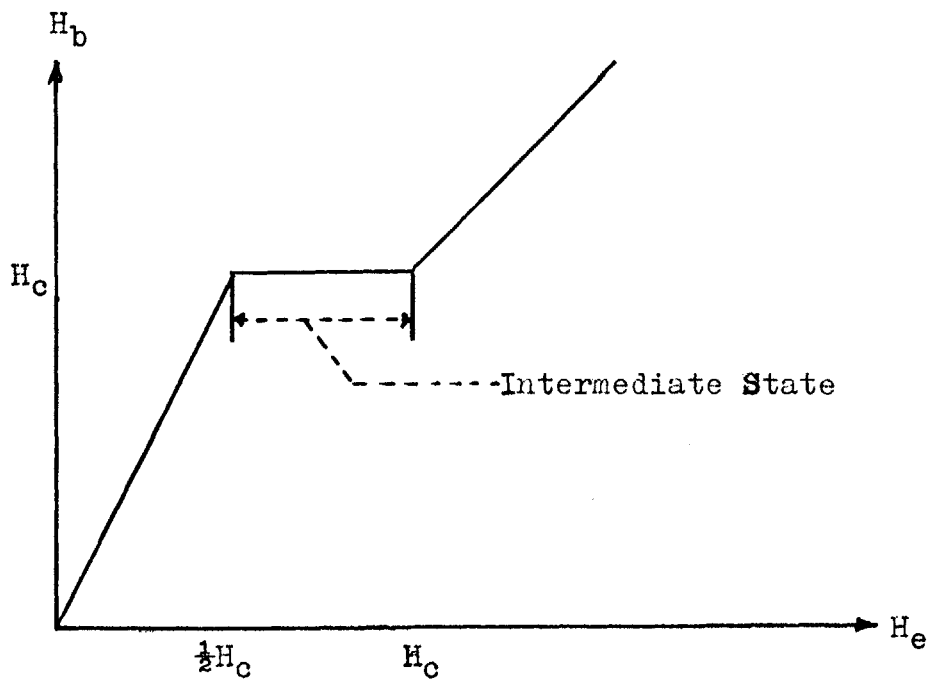


Figure 4b. Maximum surface field for an ideal superconductor in a transverse magnetic field.

develops a theoretical model for this intermediate state by postulating that the boundaries between superconducting and normal lamina are maintained by an equilibrium between Maxwell stresses and Meissner stresses.

$$\frac{1}{8\pi} \left\{ \left(\frac{B}{\gamma}\right)^2 - \left(\frac{E}{\gamma}\right)^2 \right\} = \frac{1}{8\pi} H_c^2 \quad \text{III-22}$$

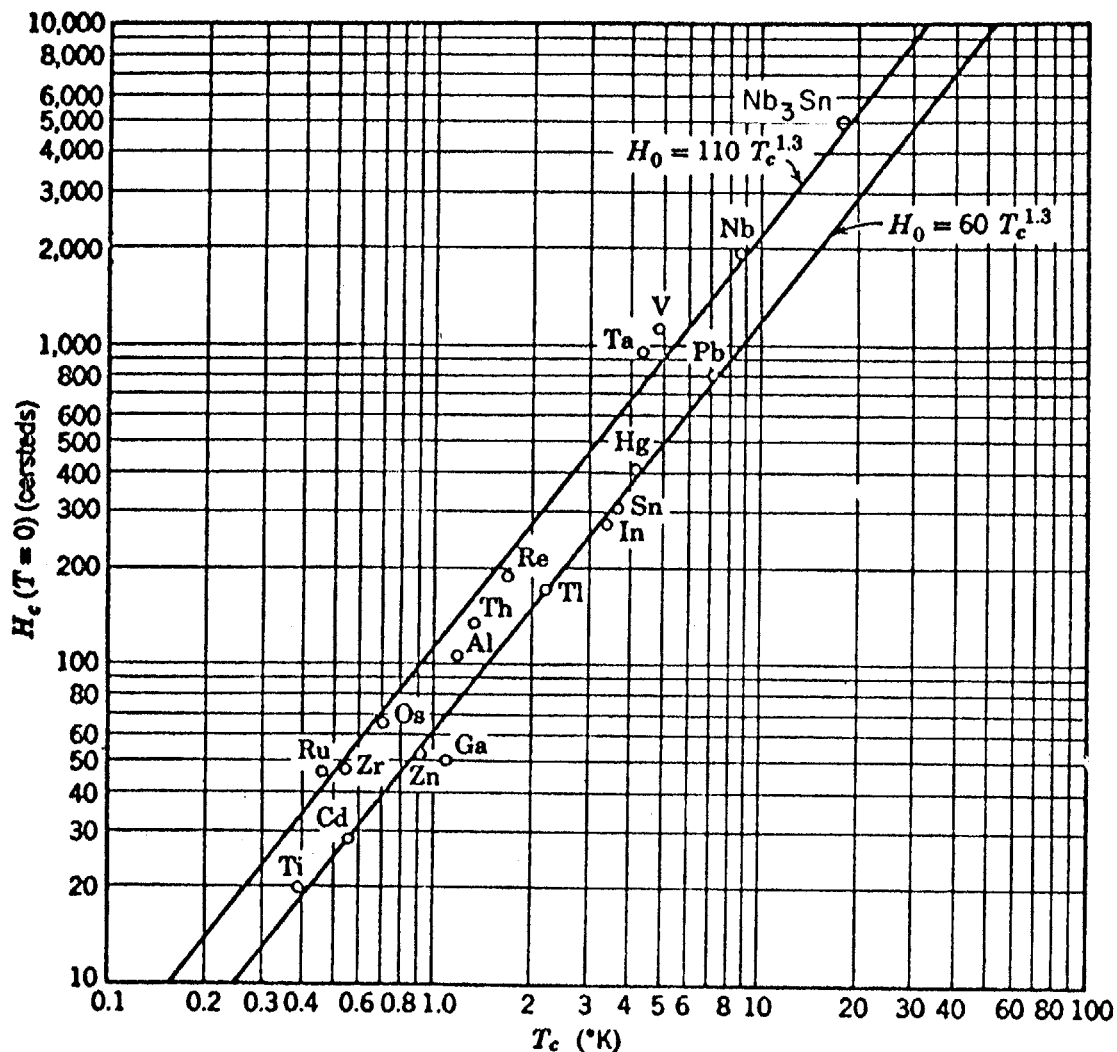
The theory is developed to the point of predicting the form of the transition curve of a wire carrying a current.

$$R = \frac{R_0}{2} \left\{ 1 + \sqrt{1 - (I_c/I)^2} \right\}, \quad I \geq I_c \quad \text{III-23}$$

It is apparent that for $I = I_c$, $R = R_0/2$ which was qualitatively substantiated by Scott⁽²⁶⁾ for Indium wires.

Non-Ideal Superconductors

To this point we have discussed the theory of ideal superconductors from which non-ideal superconductors differ by an incomplete Meissner Effect and a supercurrent carrying capability at much higher magnetic fields. Figure 5 shows the critical fields at zero temperature of various superconductors plotted against critical temperature. Plotting Nb_3Sn according to its critical temperature of $18.05^\circ K$ indicates that it should have a critical field at zero temperature of 5000 oersteds. Referring back to Figure 3 we see



Log-log plot of critical field at $T = 0$ vs. transition temperature T_c , as given by H. W. Lewis, Phys. Rev. 101, 939 (1956). This type of plot separates the hard and soft types of superconductors, or the transition and non-transition elements. [This particular graph was prepared by R. Glover from data in the book by Shoenberg and the review by J. Eisenstein, Revs. Mod. Phys. 26, 277 (1954).]

Figure 5.

that Nb₃Sn is capable of carrying substantial supercurrents at many times this field. For an explanation of this type of behaviour we begin by considering the behaviour of superconductors which are of dimensions comparable to the penetration depth.

For such a thin superconductor much of its interior will be penetrated by magnetic flux and we can indicate the degree of this penetration by an arbitrary factor m as follows

$$\underline{B} = m\underline{H} \quad \text{where } 0 < m < 1 \quad \text{III-24}$$

It can be seen that the free energy of the superconductor in the superconducting state must be lowered because of this flux penetration and equation III-4 is modified as follows

$$g_s = F(T) - \frac{H_c^2(T)}{8\pi} - \frac{(mH)^2}{8\pi} \quad \text{III-4'}$$

Since at the transition between the normal and superconducting phases the free energies must be equal we can equate III-4' to III-5 and designate this new critical field as

$$H_{c_1} = \frac{H_c}{\sqrt{1 - m^2}} \quad \text{III-25}$$

As flux penetration increases, m increases and hence H_{c_1} can increase over H_c many times.

On the basis of this thermodynamic reasoning it is theorized that non-ideal superconductors achieve their enhanced current carrying capacity at high magnetic fields by breaking down to a filamentary mesh in which the filaments are of dimensions comparable to the penetration depth. The efficiency of this theory has been demonstrated by Bean, Doyle and Pincus⁽²⁷⁾ who pressed mercury into the 20 Å pores of vycor rod and found the resulting superconductor capable of carrying greater than 10^3 amp/cm² in fields of 6000 oersteds as compared to a thermodynamic critical field of about 400 oersteds. This theory has been used to explain how extensive cold working of alloys like niobium zirconium can enhance the supercurrent capacity at high magnetic fields.

Lynton (p 46) gives a good survey of the Ginsburg and Landau phenomenological theory which accounts for penetration of the magnetic field and allows for the transition from the normal to superconducting phase to take place over a finite distance known as the coherence length. For a cylindrical filament of radius r which is small with respect to the coherence length their description for the critical field in the absence of a transport current is

$$H_{c_1} = \sqrt{8} \frac{\lambda_0}{r} H_c \quad \text{III-26}$$

or for the critical current density in the absence of an external field for a thin film is

$$J_c = \left(\frac{2}{3}\right)^{3/2} \frac{H_c}{4\pi\lambda_0}$$

III-27

An alternative theory for non-ideal superconductors is based on the surface energy between the superconducting and normal phases. London (p 125) pointed out that rather than showing a Meissner Effect an ideal superconductor should prefer to lower its free energy by admitting the magnetic flux through formation of lamina of superconducting material and normal material. If the superconducting lamina were of thickness comparable to λ and the normal lamina were extremely thin then the free energy of the superconductor could be lowered by the flux penetrating the superconducting lamina while minimizing the contribution due to the normal lamina. Consider a plate of thickness t which would then have t/λ superconducting lamina. To achieve a Meissner effect there would have to be a positive surface energy per unit area to offset this magnetic energy.

$$\frac{2t}{\lambda} u_s > \frac{H_c^2 t}{8\pi}$$

III-27

Thus the surface energy must be

$$u_s > \frac{\lambda}{2} \cdot \frac{H_c^2}{8\pi}$$

III-28

The behaviour of non-ideal superconductors has led to the question of whether all superconductors have this

positive surface energy or if indeed, some have a negative surface energy.

The surface energy is related to the coherence length and the penetration depth. London's electrodynamic theory as described previously assumes that at the surface of a superconductor the superconducting electron density changes immediately from zero to the total value determined by the temperature. Thus the magnetic field is excluded by circulating currents of these electrons in the penetration layer. Pippard (as described by Lynton p 39) found experimentally that the penetration depth was greater than that predicted by London's theory. To account for this he postulated a coherence length which is the length over which the superconducting electron density increases from zero to the temperature determined value. This coherence length is directly related to the electronic mean free path. Thus according to Pippard the shielding currents cannot exert their full influence right at the surface and hence there is greater field penetration than predicted by London. The overlapping of coherence length and penetration depth is illustrated schematically in Figure 6a.

Referring to the inequality III-28 it is possible to define a surface energy parameter

$$u_s \equiv \delta \frac{H_c^2}{8\pi}$$

III-29

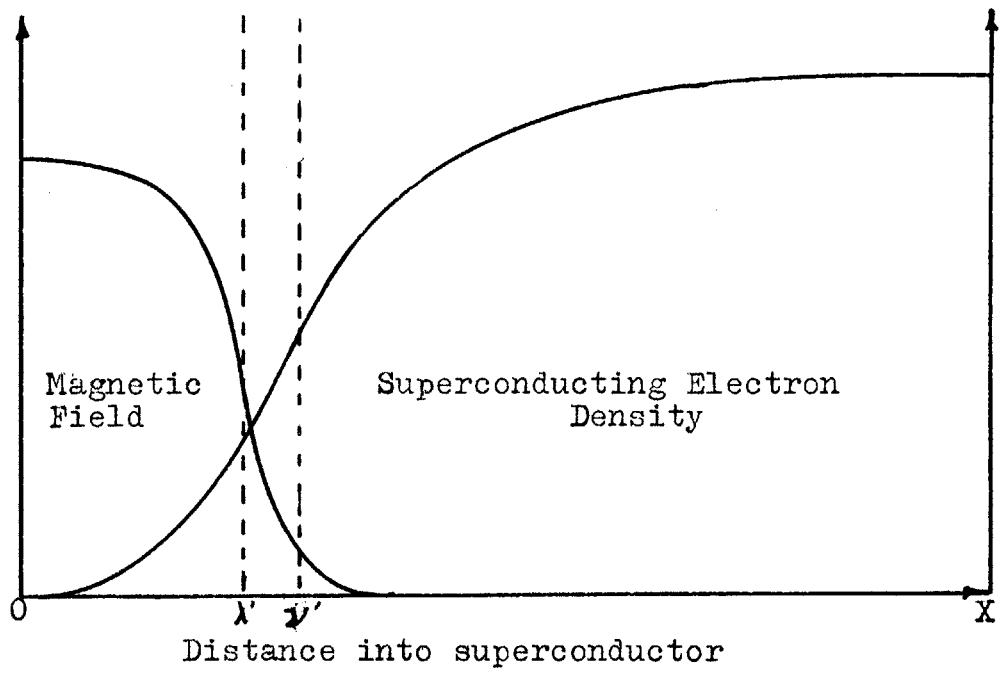


Figure 6a. Graphical illustration of the coherence length and penetration depth.

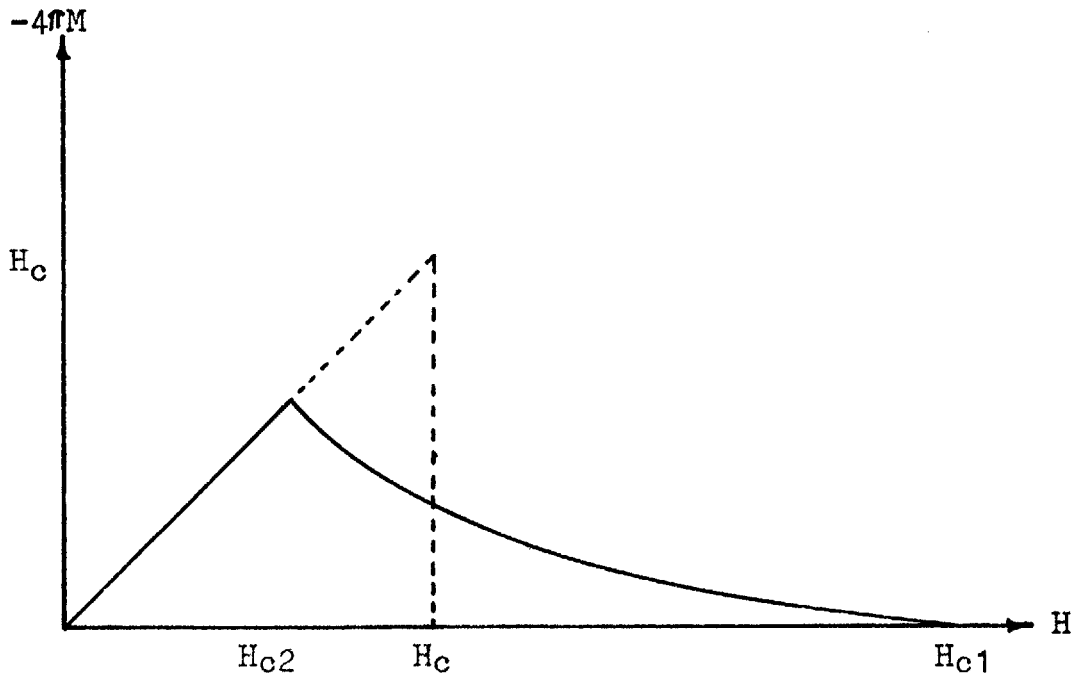


Figure 6b. Magnetization curve for a negative surface energy superconductor.

where $\delta > \frac{\lambda}{2}$. Referring to Figure 6a we can imagine a pseudo coherence length v' which could be represented by the distance from the surface at which the superconducting electron density would change abruptly from zero to the interior value and still maintain the actual superconducting free energy. This would lead to a surface energy parameter $\delta = v'$. Similarly, we can imagine a pseudo penetration depth λ' at which the external field would vanish and still maintain the actual amount of penetrating flux. This would lower the free energy by the penetration of the field and must be subtracted from the surface energy due to the coherence distance. Thus we have

$$\delta = v' - \lambda'$$

or

$$\delta \approx v - \lambda \tag{III-30}$$

It is now apparent that the surface energy will be positive for $v > \lambda$ and negative for $v < \lambda$.

In the course of developing their phenomenological theory Ginzburg and Landau define a parameter

$$k^2 \equiv \frac{2e^2}{\hbar^2 c^2} H_c^2 \lambda_0^4 \tag{III-31}$$

which can be shown to be as follows

$$k \approx 0.96 \frac{\lambda_0}{v_0} \tag{III-32}$$

Further, they develop the equation

$$\frac{H_{c1}}{H_c} = \sqrt{2} k \quad \text{III-33}$$

Then for the regime $k > 1/\sqrt{2}$, H_{c1} exceeds H_c and the surface energy is negative, (precisely according to the G-L theory and roughly according to the above approximate theory).

Abrikosov (again as described by Lynton) has extended this theory for $k > 1/\sqrt{2}$ and calls the state below H_{c1} the mixed state which extends down to a value of the field given by

$$H_{c2} = \frac{1}{2k} (\ln k + 0.08) \quad k \gg 1 \quad \text{III-34}$$

below which normal phases are unstable and the non-ideal superconductor behaves as an ideal superconductor. Figure 6b in which the dotted curve represents a superconductor with a positive surface energy describes graphically the Abrikosov theory.

Neither the filamentary model nor the negative surface energy model have been developed to the point of accounting for a transport current in the presence of a magnetic field.

Abrikosov's theory would require drastic modification to be able to handle the presence of a transport current. Indeed, Kamper⁽²⁸⁾ maintains that a superconductor following



77 Massachusetts Avenue
Cambridge, MA 02139
<http://libraries.mit.edu/ask>

DISCLAIMER NOTICE

Due to the condition of the original material, there are unavoidable flaws in this reproduction. We have made every effort possible to provide you with the best copy available.

Thank you.

Despite pagination irregularities, this is the most complete copy available.

Page 32 does not exist.

the negative surface energy model is incapable of carrying a transport current in the presence of an external magnetic field which is strong enough to produce the mixed state, unless the superconductor contains enough structural defects to stabilize the current against the Lorentz force. Kamper holds that a structurally perfect non-ideal superconductor should follow a modified Silsbee rule which allows that no point on the surface of the superconductor can the magnetic field exceed H_{c2} , the field of first penetration. This Kamper Rule is given by

$$\frac{I_c}{5r} + \frac{H_e}{(1-D)} = H_{c2} \quad \text{III-35}$$

He substantiates his argument experimentally by measuring the current in a **lead**-indium ring in the presence of an axial magnetic field and obtains the type of results indicated in Figure 7(a). The current in the ring rises with applied field and if equation III-35 is valid the current should peak and then follow the dotted line to become zero at $H = H_{c2}/2$ for a cylindrical section ring with demagnetization coefficient 1/2.

Kamper's results are corroborated by Heaton and Rose-Innes⁽²⁹⁾. Heaton and Rose-Innes investigated the the behaviour of tantalum-niobium wire with respect to magnetization and supercurrent capacity in transverse magnetic fields. Their results are shown in Figure 7(b) and indicate

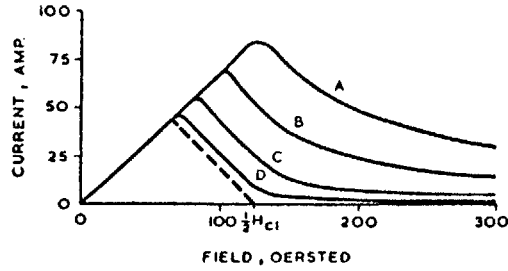


Fig. 1. Persistent current versus magnetic field for lead-indium rings in successive stages of anneal and polish. A) as prepared, D) after two days at 270°C followed by chemical polish to a depth of 0.010".

Figure 7a. Results of Kamper for persistent currents in a non-ideal superconducting ring. Extracted from reference 28.

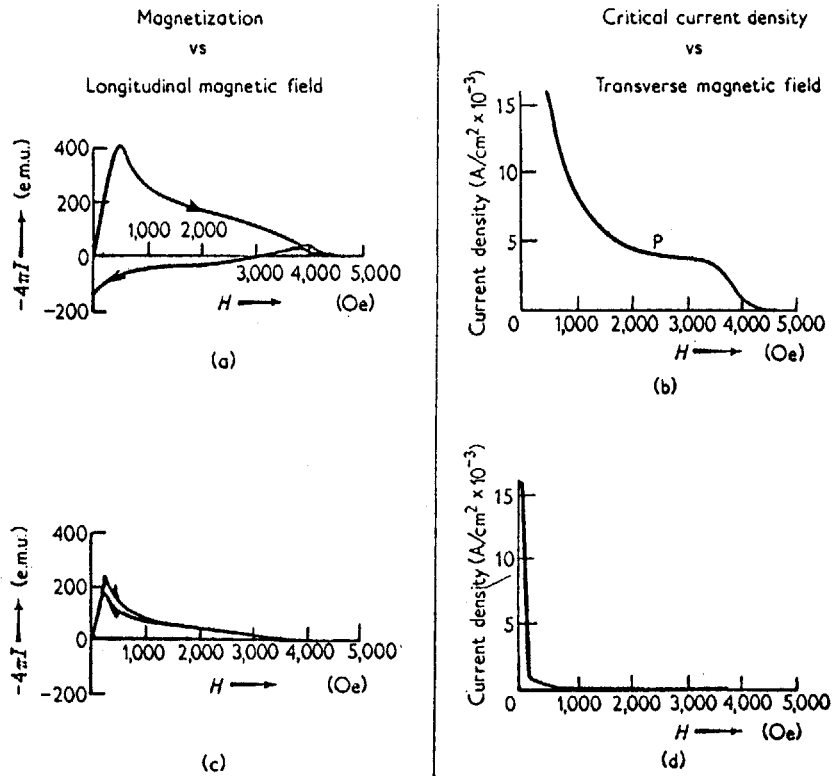


Figure 2. Critical currents and magnetizations of $Ta_{65}-Nb_{35}$ wires at $4.2^\circ K$

Figure 7b. Results of Heaton and Rose-Innes for non-ideal superconductors. Extracted from reference 29.

clearly that a high degree of structural perfection, associated with a reversible magnetization curve yields a very poor supercurrent capacity in the mixed state. Alternatively, the supercurrent capacity at high magnetic fields is enhanced by structural defects associated with the large amount of flux trapping indicated by the irreversible magnetization curve. Heaton and Rose-Innes also report that the "knee" in the current density curve is independent of the amount of annealing of the specimen and of whether the magnetic field is applied transversely or longitudinally. Thus, it seems that the magnetic field limit of the supercurrent capacity is not affected by the Lorentz force.

Apparently, the filamentary model and the negative surface energy model must be combined in order to explain the high supercurrent capacity at high fields of non-ideal superconductors. Accordingly, Bean⁽³⁰⁾ has postulated a macroscopic model as follows: a filamentary structure capable of sustaining a supercurrent up to a critical current density J_c : this critical current density is a function of magnetic field, becoming zero at the critical field of the filaments; however, this function of magnetic field is assumed to be extremely weak until the critical field of the filaments is approached; this means that at fields much less than the critical field of the filaments, J_c can be assumed independent of the field: the mesh is supported in a matrix of ideal superconductor with a critical field

H_c : the magnetic field is shielded by the ideal superconductor up to a field H_c ; and then further shielding is accomplished by currents circulating in the mesh; these mesh currents flow at a value J_c to a depth necessary to reduce the field to H_c . Bean computes magnetization curves for a cylindrical model and obtains curves similar in form to the Abrikosov model with the significant distinction that the magnetization is dependent on the dimensions of the sample. Bean goes on to verify experimentally that this size dependence of magnetization is valid by measuring the magnetizations of two sizes of Nb_3Sn cylinders. The crux of Bean's theory is that the field penetration depth is very strongly field dependent.

Kim, Hempstead and Strnad^(31,32) have extended Bean's theory substantially. Where Bean assumed a constant critical current density, K-H-S assume that the critical current density is a linear function of the magnetic induction as follows:

$$\alpha/J_c = B_0 + B \quad \text{III-36}$$

K-H-S also define a critical state wherein the local current densities throughout a superconductor are all at the critical value as determined by the local magnetic field. It should be noted that for high magnetic fields $B \gg B_0$ the critical current density is strongly influenced by the Lorentz force; $\alpha \approx J_c B$. Experimentally, K-H-S are able

to trace and retrace these critical states for cylindrical tubes and by normalizing their data to the theory through the constants α and B_0 are able to predict the form of the critical states on a plot of the magnetic field inside the tubes against the external field. They find that the critical current density is independent of size and hence that total current is proportional to the cross sectional area of the sample. The data for Nb_3Sn seem to fit nicely for $B_0 = 5$ kilogauss which in fortuitous agreement with the thermodynamic critical field. K-H-S also determine α as a function of reduced temperature, T/T_c , for powdered niobium and niobium-zirconium tubes, as is shown in Figure 8. Extrapolations of their data lead to $\alpha = 0$ at $T/T_c < 1$ which implies the unacceptable consequence of zero supercurrent capacity at $T/T_c < 1$. One would expect these curves to fair into the abscissa in a non-linear manner.

One can expect a sort of thermodynamic cut-off point for equation III-36 associated with H_{c1} of the Abrikosov theory together with a functional modification corresponding with the "knee" in the Heaton-Rose-Innes I_c -H curves. Otherwise, III-36 implies an infinite critical field.

Heretofore in our discussion of non-ideal superconductors the supercurrents involved have been magnetically induced. LeBlanc⁽³³⁾ has considered the effect that an electric field induced transport current has on the magnetization of non-ideal superconductors. LeBlanc finds that

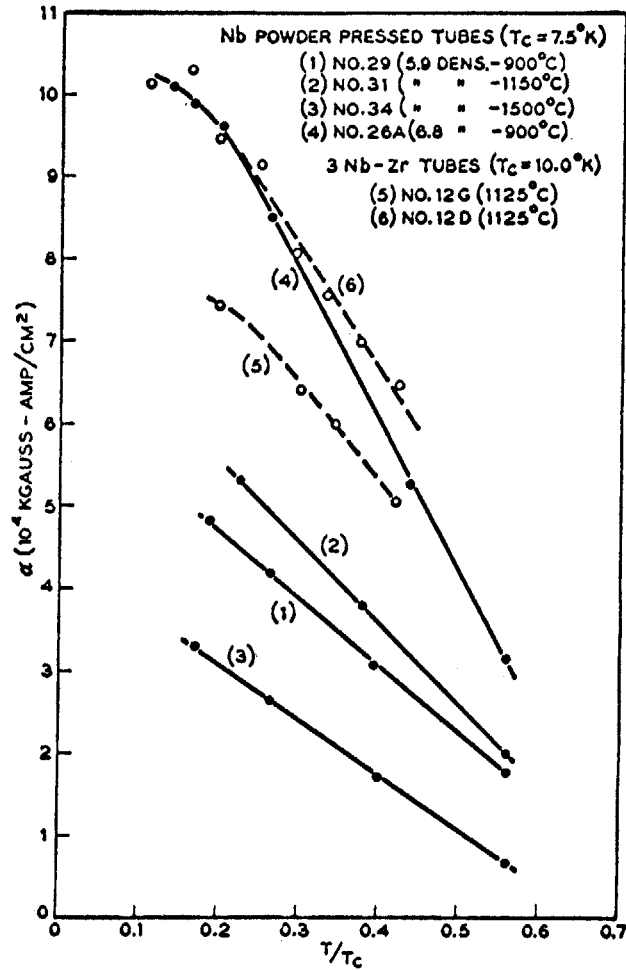


FIG. 2. α as a function of T/T_c for various tube samples. The solid circles are experimental values for Nb powder pressed samples of different densities.

Figure 8. Temperature dependence of the defect density factor α , of Kim, Hempstead and Strnad. Extracted from reference 31.

the magnetization is influenced by a transport current roughly as follows,

$$\frac{M(I)}{M(0)} = 1 - \left(\frac{I}{I_c}\right)^n \quad \text{III-37}$$

where the index n is a function of the sequence of application of the current and the field and of the previous history of the current. If the magnetization is measured with the sample in a critical state, $n = 2$. LeBlanc corroborates the K-H-S concept of the critical states and verifies that the critical state is determined by a critical current density. A transport current reduces the shielding capability by simultaneously reducing the superconducting electrons available for shielding and by increasing the internal magnetic induction.

Summary

The foregoing abridgement of the phenomenological theory of superconductors will serve as a basis for discussing the experimental results later. It is apparent that there is not available a quantitative basis from which we can compute a theoretical result to verify experimentally. Nonetheless, it is useful to summarize what is known about non-ideal superconductors to attempt a qualitative prediction.

A pure homogeneous non-ideal superconductor will have a negative normal-to-superconducting interface energy which will allow it to admit magnetic flux while in the superconducting state. As a consequence of this flux admission, such a superconductor can lower its free energy and maintain the superconducting state to magnetic fields higher than the thermodynamic critical field. In a pure form with a perfect microstructure this type of superconductor cannot maintain a net current in a transverse magnetic field which penetrates to the interior because the current would, in effect, be "blown out" by the Lorentz force.

In a negative surface energy superconductor a mesh of defects in the microstructure can play a dual role. In accordance with the Bean model this mesh can act as a network to support currents against the Lorentz force. This mesh can also form a network of localities where the normal to superconducting surface energy is in varying degrees, more negative than that of the pure structure. This would allow superconducting regions to exist in the material to fields greater than H_{c1} associated with the pure material as is exemplified by the curves of Heaton and Rose-Innes shown in Figure 7(b). One can then postulate the behaviour of a current carrying superconductor in a transverse magnetic field as follows: At fields below H_{c2} extremely high supercurrents are possible because the interior of the superconductor is shielded from the magnetic field. As the applied

field exceeds H_{c_2} , the flux begins to penetrate and both the induced currents and the transport current near the surface require support from the defect mesh and are determined by the local magnetic field. When the flux permeates the interior completely the critical current density approaches linearity in terms of field and transverses the so-called plateau on the J_c - H plot. This linearity persists until the field reaches H_{c_1} corresponding to the pure material. From this point the critical current density depends both on the ability of the defect mesh to withstand the Lorentz forces but also on its ability to sustain regions of superconducting material. In other words, the superconducting network begins to shrink in density at H_{c_1} (pure) until it is totally quenched at H_{c_1}' (impure). Further, data by Heaton and Rose-Innes shown in Figure 9 indicate that the value of α which governs the supercurrent capacity at moderately high fields has a correspondence with H_{c_1}' (impure) implicitly through the defect density. One could consider α as a defect density parameter.

The question with which this thesis is concerned is the possibility of obtaining a measure of the defect density parameter at low currents in the earth's magnetic field and at temperatures approaching the critical temperature. Budnick⁽³⁴⁾ has reported on a decrease in critical temperature corresponding to an increase in residual resistance for

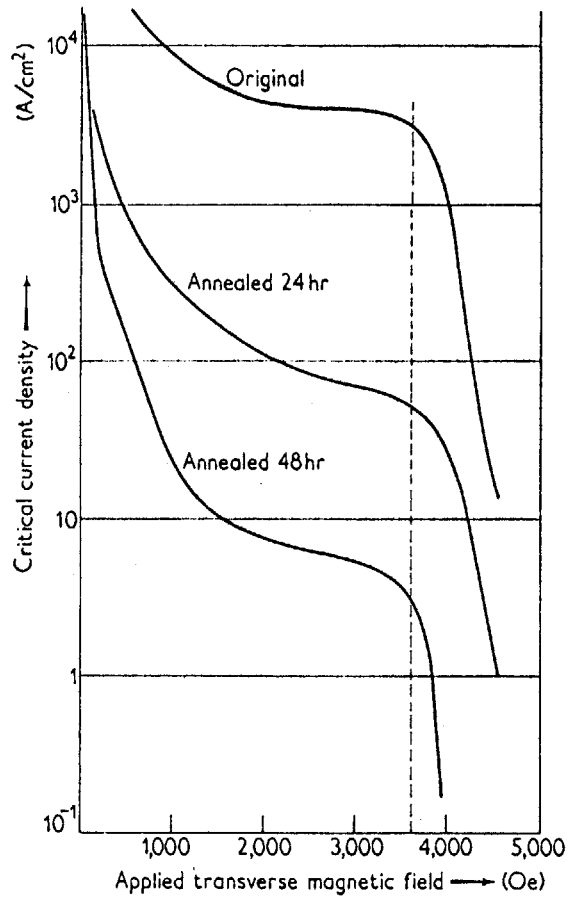


Figure 3. Critical currents at 4.2° K

Figure 9. Supercurrent capacity dependence on annealing time, by Heaton and Rose-Innes. Extracted from reference 29.

tantalum wire of variable purity. The increase in residual resistance could be expected to relate to a defect density. Such a result would imply a crossover on plots of α against temperature whereby high α at low temperature would correspond to low α at high temperature. Reference to Figure 8(a) indicates that such a crossover is indeed possible. According to Lynton (p 132) the depression of T_c goes linearly with the reciprocal electronic mean free path which means that a high defect density (high α) would decrease the average mean free path and result in a greatly depressed T_c . From the results of Budnick⁽³⁴⁾ depressions in critical temperature are not of the order to correspond to linear extrapolations of the curves in Figure 8(a). Nonetheless, it is an effect such as described above which was sought in the experiments to be described subsequently.

IV. EXPERIMENTAL METHOD

The Superconductor

The superconductor used in this study was chosen mostly for its availability. It is a composite ribbon of tin, Nb_3Sn , niobium, Nb_3Sn and tin and is manufactured by the National Research Corporation by rolling tin-clad niobium and reacting in an oven. In some instances the reaction consumes all the tin resulting in a Nb_3Sn clad niobium ribbon. The ribbon used in these experiments was of two widths, 1/16 inch and 1/8 inch and varied in thickness from 0.001 inch to 0.002 in. In order to obtain as wide a range of quality as possible, samples were selected from pilot runs of the manufacturing process for which accurate process data were not available. However, process data is not necessary for the purposes of this thesis.

At high temperatures and high magnetic fields the supercurrent carrier was the two layers of Nb_3Sn . The quality variables are essentially the thickness of these layers in proportion to the thickness of the entire ribbon and the homogeneity and purity of these Nb_3Sn layers.

The samples are designated by their N.R.C. process numbers plus a suffix which indicates its position in this sequence of tests. For example, a sample designated 2BH8-T32

refers to N.R.C. batch 2BH8, the third sample from this batch which was used in the temperature test project and the second temperature test of this sample. If the last digit in the suffix is a zero, it refers to the magnetic field test of the same sample (eg. 2BH8-T30).

Current contacts were made to the samples by copper plating the ends of the samples over a length of about four inches and then soft soldering to copper leads. The copper plating process is given in Appendix A. In the magnet tests the contacts were sufficiently removed from the main magnetic field that flux trapping by the lead in the soft solder contacts was not a problem. Otherwise, tin-indium solder would have been used since neither tin nor indium are superconducting at 4.2°K . In some of the early temperature tests the contacts were made by ultrasonic soldering with tin-indium solder on the bare ribbon but this type of contact was judged no better than the soft solder technique considering the complexity of the ultrasonic soldering process.

Voltage contacts were made by taping the voltage leads to the sample and using silver paint to facilitate electrical contact.

Apparatus

The experiments were carried out in two phases: the high temperature phase with magnetic field fixed (i.e., the

earth's magnetic field) and temperature and current as variables and the high magnetic field phase with temperature fixed (i.e., the normal boiling point of helium) and magnetic field and current as variables. The high temperature apparatus is pictured in Plate 1 while the high field apparatus is pictured in Plate 2.

The two sets of experiments had a common component which was the low voltage current source for the superconducting samples. The current source was a six volt automotive type wet cell battery. Current control was achieved by controlling the bias on four watercooled 60 ampere power transistors which were connected in parallel. The circuit diagram from which the current control was constructed is given in Appendix B. On short circuit the current could be controlled from a minimum of 0.5 milliamperes to a maximum of 200 amperes. In use with a superconducting sample plus the leads, ^{the} maximum current obtainable was 140-160 amperes depending on the condition of the battery. In general, the current could be controlled within tolerances less than could be read on a three figure ammeter. The battery charge was maintained by a commercial automotive trickle charger.

The high temperature test apparatus is shown schematically in Figure 10. The essential part of the apparatus was the copper temperature control body which through intimate thermal contact with the portion of the superconductor under test provided the means whereby the temperature of the

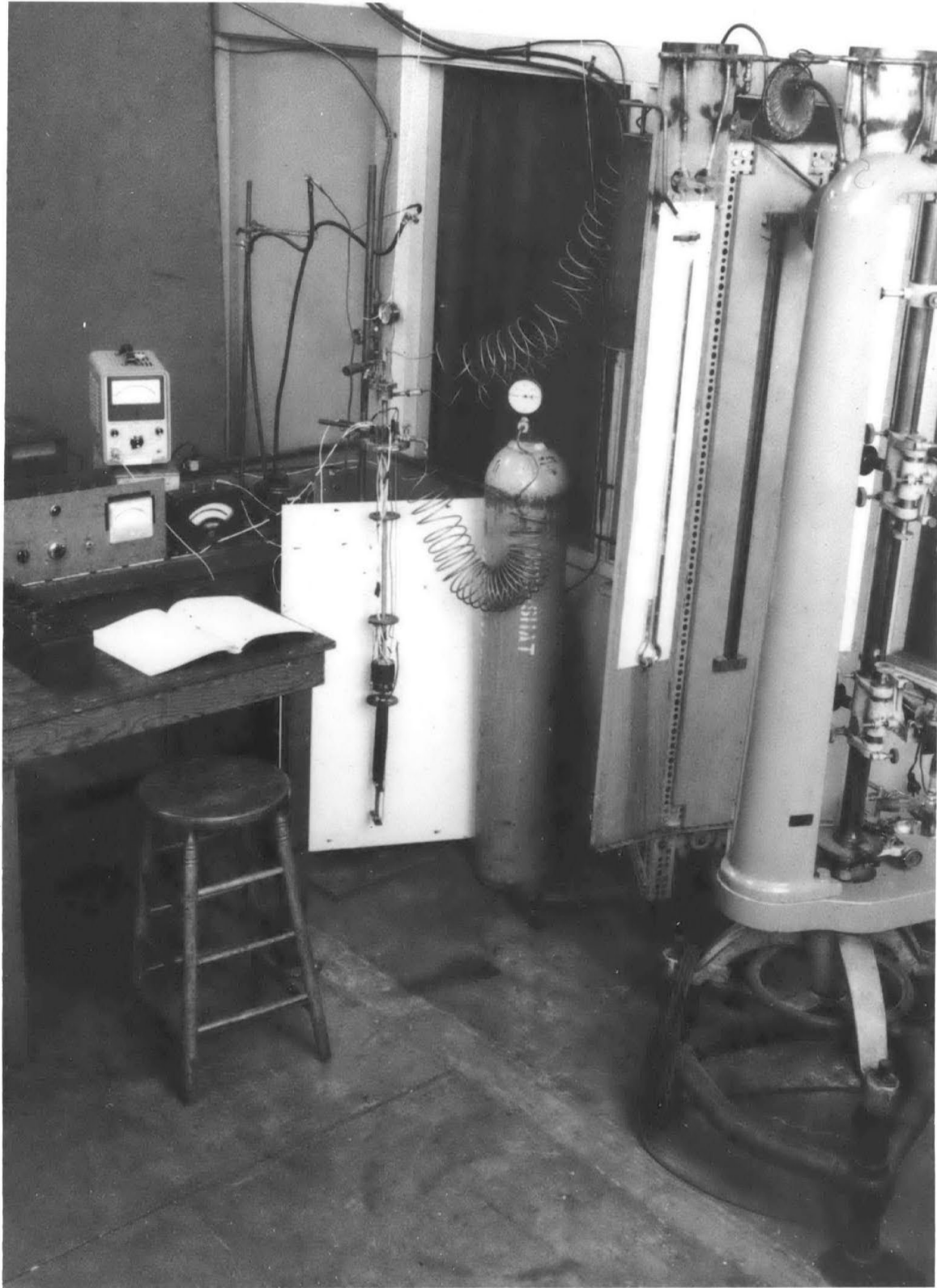


PLATE 1. TEMPERATURE TEST APPARATUS

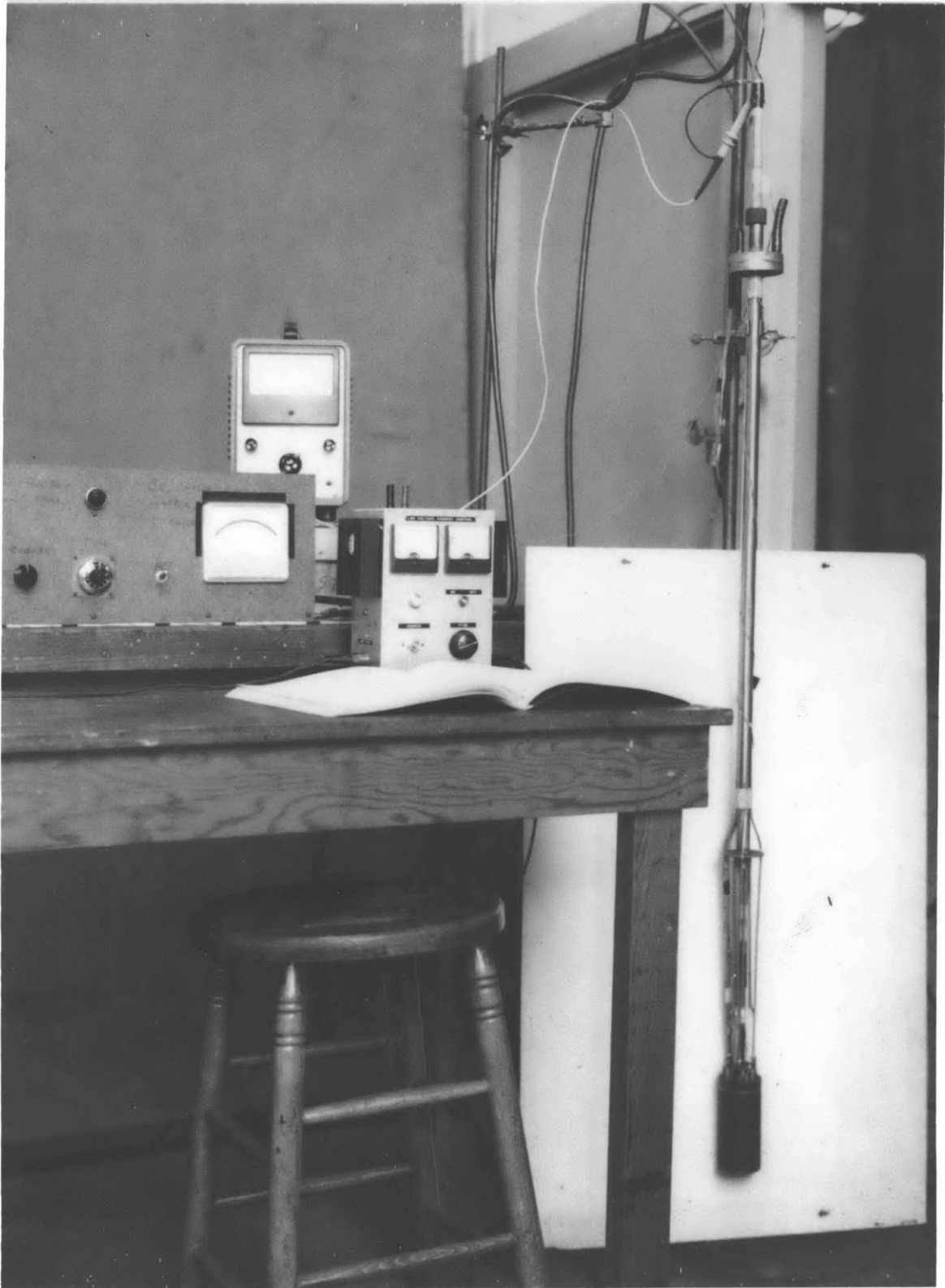


PLATE 2. MAGNETIC FIELD TEST APPARATUS

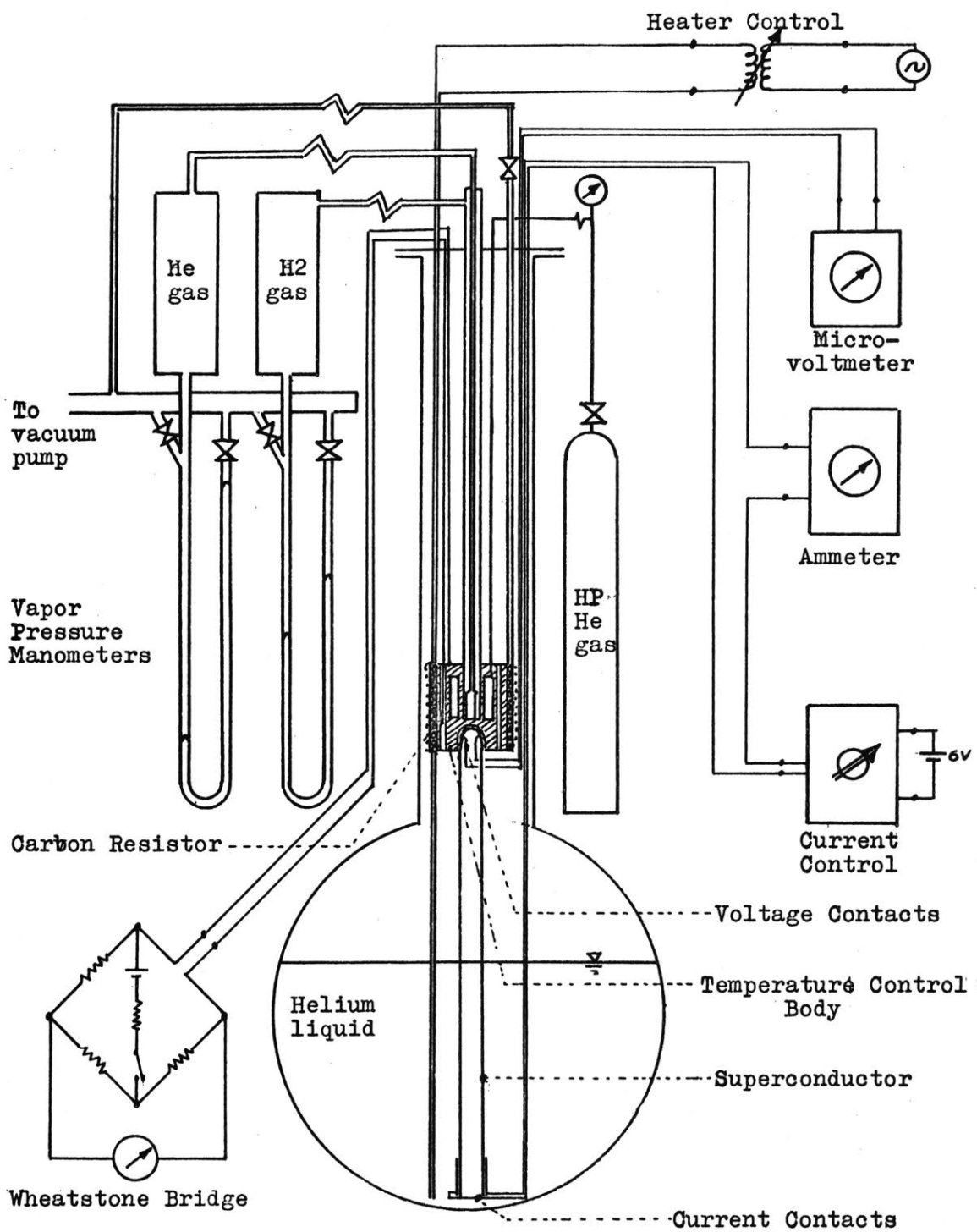


Figure 10. Schematic of the temperature test apparatus.

test sample was controlled and measured. The temperature of this control body was controlled in three ways. The apparatus was lowered into the 3.5 inch diameter neck of a special 25 liter liquid helium dewar and the relative positions of the control body in the neck and the liquid level in the dewar provided a coarse adjustment on the temperature of the control body. The outside of the control body was wrapped with a coil of 1/8 inch thin wall copper tubing. The coil was bonded to the body by soft solder. One end of the coil was connected to a cupro-nickel tube which extended down to the bottom of the dewar below the liquid helium level. The other end of the coil was connected to another cupro-nickel tube which lead out of the neck of the dewar and was connected through a needle valve to the laboratory's 135 cfm vacuum pump. Once the position of the control body was fixed additional refrigeration could be supplied to it by controlled pumping of two-phase helium through this coil system. Outside of the refrigeration coil was wrapped a layer of 0.005 inch aluminum foil, a layer of 0.0005 inch Mylar and a coil of 24 gage nichrome heating wire which had a total resistance of 10 ohms. By supplying alternating current via a Variac through this heater coil the temperature of the control body could be raised above its equilibrium temperature corresponding to the position in the neck of the dewar.

For the purposes of this experiment the control body was assumed isothermal. The normal heat leak into the dewar with the apparatus removed and micarta baffle stack in the neck resulted in a liquid helium boil-off of 0.12 liters/hr. The liquid helium boil-off averaged over the period of an experiment was 0.2 liters/hr. If all the additional heat leak was assumed to flow through the control body which is unlikely in view of the refrigeration necessary to cool the apparatus and the increased connection paths available, the resultant temperature gradient in the control body would be $0.002^{\circ}\text{K}/\text{cm}$. Hence, the assumption of an isothermal body is reasonable.

The superconducting sample was mounted on a micarta holder as shown in Plate 3. The sample was bent on a 0.5 inch diameter over the head of the holder and current contacts made at the lower end. Voltage contacts were made at the head end of the holder so that the 0.75 cm of the sample over head of the holder was the section of the sample actually under test. The head of the sample holder was clamped into the interior of the control body while the lower end extended down to the bottom of the dewar to hold the current contacts below the liquid helium level. By means of a clamping arrangement of two micarta wedges and a nylon draw rod which was designed to tighten as it was cooled, the head of the sample holder and hence the sample test section was held in intimate thermal contact with the temperature control body.

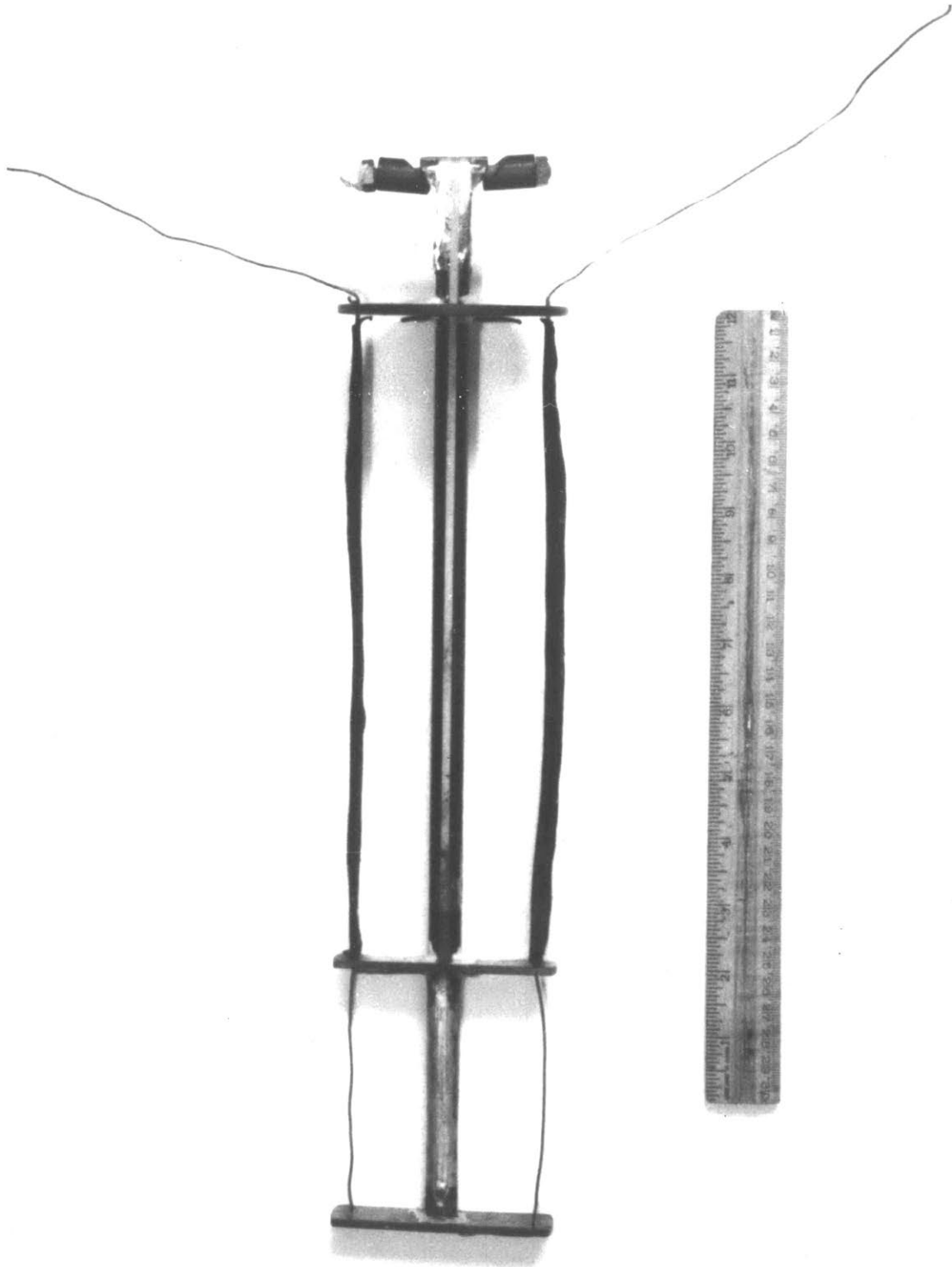


PLATE 3. TEMPERATURE TEST SAMPLE HOLDER

The effectiveness of the clamping arrangement was tested in the following manner. At positions on the sample holder head where the voltage contacts were to be made, two gold wires were embedded laterally and filed smooth until the exposed surface was flush with the head of the sample holder. Thus the gold wires presented two electrical contacts transverse to the ribbon and a circuit could be completed from one gold wire through the ribbon to the other gold wire when the sample holder was clamped tightly against the control body. Several clamping arrangements were tried before it was found that the one described above would maintain the electrical circuit at test temperatures. A strip of 0.0005^{in.} mylar was used to electrically isolate the sample from the control body.

In the control body was a 15.5 cubic centimeter cavity which was connected through a valve to a high pressure cylinder filled with helium gas. Assuming a constant pressure of 100 atmospheres this device provided the control body with a thermal inertia ranging from 4.6 calories/^oK at 20^oK to 18.2 calories/^oK at 5^oK.

Also in the temperature control body were hydrogen and helium bulbs of volumes 11.6 cubic centimeters and 0.756 cubic centimeters respectively. These temperature sensing bulbs were connected in series with two room temperature reservoirs (9.4 liters for hydrogen and 5.44 liters for helium) to two mercury manometers. The filling pressure

was 816 MM Hg., and room temperature volume of the hydrogen vapor pressure thermometer were selected so that the bulb would begin to fill with liquid hydrogen at 20°K and would be full at 15°K. Similarly, the helium vapor pressure thermometer bulb was designed to begin filling at 4.26°K by charging to a pressure of 840 MM Hg.

The purity of the gases filling the vapor pressure thermometers was assured by successive purging of the systems after they had been pumped to 10^{-7} MM Hg pressure for an extended period. The filling gases were introduced through a trap filled with activated charcoal and refrigerated to 77°K by liquid nitrogen.

The temperature control body was provided with two vertical holes with transverse set screws at a level adjacent to the test section of the superconductor. The set screws were used to clamp one lead of each of two Ohmite carbon resistors to the control body to assure electrical and thermal contact. Either of the carbon resistors were connected to form one arm of a Wheatstone Bridge circuit in which the temperature control body was live.

The vapor pressure connecting tubes were used to suspend the temperature control body in the neck of the dewar. A brass plate which could be bolted to a 6 bolt-hole flange on the top of the dewar was the suspension point. An O-ring between the plate and the flange provided the means to seal the dewar once the apparatus was in place. A valve

connected through the plate to the inside of the dewar allowed the dewar to be vented when necessary and could be closed to prevent the entrance of air. All electrical connections were detachable at the mounting plate. The gas and vapor conduit connections were made sufficiently flexible that the apparatus could be lifted from the dewar to change samples without disconnecting them.

The high magnetic field test apparatus is shown schematically in Figure 11. The magnetic field was produced by either of two Magnion superconducting solenoids with niobium-zirconium wire windings. One had a 0.5 inch bore and was capable of producing in excess of 30 kilogauss with some coaxing. The other had a one inch bore and was capable of 40 kilogauss with coaxing. The 0.5 inch bore solenoid would accept 0.375 inch diameter sample holders on which the samples were mounted in a groove over the end as shown in Plate 4. It was necessary to immobilize the the samples against Lorentz forces during the magnet tests yet it was also necessary to avoid stressing them at the same time. Motion due deflecting under Lorentz forces could cause premature quenching due to Joule heating by eddy currents in the normal part of the conductor. By the same token excessive stressing of the sample could degrade its performance. Voltage contacts were attached so that the same 0.75 centimeter of each sample which was temperature tested was monitored while subjected to the transverse magnetic field. The

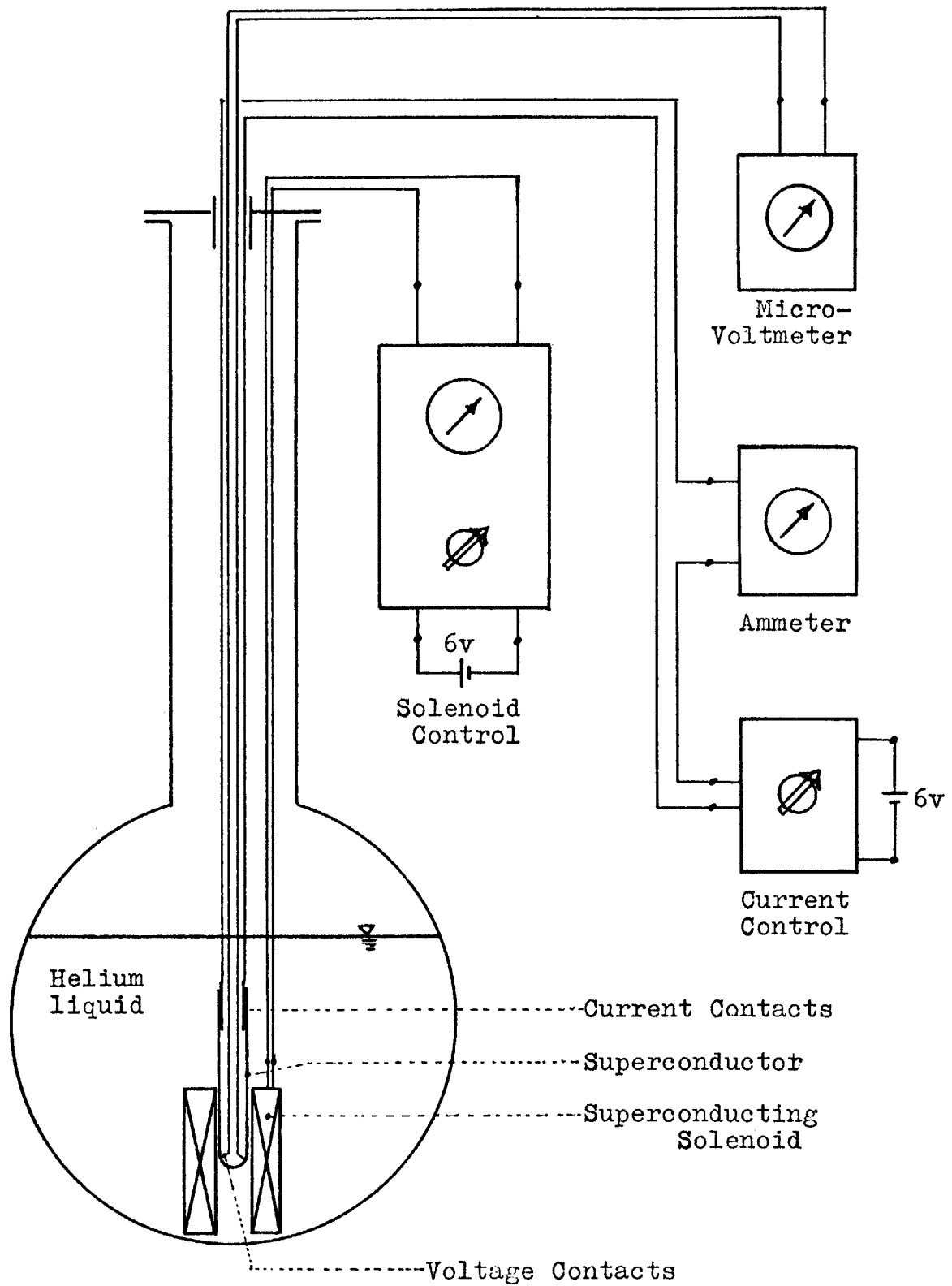


Figure 11. Schematic of the magnetic field test apparatus



PLATE 4. MAGNETIC FIELD TEST SAMPLE HOLDER

one inch bore magnet would accept 0.75 inch diameter probes and approximately half of the samples were tested in each magnet.

To power the solenoids a low voltage current source was constructed from essentially the same circuit diagram as given in Appendix A. However, a single air-cooled 60 ampere power transistor was used in lieu of the four water cooled transistors. Because of the inferior cooling, the transistor was derated by fifty per cent which gave the current source a maximum output of 30 amperes which was comfortably in excess of the solenoid requirements. Since less fine current control was required for this purpose a three turn helipot was substituted for the ten turn helipot.

The superconducting solenoid was mounted in the same 25 liter helium dewar as was used for the temperature tests.

Instrumentation and Calibrations

In both the temperature and magnet tests the voltage across the test section of the sample was sensed by a Hewlett-Packard Model 425A micro-volt-ammeter. The most sensitive scale of this instrument was ten microvolts full scale. The quoted accuracy of this meter was 3 per cent of full scale which was reflected very well in that repeatable data could be obtained by taking 1.0 microvolts as the gate between the superconducting state and the normal conducting state.

In the low current temperature tests the current was monitored by a Weston Model 931 milliammeter which had a quoted accuracy of 1 per cent. In the higher current, temperature tests and in the magnet tests the current was monitored by a Weston multirange millivoltmeter in conjunction with a 3 ampere, a 15 ampere and a 200 ampere 50 millivolt shunts. The quoted accuracy of the millivoltmeter was 0.5 per cent and of the shunts 1.0 per cent.

The superconducting solenoids were calibrated against the ammeter on the current control. In actuality, the manufacturer's calibrations were used. These calibrations were checked at several points by means of a Sensitive Instruments Flux meter Model FM of quoted accuracy 0.5 per cent in conjunction with a 16 turn pull coil with an average cross sectional area of 0.67 square centimeters. The Fluxmeter equation was as follows.

$$\text{Kilogauss} = \frac{.10 \times \text{Deflection}}{\text{Turns} \times \text{Cross sectional Area}} \quad \text{IV-1}$$

The calibrations with the check points indicated are given in Appendix C.

The mercury ~~levels~~ in the vapor pressure manometers were measured by a Society Genevoise Model CA 250 A cathetometer to an accuracy of 0.02 millimeters. For the helium vapor pressure to temperature calibration the values tabulated on page 104 of White⁽³²⁾ for the range 800-760 mm Hg were used.

For the hydrogen vapor pressure to temperature calibration the following equation for normal liquid hydrogen was used.

$$\log_{10} p_{\text{MM Hg}} = 4.66687 - \frac{44.9569}{T} + 0.020537T \quad \text{IV-2}$$

This equation was taken from Scott⁽³⁶⁾ page 298 and corresponds to normal hydrogen (i.e., 75 per cent ortho-hydrogen). The constants in equation IV-2 vary with the concentration of ortho-hydrogen in the liquid which becomes 0.21 per cent in its equilibrium state at 20.4°K. Scott (p 290) gives the uncatylyzed conversion rate of ortho-hydrogen as

$$- \frac{dx}{dt} = 0.0114 x^2 \left(\frac{1}{\text{hr}} \right) \quad \text{IV-3}$$

If one assumes that the uncatylyzed conversion takes place over the duration of a 5 hour experiment the resulting temperature error at 18.00°K is less than 0.001°K which is less than the tolerance of these experiments. Further, the hydrogen liquid was not completely condensed in the bulb over the full time of the experiment so that the assumption that equation IV-2 is valid is justified for these experiments. Equation IV-2 was put on a computer and tabulated at intervals of 0.050°K which allowed a linear interpolation. This tabulation is given in Appendix D.

Interpolation between vapor pressure readings was achieved by measuring the resistance of a 500 ohm carbon

resistor which was mounted as described previously and connected as one arm of a Wheatstone Bridge. The Bridge circuit is given in Appendix E and was designed so that power dissipation in the temperature sensing resistor was less than 10^{-7} watts. There was no detectable drift of the Bridge reading with respect to vapor pressure readings so that power dissipation in the sensing resistor was adequately low. The null sensing device of the Bridge circuit was a Rubicon galvanometer Model 3412 with a quoted sensitivity of 0.009 microamperes per millimeter deflection.

In some of the early experiments data were taken at temperatures less than 14°K in which cases the following equation taken from White (p 127), was used for interpolation between vapor pressure measurements.

$$\log_{10} R + k/\log_{10} R = A + B/T \quad \text{IV-4}$$

The constants were evaluated at two temperatures in the hydrogen vapor pressure range ($14\text{-}20^{\circ}\text{K}$) and at one temperature in the helium range (about 4.26°K).

Most of the experiments were conducted in the hydrogen vapor pressure range in which cases graphical interpolation was made between several vapor pressure readings to obtain a curve of resistance against temperature for the carbon resistor. The resistor was calibrated for each experiment because the calibration would not hold if the resistor was cycled to room temperature and back to operating temperature.

This variation in calibration is illustrated by some typical calibrations in Figure 12.

The Wheatstone Bridge carbon resistor combination was the limiting factor in the sensitivity of the temperature measurements. In practice temperature measurements were made to a sensitivity of 0.003°K which was deemed adequate for these experiments.

Procedure

As a prerequisite to the temperature tests of the superconductors it was necessary to make the coarse adjustment of the temperature of the control body. By trial and error the temperature control body was located at a position in the neck of the dewar such that with the liquid helium level at the base of the neck, the control body came to equilibrium at about 12°K and with the dewar almost empty of liquid helium the equilibrium temperature was about 16°K . With the dewar full to the neck with liquid helium it was possible through using the refrigeration system to its capacity, to lower the temperature of the control body to about 4.2°K .

When the apparatus was lowered into the dewar and before commencing an experiment, the apparatus had to be allowed to come to thermal equilibrium with its surroundings. After equilibrium was attained, judicious application of the heater or refrigeration could change the temperature of the

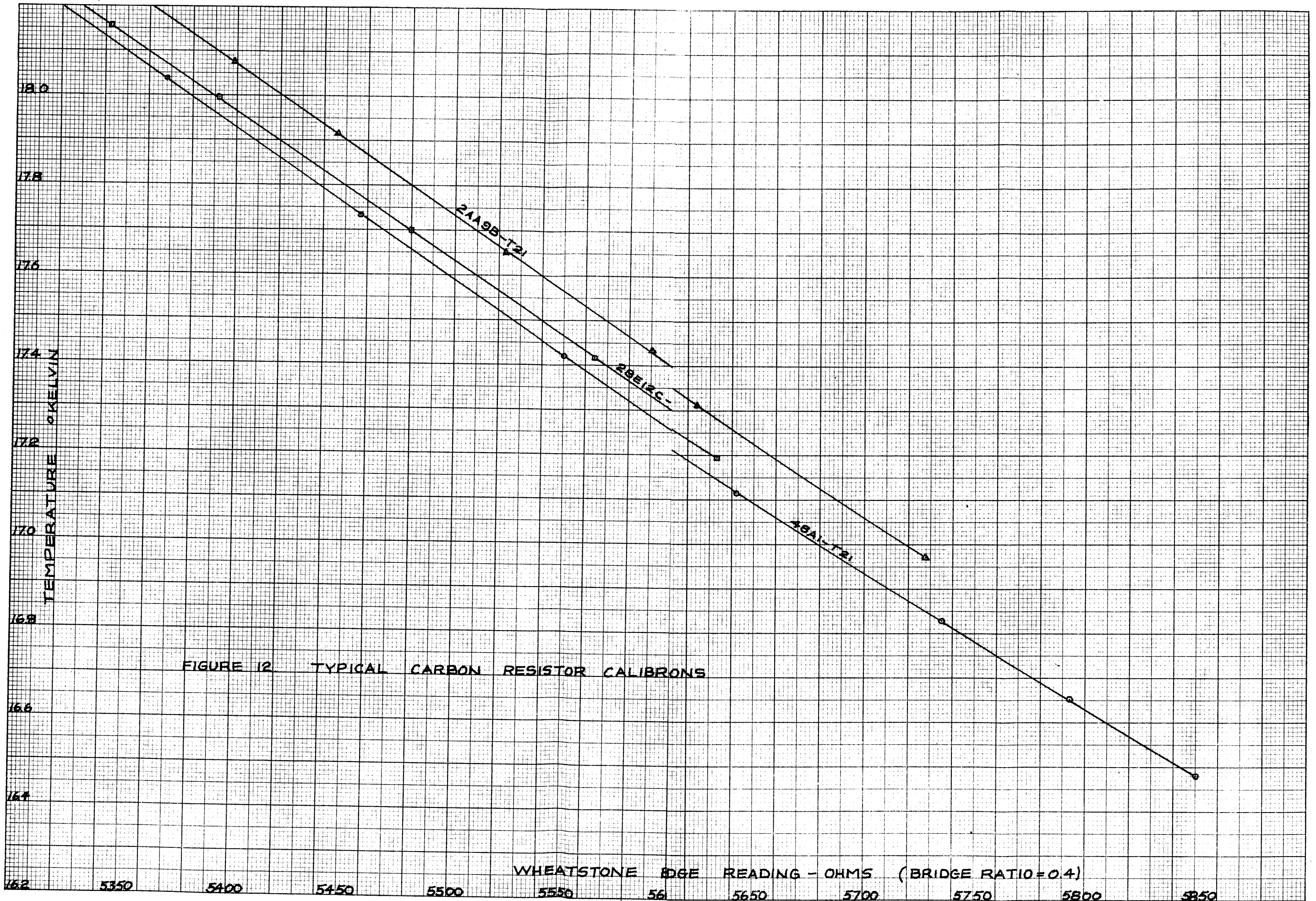


FIGURE 12 TYPICAL CARBON RESISTOR CALIBRONS

control body to a desired value. Temperature control was somewhat capricious when high currents (> 20 amperes) were run through the superconductor. The high currents dissipated considerable joule heat in the normal conductors below the liquid helium level and the liberated helium vapor applied sporadic refrigeration to the control body as the currents were applied. Under these circumstances the apparatus required two operators. One operator applied the measuring current and the heater current simultaneously while the other operator monitored the resistance thermometer via the Wheatstone Bridge.

If data were to be taken below the hydrogen vapor pressure range the following procedure was followed. The apparatus was allowed to reach equilibrium with the valve to the high pressure helium bottle closed. With the high pressure helium thermal ballast excluded from the control body, refrigeration was applied until a calibration point could be taken for the carbon resistor in the helium vapor pressure range. Then the thermal ballast was admitted to the control body and two calibration points for the carbon resistor were taken in the hydrogen vapor pressure range. Following the resistor calibration the data could be taken while the temperature was monitored via the Wheatstone Bridge.

If data were to be taken only in the hydrogen vapor pressure range resistor calibration points were interspersed among the superconductor data.

Precise point control of temperature was not feasible in terms of the time required to stabilize the temperature of the control body at a predetermined value. It was much easier to set the temperature of the control body in a slow drift (about 1.0°K/hr) upwards from a point at the low end of the temperature range involved. If the low point was below the hydrogen range, in the absence of applied refrigeration the temperature of the control body would drift slowly to the equilibrium value. Above the equilibrium temperature a stepwise application of the heater, would result in a stepwise drift of temperature with the control body approaching each new higher temperature asymptotically. The carbon resistor reflected the various heat inputs very faithfully as did the vapor pressure thermometer, during the slow temperature changes. However, some lag was detected in the vapor pressure thermometers under rapid temperature changes. Hence, as an added precaution, resistor calibration points were taken as the control body approached each new equilibrium temperature.

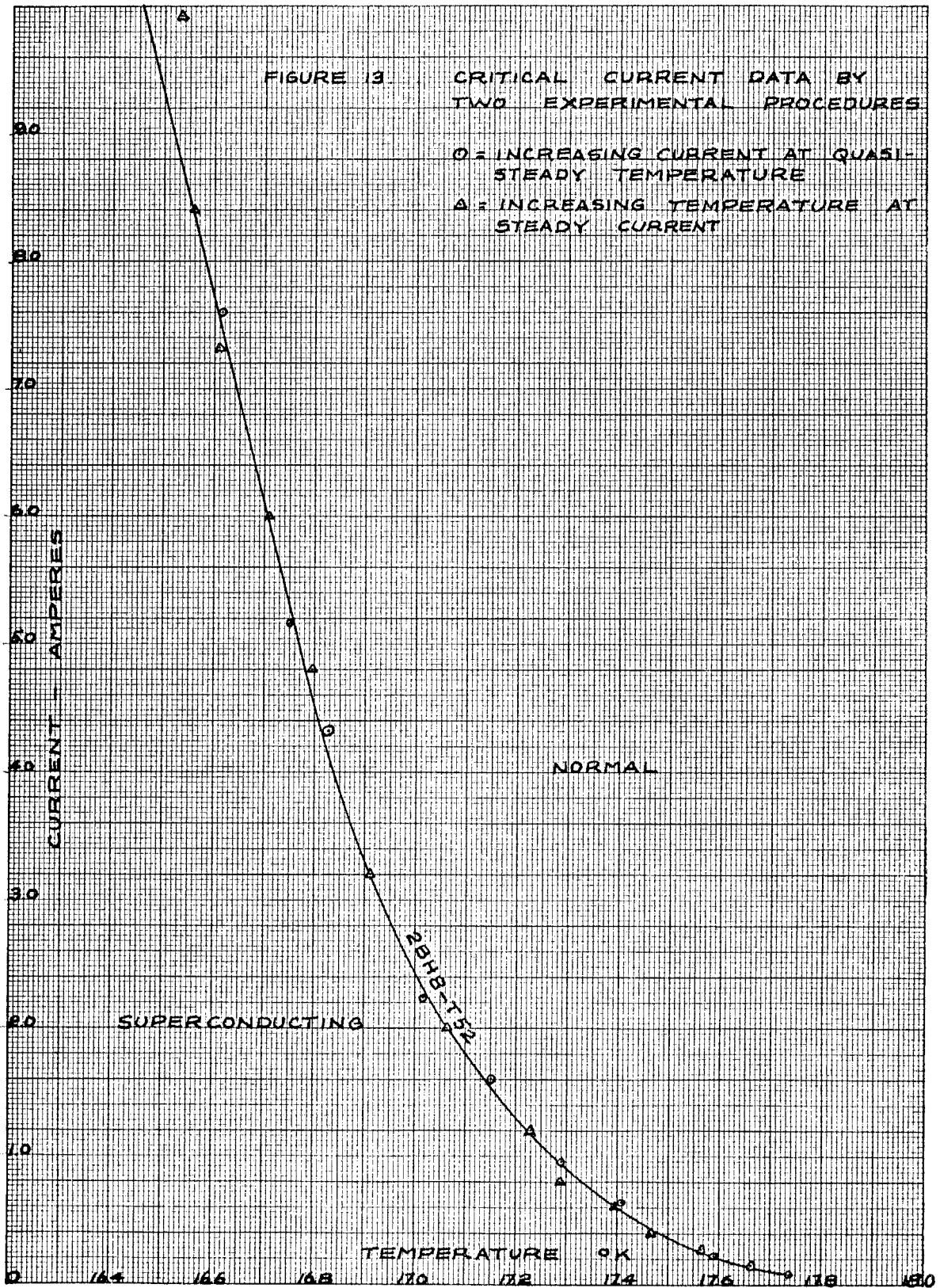
If critical currents were to be measured, the temperature drift was initiated from the lowest temperature desired and the current was applied to a value necessary to cause an electrical resistance in the superconductor. The current was reduced by a desired amount and the temperature monitored until the resistance reappeared. This procedure was continued until the critical temperature of the superconductor was exceeded. The equivalence of this manner of

taking a critical current curve to the procedure whereby the temperature is set and the current raised to its critical value is demonstrated in Figure 13.

The temperature drift allowed resistive transitions at constant current to be measured with facility by monitoring the voltage as the temperature increased.

Measurements in a magnetic field were relatively straightforward. The superconducting solenoids operated at the normal boiling point of liquid helium. Magnetic field data were taken for the samples at the same temperature. With the sample holder located so that the head was at the axial midpoint of the solenoid, current was applied to the solenoid gradually and with pauses to allow for the dissipation of Joule heat generated by eddy currents in the normal portions of the windings. The 30 kilogauss solenoid behaved best if the applied voltage was not allowed to exceed 0.1 volt. With each cooling it was necessary to train this 30 kilogauss solenoid up to its maximum field by raising the current and then removing it in successively increasing steps. Once the solenoid had reached the maximum field, the current could be removed and brought up again smoothly so long as the temperature of the solenoid was maintained at 4.2°K. The 40 kilogauss solenoid was not so sensitive in this regard.

When the 30 kilogauss solenoid was set at a given field there was a small amount of drift about the set field.



This drift was not excessive and could be accounted for while taking voltage and current readings. The 40 kilogauss solenoid was fitted with a persistent current loop and was perfectly stable on a field setting when the activating current was flowing through the persistent current loop and the current source disconnected.

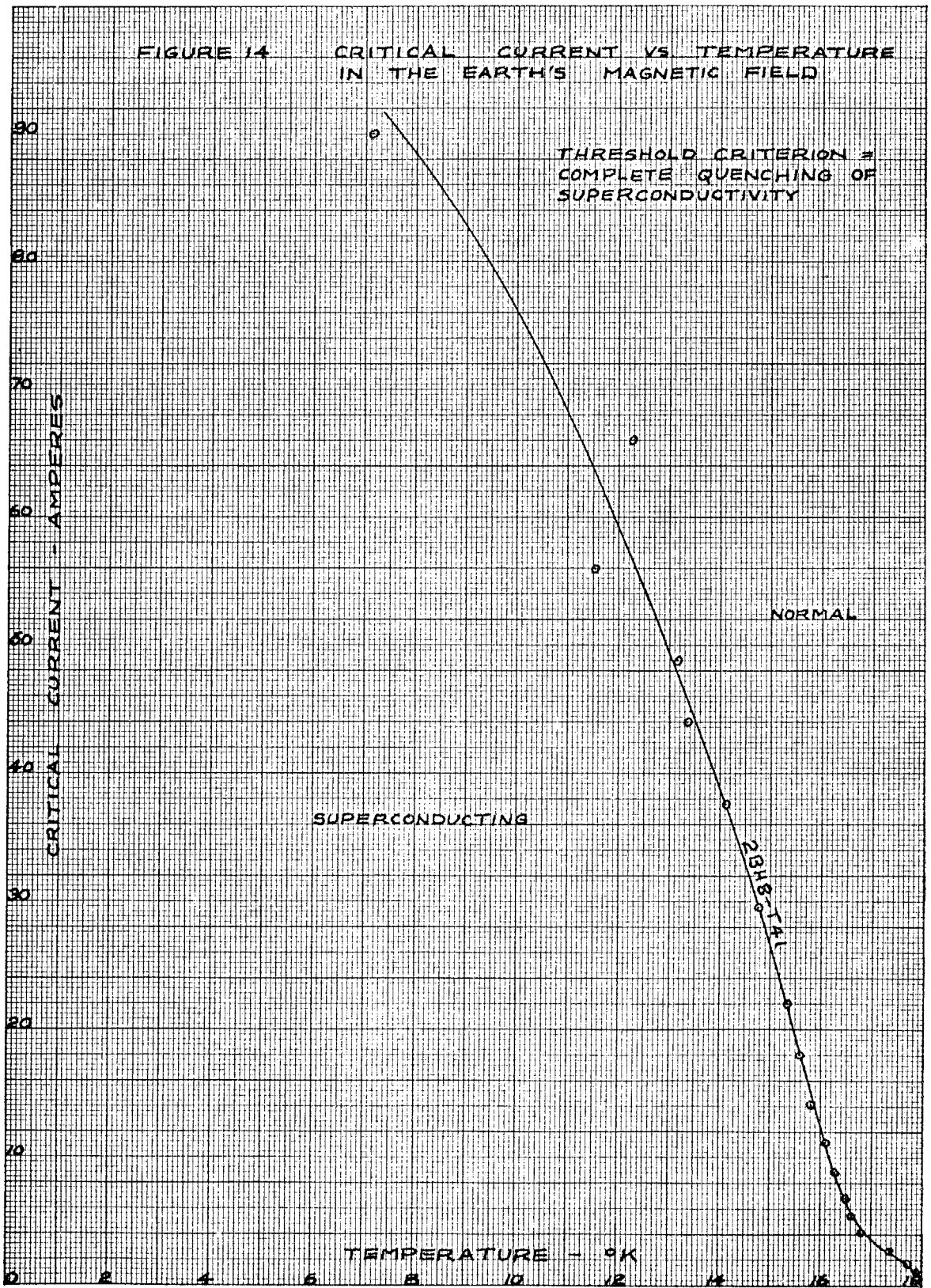
The sequence for taking magnetic field data was as follows. The magnetic field was set at the highest value and then the current through the sample was raised smoothly until a voltage was detected. Then the current was increased in a stepwise manner with current and voltage measurements being taken at regular intervals until the sample was quenched of all superconductivity and the current and voltage went through a sharp discontinuity. The field was then lowered to the next value and the voltage and current readings repeated. The 30 kilogauss solenoid was prone to quenching when the sample quenched which meant that the field had to be raised to the next value from zero. However, the consistent pattern was to work from the high fields to the lower fields so that complete data could be obtained before the sample burned out at the high currents possible in low fields, if this were the case.

V. EXPERIMENTAL RESULTS

Preliminary Tests

The first tests conducted with the temperature test apparatus were aimed at learning of the characteristics of the apparatus and at determining the form of critical current curve at high temperatures. In Figure 14 is shown the critical current against temperature for a typical superconducting sample. The criterion for the threshold between the superconducting state and the normal state was taken as the full quench of all superconductivity as indicated by an abrupt fall in current due to the inability of the applied voltage to sustain the current in a resistive ribbon. The scatter of the data at currents above 50 amperes indicates the difficulty in making accurate measurements when Joule heating of the current leads in the liquid helium created substantial refrigeration to the temperature control body which had to be offset by the heater. The shape of the critical current curve at high temperatures appears to be similar to that expected at high magnetic fields as shown in Figure 7b. Further, an extrapolation of the curve above 10 amperes would intersect the temperature axis at less than the critical temperature as is implied by the K-H-S results (See Figure 8) for the defect density factor α .

FIGURE 14 CRITICAL CURRENT VS TEMPERATURE
IN THE EARTH'S MAGNETIC FIELD



The single critical current curve as shown in Figure 14 is deceptive because it implies an abrupt transition through an infinitesimally narrow threshold between the two states. This is in fact not the case. In Figure 15 it is seen that there is a band of an intermediate state which divides the superconducting from the normal state. If the sample were an ideal superconductor this intermediate state could be explained in terms of London's theory as given in Chapter III. However, in a non-ideal superconductor penetration of the magnetic flux due to the transport current simply implies that the mesh must take up the shielding load. On the other hand, one could attribute this intermediate state to the appearance of small discontinuities in the superconducting mesh which gradually grow in size and number until the Joule heating in the discontinuities drives whole mesh into the normal state.

At high currents it is evident that the Joule heat accelerates the transition and the intermediate band is relatively narrow. At low currents the Joule heat is not as significant and the transition zone is expanded until near the critical temperature the transition is smooth and the onset of full resistance is not detectable by a current discontinuity.

If one wishes to define the transition by a line there is a certain amount of arbitrariness involved. Figure 16 illustrates two threshold criteria. The criterion of

FIGURE 15 TRANSITION BAND OF RESISTANCE FOR CRITICAL CURRENT AGAINST TEMPERATURE SAMPLE 28H8-T52

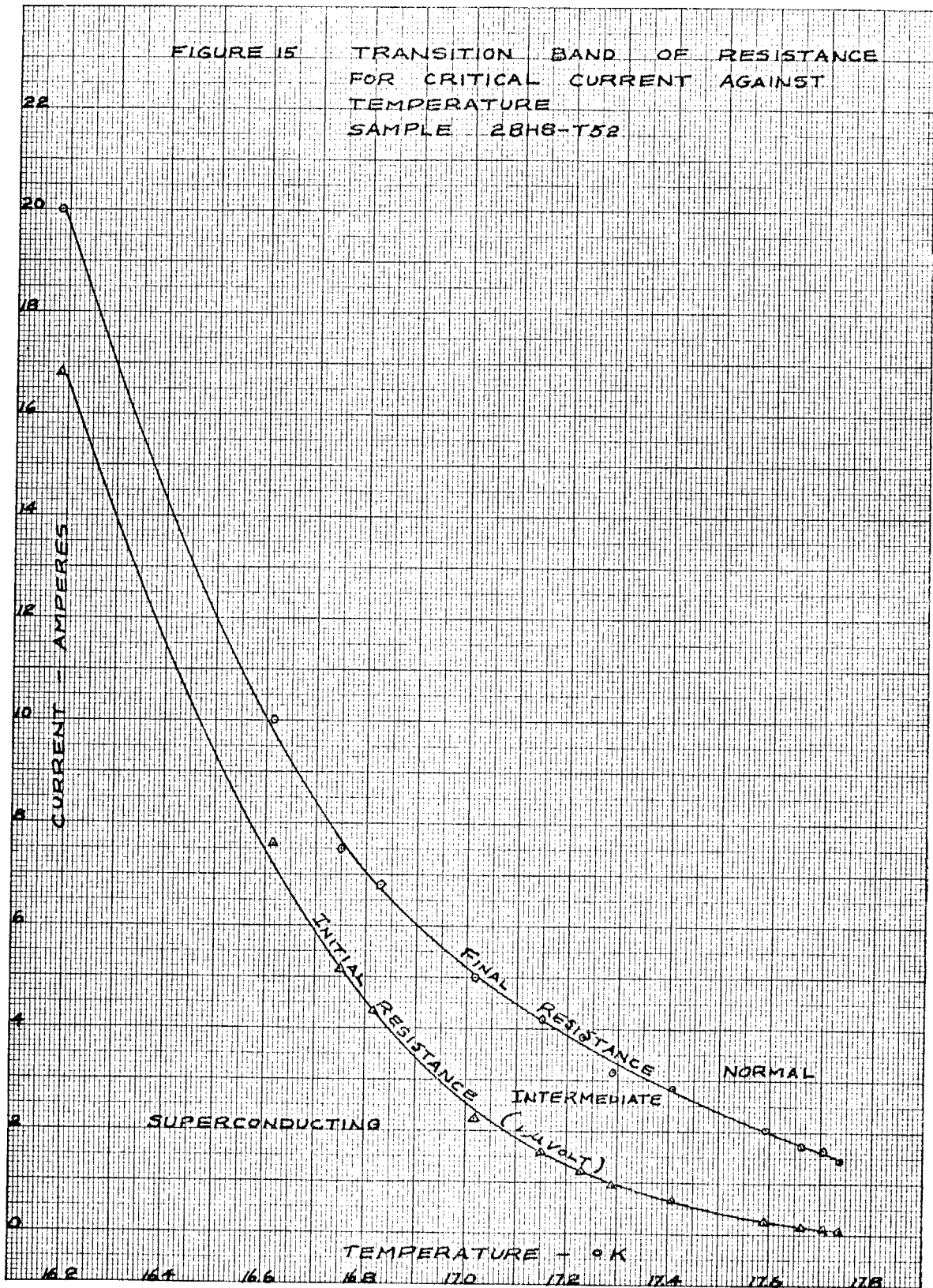
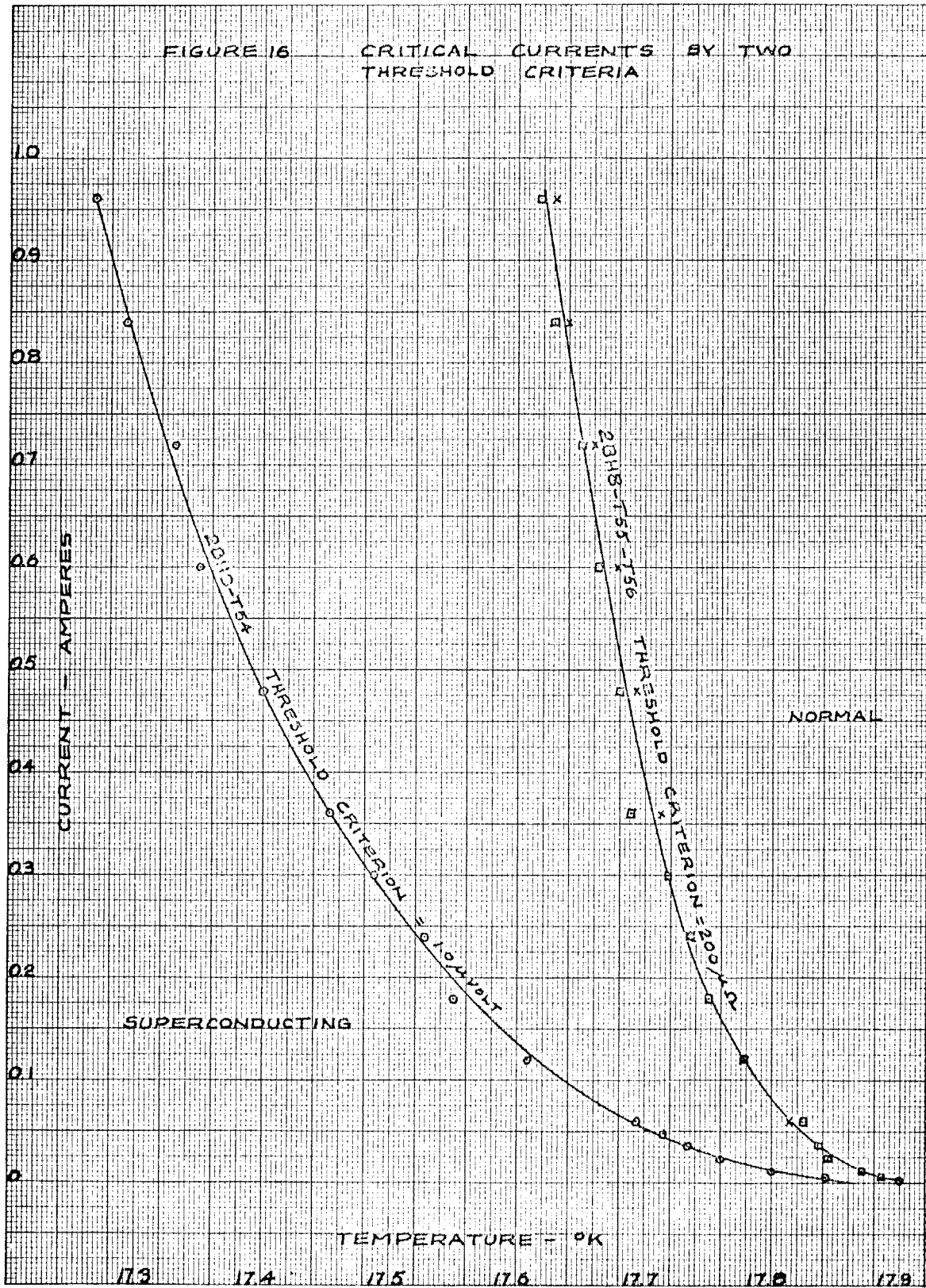


FIGURE 16 CRITICAL CURRENTS BY TWO THRESHOLD CRITERIA



one microvolt depends on the current and does not necessarily represent a state of the superconductor. The 200 micro-ohm criterion was chosen because it represented the smallest resistance detectable at the lowest current. Using a resistance threshold criterion has the virtue of representing to an extent the state of the superconductor. The two sets of points defining the 200 micro-ohm curve indicate the worst case as far as repeatability of these data is concerned.

Using the 200 micro-ohm threshold criterion data were taken on three samples and compared to magnetic field data. These data are shown in Figures 17 and 18 and indicate a correspondence similar to the one expected from the discussion in Chapter III. Using the magnetic field data to determine the constants α and B_0 in equation III-36 the results were compared to the critical currents at 17.9°K and the critical temperature for a test current of 100 milliamperes. The comparison is shown in Table I.

Table I
Preliminary Test Comparison

Sample	2BH8-T5	3AC7C-T1	3AC7B-T1
B_0 - Oer x 10^{-3}	2.34	2.09	1.895
α - Oer-Amp x 10^{-6}	15.0	13.5	11.2
I_c (17.9°K) -ma.	30	800	920
T_c (I=100ma) -°K	17.788	17.894	17.898

FIGURE 17 COMPARATIVE CRITICAL CURRENT DATA FOR THREE SAMPLES
THRESHOLD CRITERION = 200 μ A

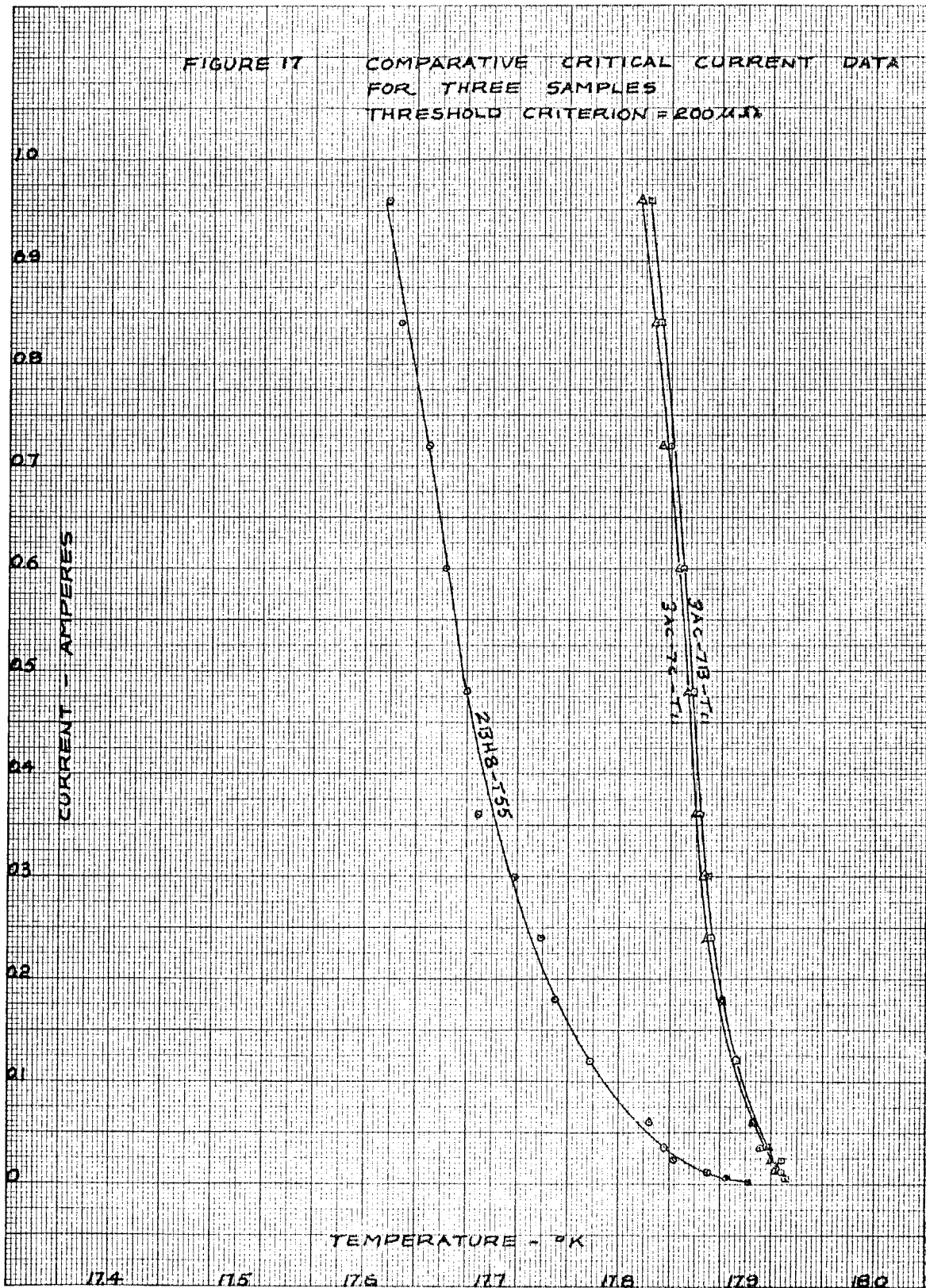
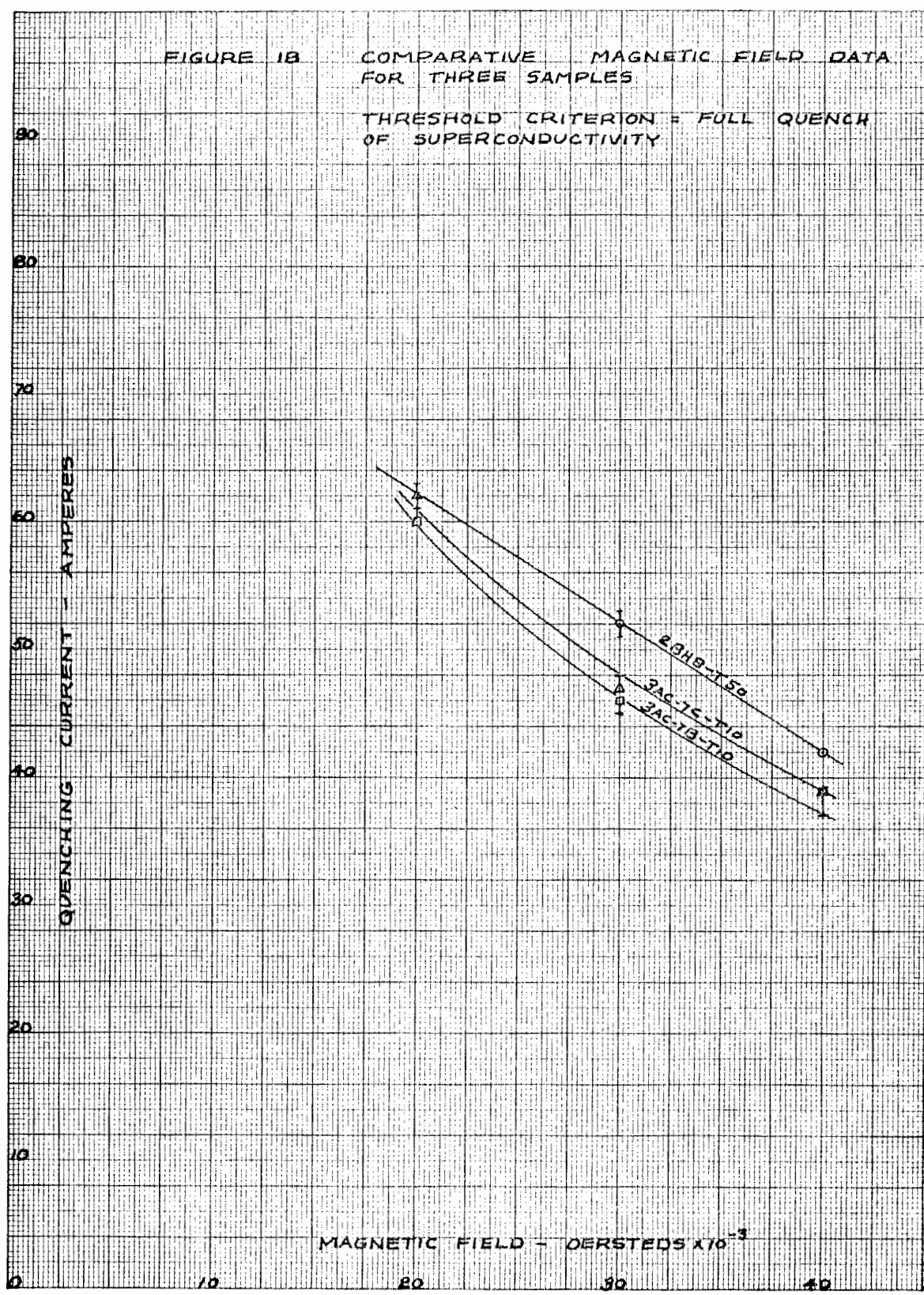


FIGURE 1B COMPARATIVE MAGNETIC FIELD DATA FOR THREE SAMPLES

THRESHOLD CRITERION = FULL QUENCH OF SUPERCONDUCTIVITY



For a truly favorable correspondence, one would have preferred the α and B_0 values for the 3AC7C-T1 and 3AC7B-T1 samples to be almost identical. However, there was enough scatter in the magnetic field data to accomplish this effect. Also the data were not reduced in terms of current densities, although the samples were of approximately the same dimensions. Nevertheless, the results of this set of tests were sufficiently good to encourage pursuing the problem further.

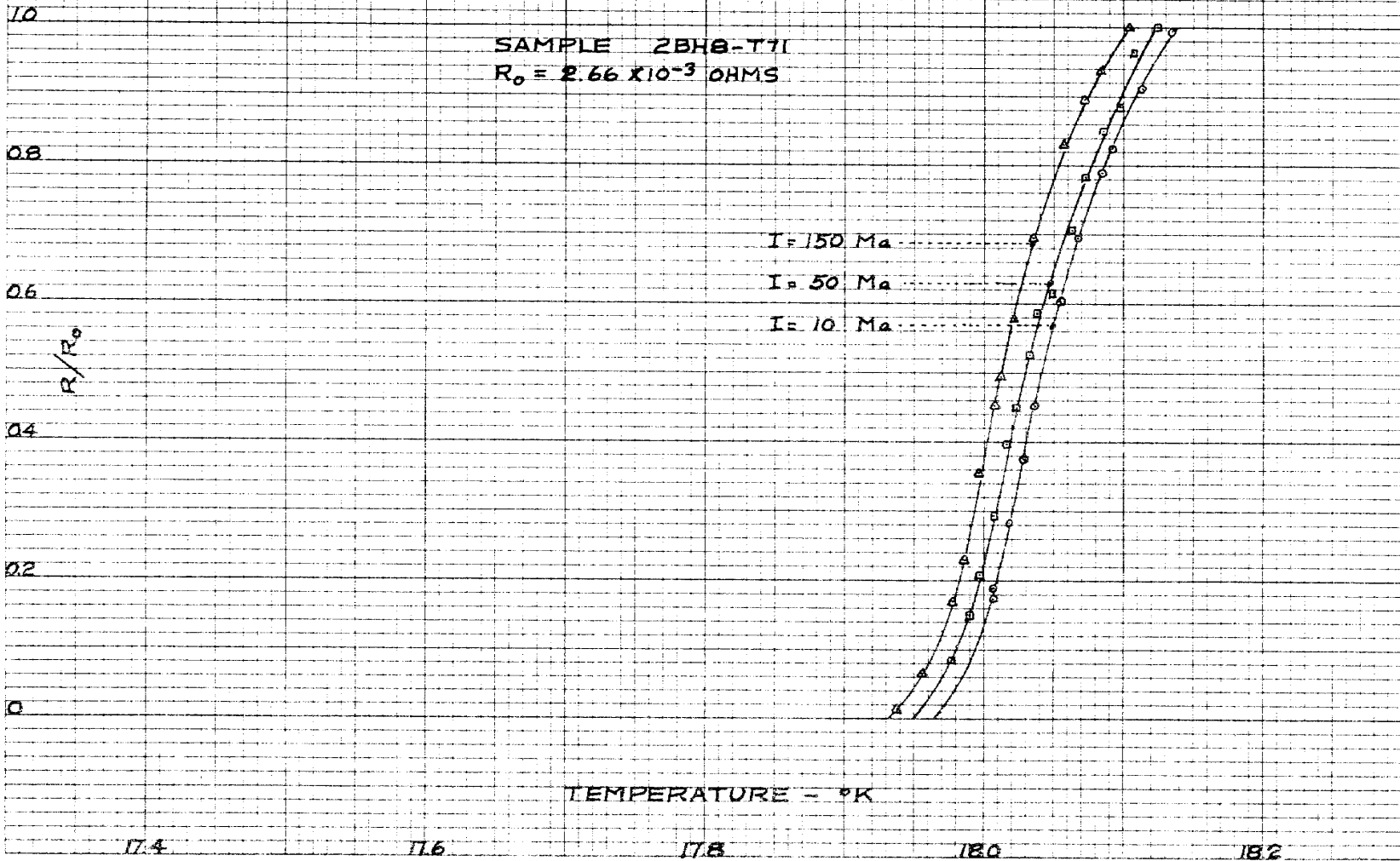
Referring back to Figure 17, it can be seen that critical current curves could take forms such that it would be impossible to correlate critical currents in terms of a single temperature. One would then have to correlate critical temperatures in terms of a single current. Since these critical temperatures would correspond to an arbitrarily chosen resistance, it was decided to take the temperature data in the form of resistance transition curves taken at a given current density. The current dependence of the resistance curves is shown in Figure 19.

Temperature Transitions

The test current density for the temperature transitions was chosen partly for experimental expediency. The current was sufficiently low so that Joule heating would not accelerate the transition excessively and make it impossible to maintain the current constant throughout the transition.

FIGURE 19 THE EFFECT OF TEST CURRENT ON TEMPERATURE TRANSITIONS

SAMPLE 2BH8-T71
 $R_0 = 2.66 \times 10^{-3}$ OHMS



Given the range of dimensions of the samples the current density of 80 amperes/cm² allowed all current readings to be taken on the same 0-150 milliampere meter.

Further, the correlation sought could hopefully be applied to a long length of ribbon coiled on a spool and immersed in a temperature controlled bath. A simple calculation on a coil of 5000 feet of 0.0015 inch thick ribbon wound on a spool of one inch inner diameter gives the stress in the inner turn as

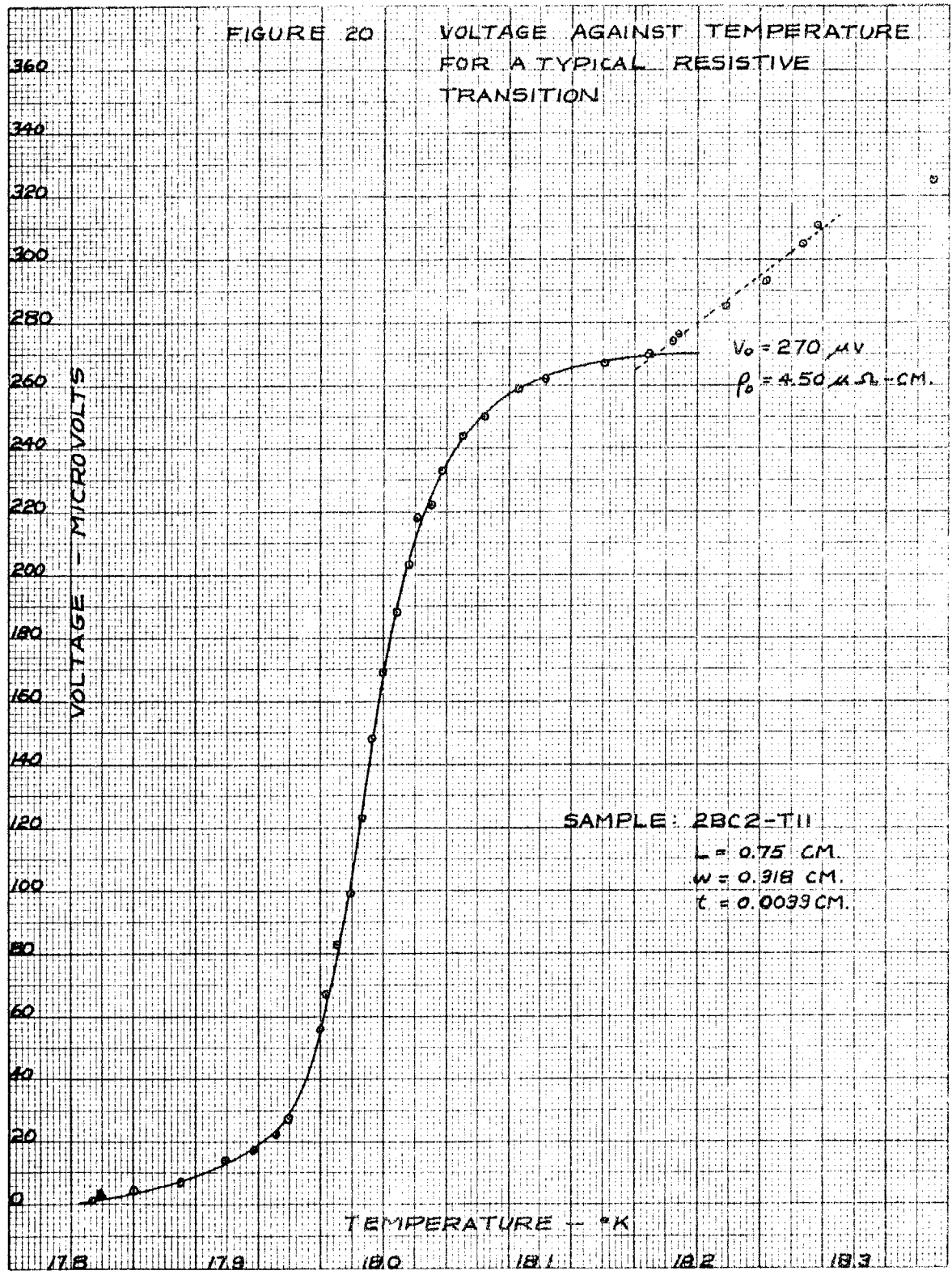
$$\text{Stress} \approx 20 I^2 \text{ psi} \quad \text{V-1}$$

if the inner turn is unsupported radially. Muller and Sour⁽²¹⁾ found that resistive transitions could be depressed about 0.1°K by tensile stresses of the order of 30,000 psi. Reference to equation V-1 indicates that for currents less than one ampere there is a safety factor of more than 10³ in this regard.

A plot of voltage against temperature for a typical resistive transition is shown in Figure 20. The linear rise in voltage at the upper end of the transition was apparently due to the fact that the voltage contact covers a finite length of the ribbon. While superconductivity persisted the voltage contact was on an equipotential surface and the contact picked up only the voltage between its inner boundaries. As the final loss of superconductivity occurred the contact then picked up the residual resistance along its length. The residual resistance was evaluated at the intersection

FIGURE 20

VOLTAGE AGAINST TEMPERATURE
FOR A TYPICAL RESISTIVE
TRANSITION



of the S-curve and the linear offshoot. The data were normalized in terms of this residual resistance and the resulting temperature transitions are given in Figures 21-40.

Magnetic Field Transitions

In Figure 41 is shown the form in which magnetic field transitions were measured. Full quench of the superconducting phase is indicated by the points with lateral arrows. One is again faced with choosing a threshold criterion to determine a critical current. As will be seen from the data presented later, the choice of threshold criterion can govern the rank of performance of the various samples. Because of this effect, the author chose three criteria for consideration.

The first criterion was that of 1.0 microvolt voltage rise across the sample. This voltage was the lowest that could be reliably measured. As a threshold criterion it has the fault that the single microvolt represents various rates of power dissipation from the sample depending on the current at which it is sensed. The various rates of power dissipation in turn imply various temperatures of the samples with respect to the environment temperature.

The second criterion was one of equal power dissipation per unit width of ribbon. Assuming that the power was dissipated from equal lengths of ribbon and that the

FIGURE 21. TEMPERATURE TRANSITION

$J = 80 \text{ AMP/CM}^2$
 $L \approx 0.05 \text{ CM.}$

○ - 2AA9B-T11
 $R_0 = 8.00 \text{ m.}\Omega$
 $w = 0.159 \text{ CM.}$
 $t = 0.0036 \text{ CM.}$

+ - 2AA9B-T21
 $R_0 = 7.85 \text{ m.}\Omega$
 $w = 0.159 \text{ CM.}$
 $t = 0.0038 \text{ CM.}$

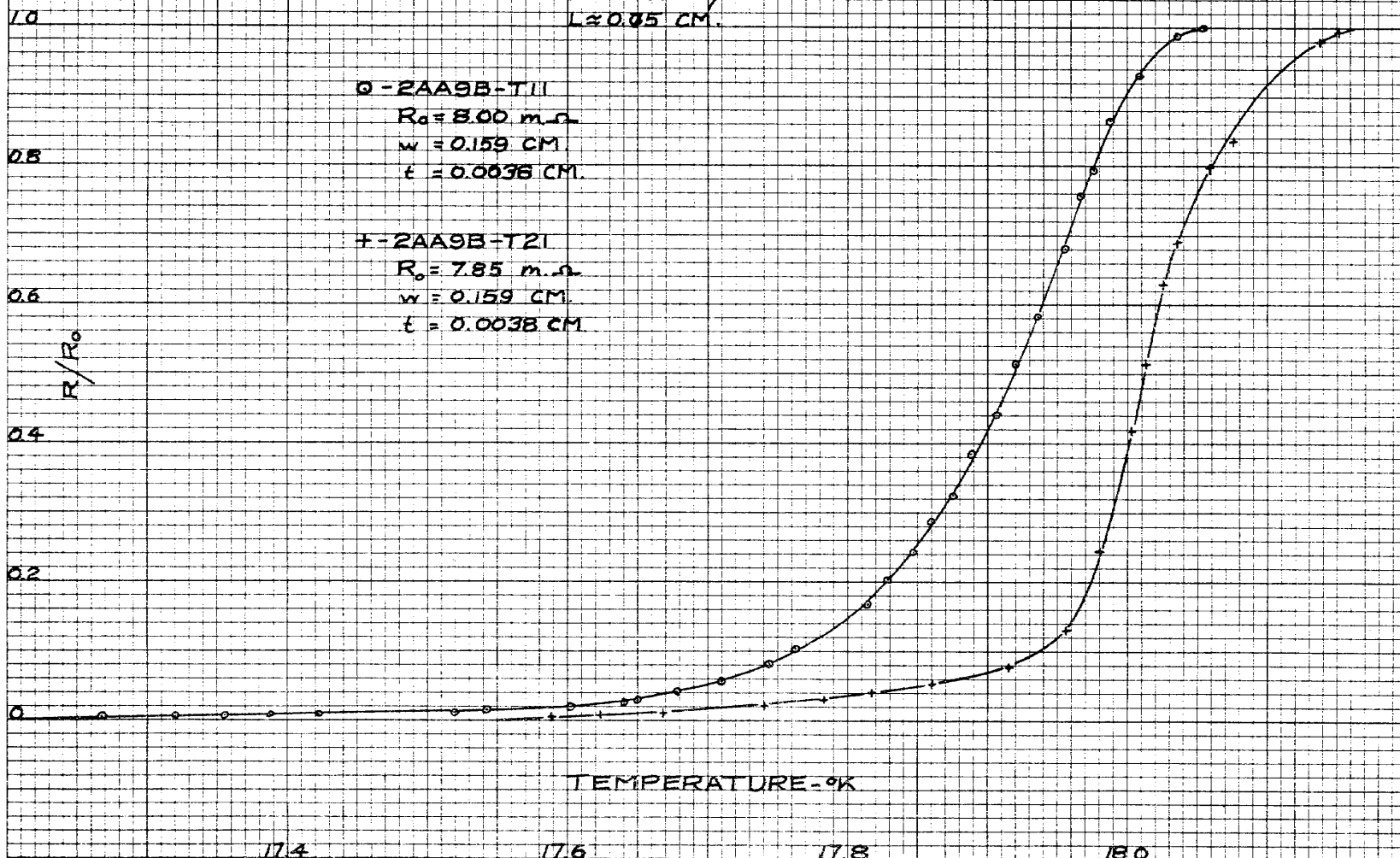


FIGURE 22. TEMPERATURE TRANSITION

$J = 80 \text{ AMP/CM}^2$
 $L \approx 0.75 \text{ CM}$

$\phi - 2\text{BAI-B-TII}$
 $R_0 = 10.04 \text{ m}\Omega$
 $w = 0.159 \text{ CM}$
 $t = 0.0051 \text{ CM}$

1.0

0.8

0.6

0.4

0.2

0

R/R_0

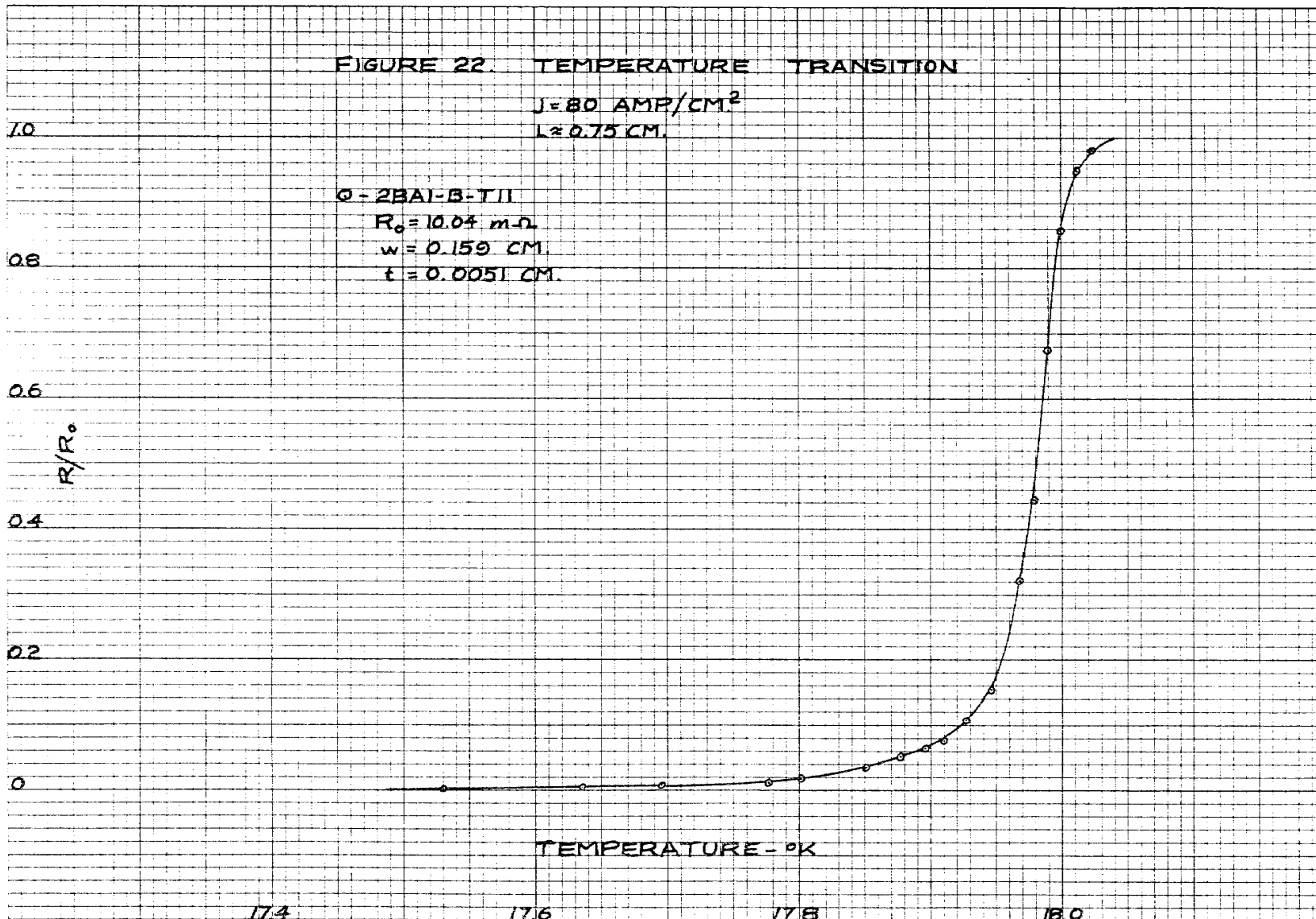
TEMPERATURE - °K

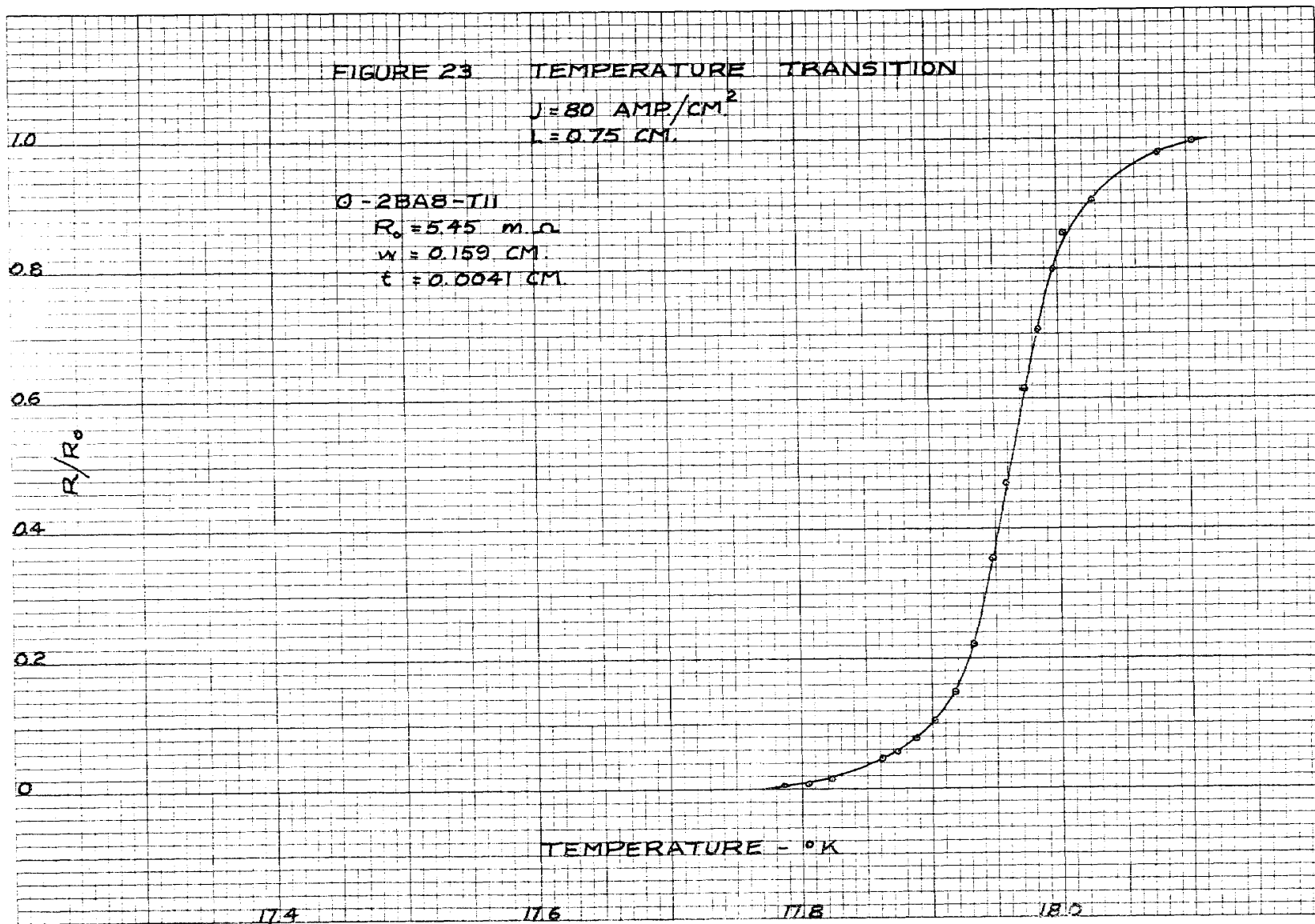
17.4

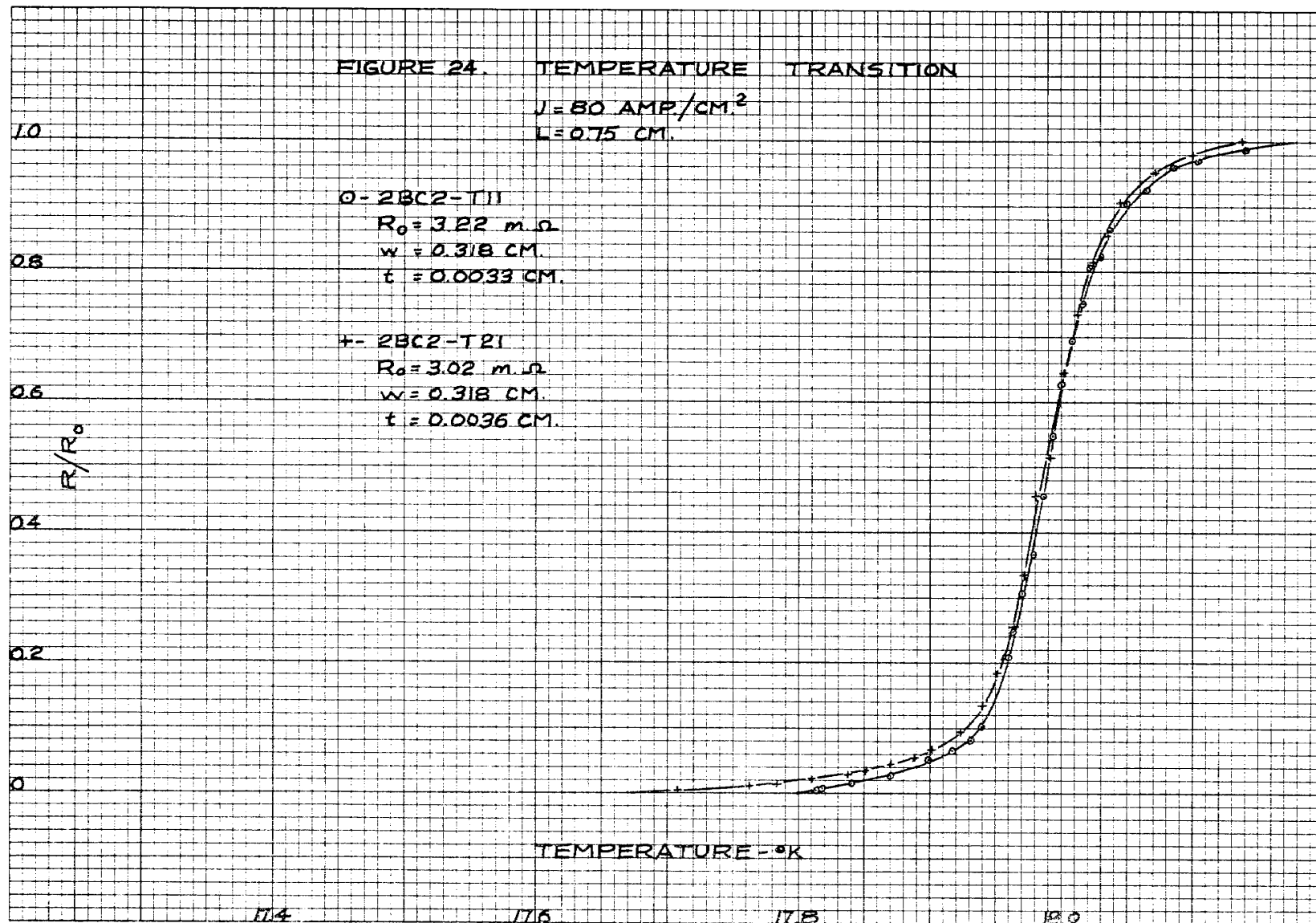
17.6

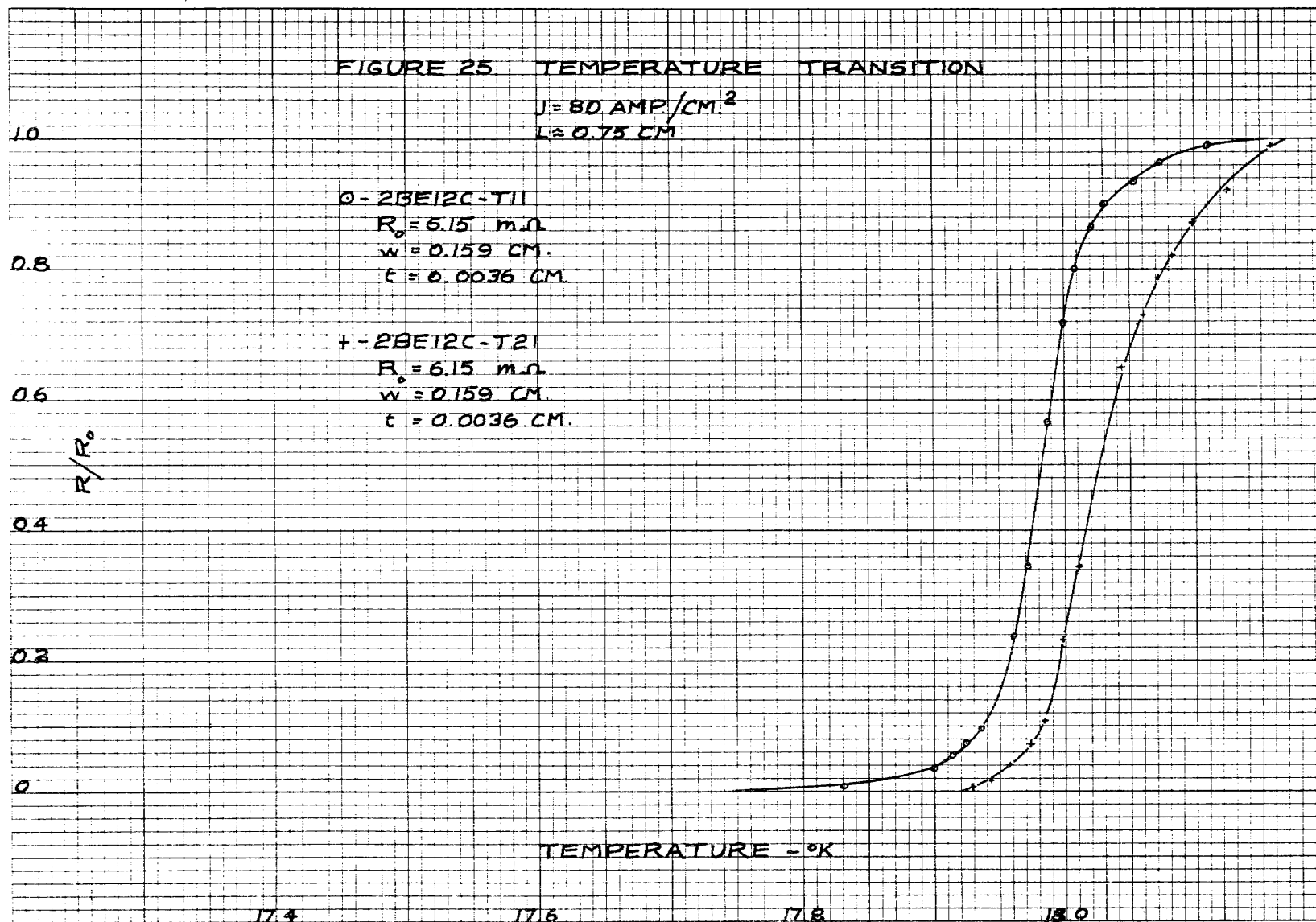
17.8

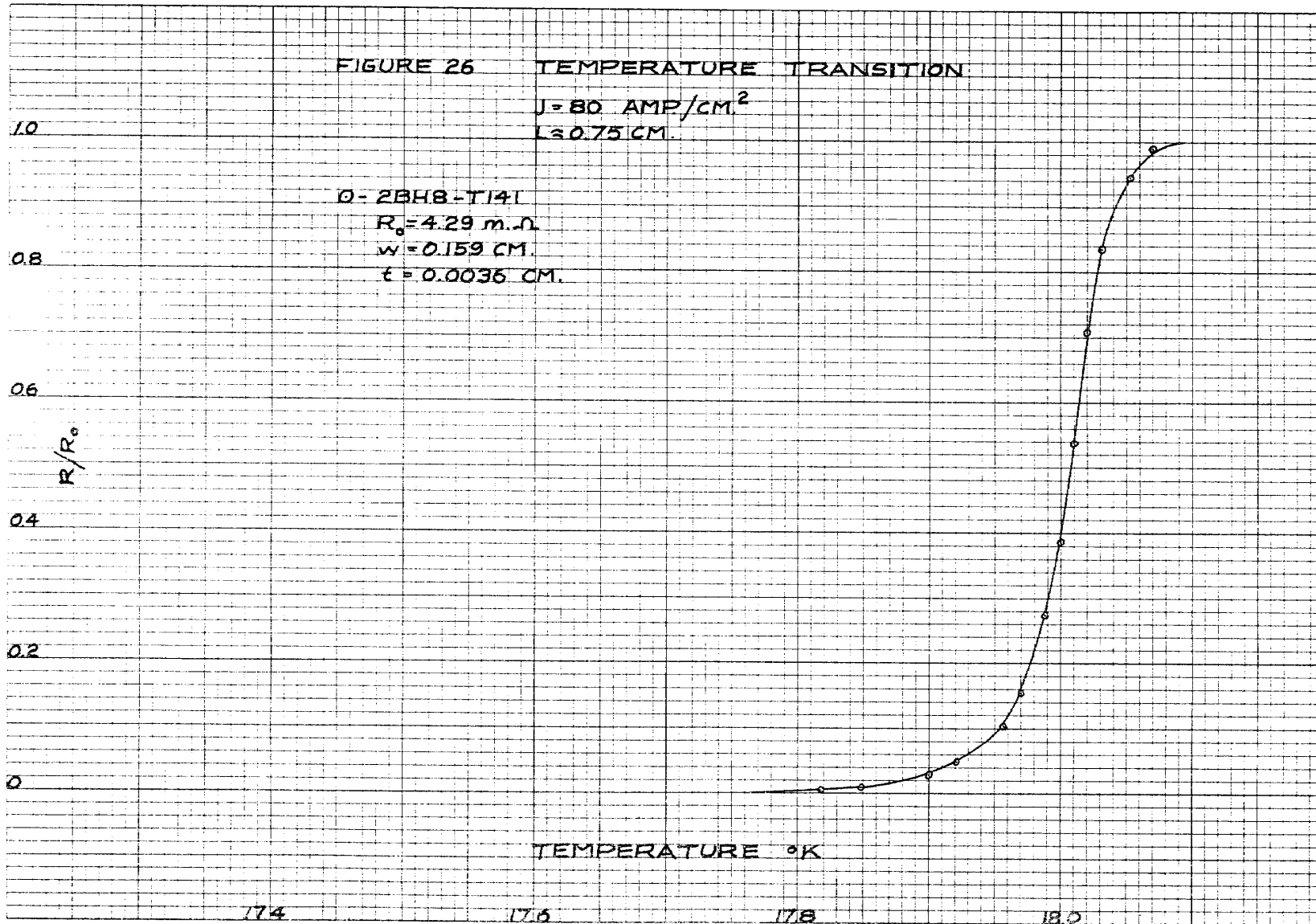
18.0









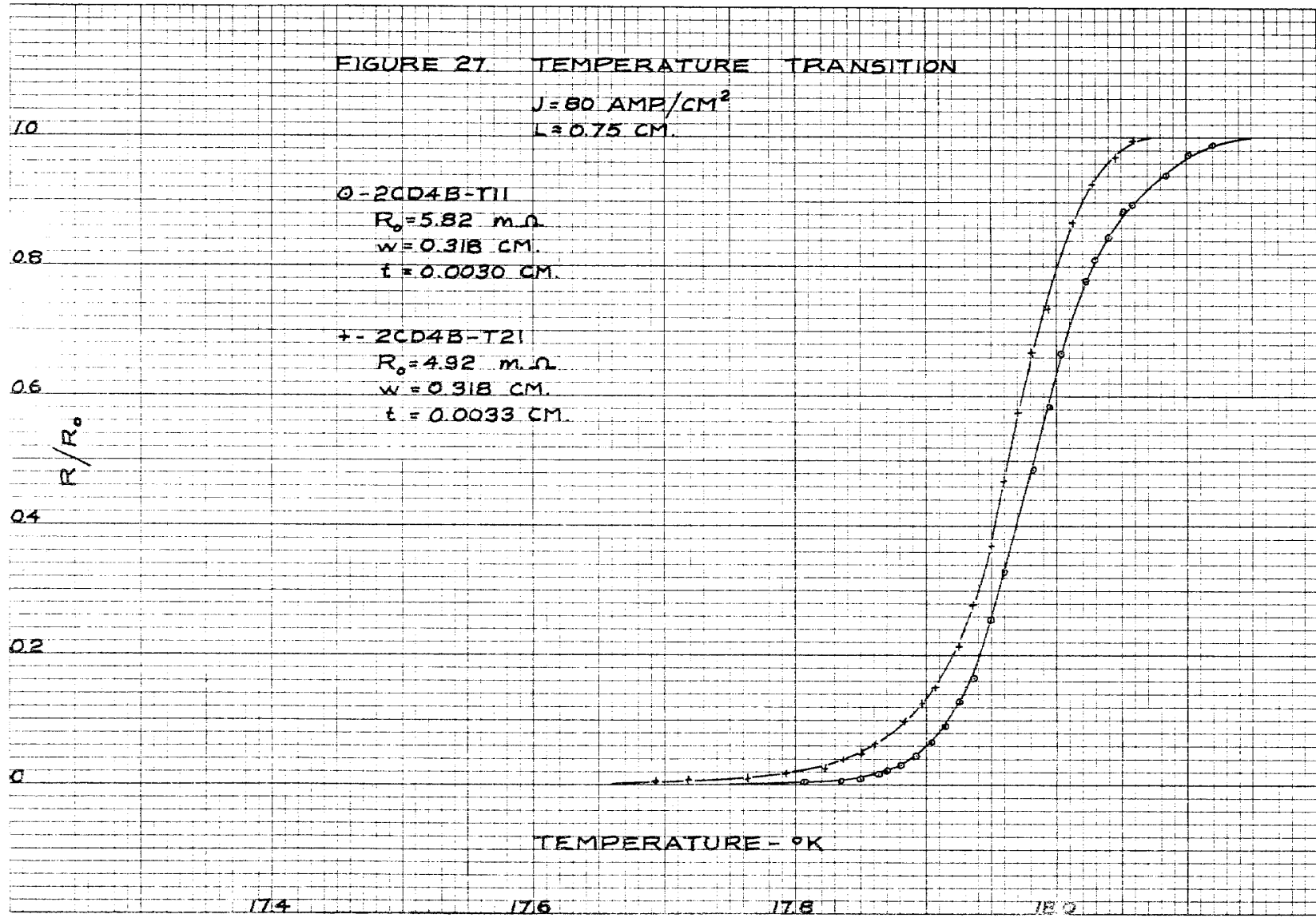


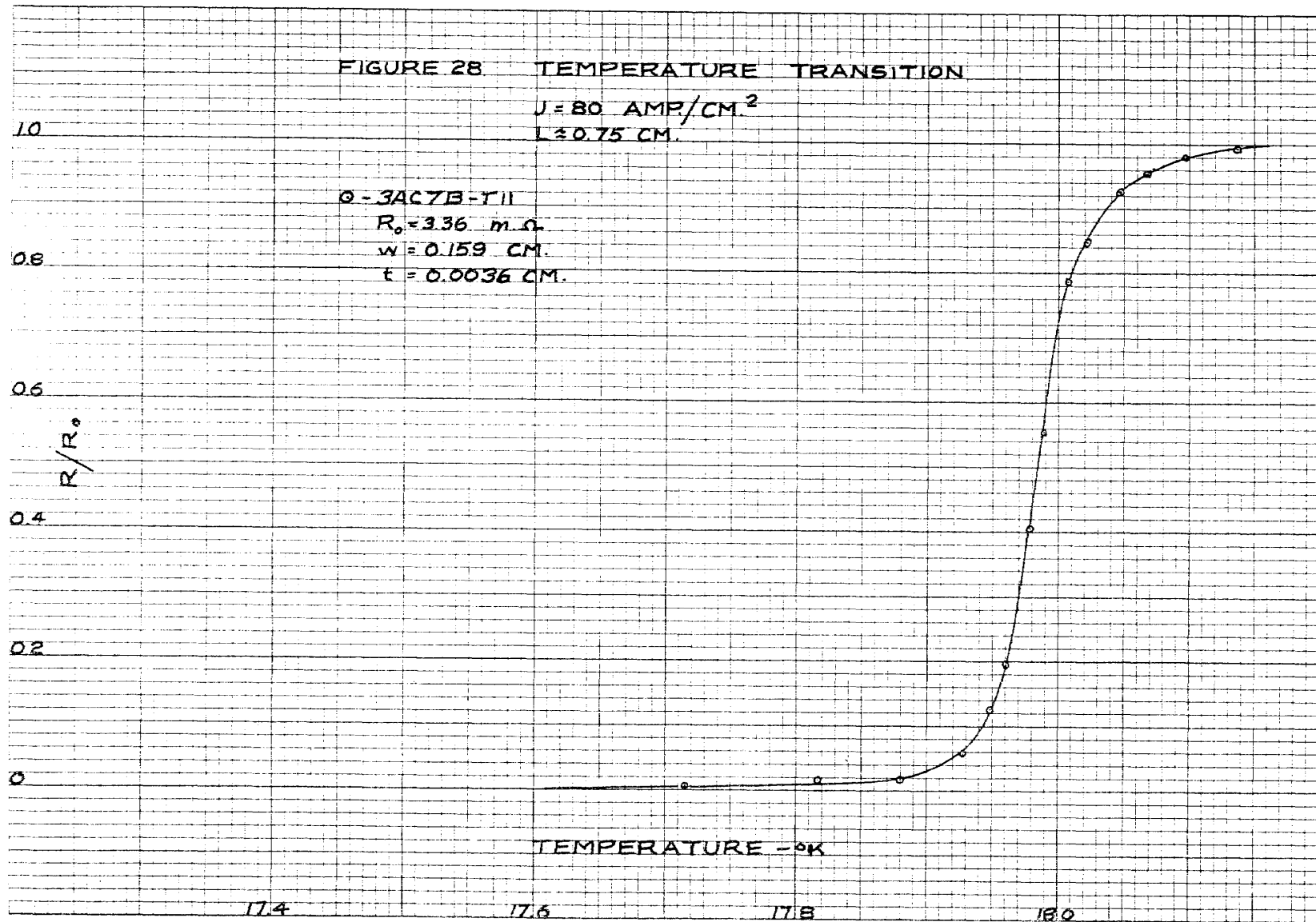
174

176

178

180





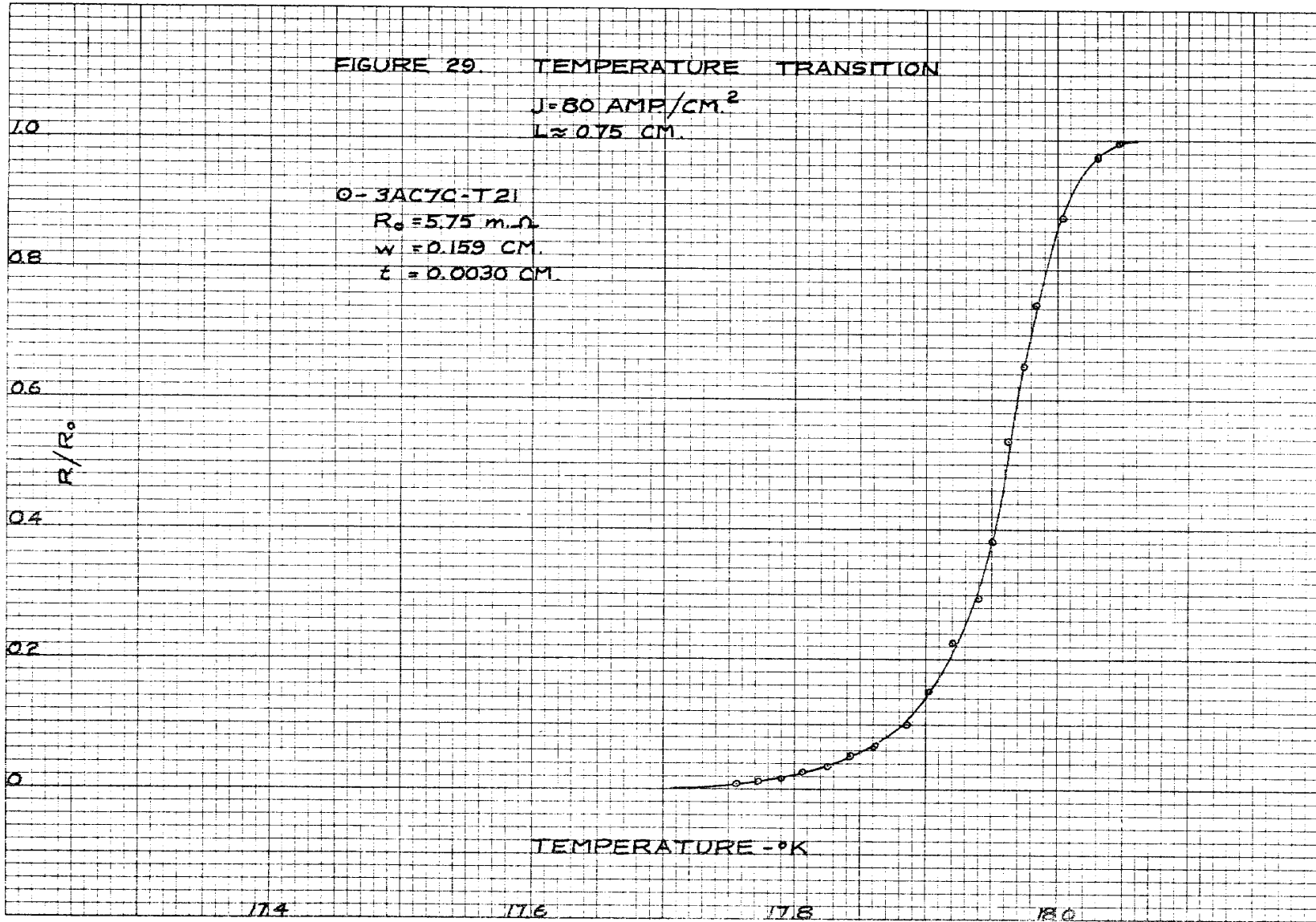
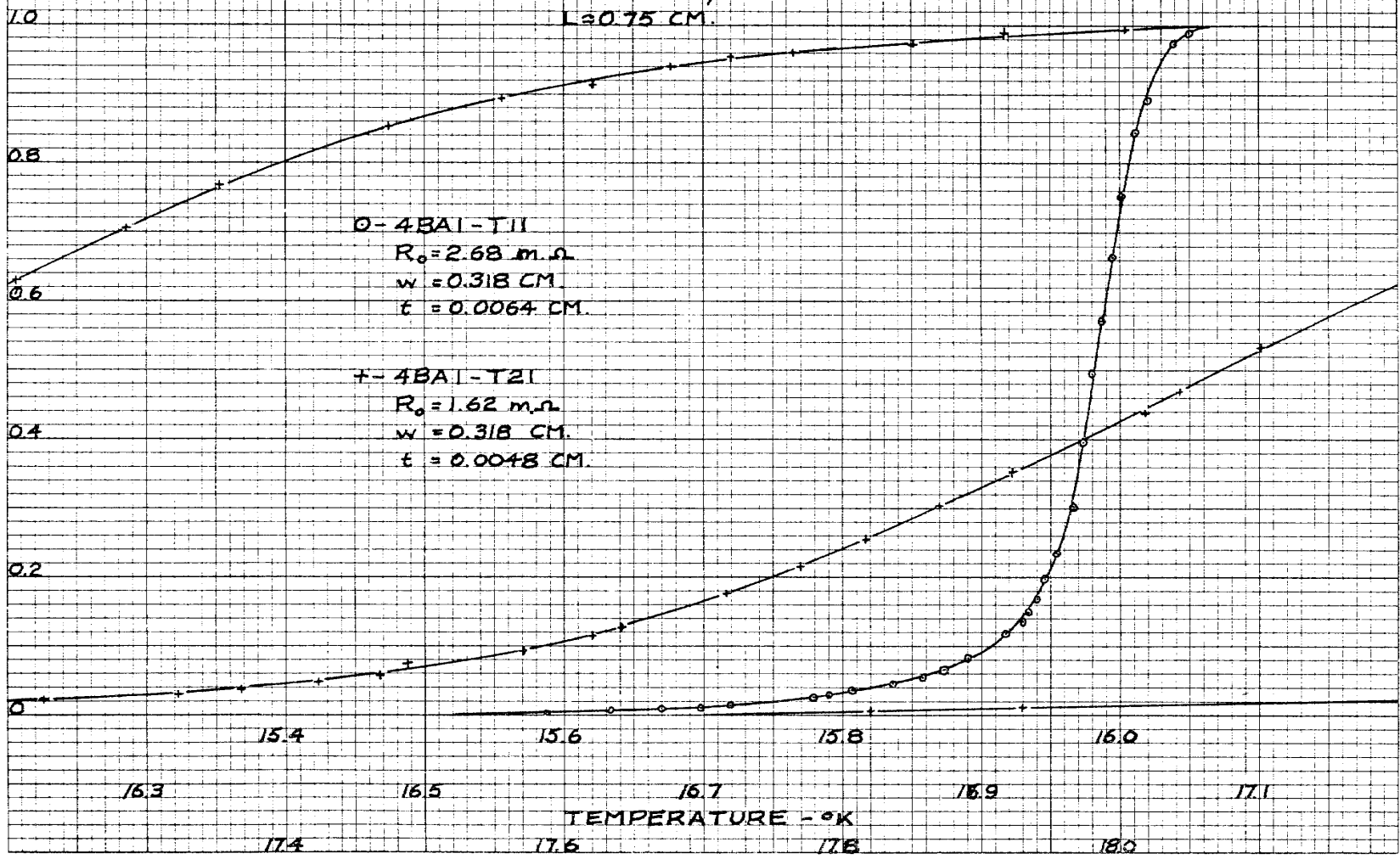


FIGURE 30 TEMPERATURE TRANSITION

$J = 80 \text{ AMP/CM}^2$
 $L = 0.75 \text{ CM.}$



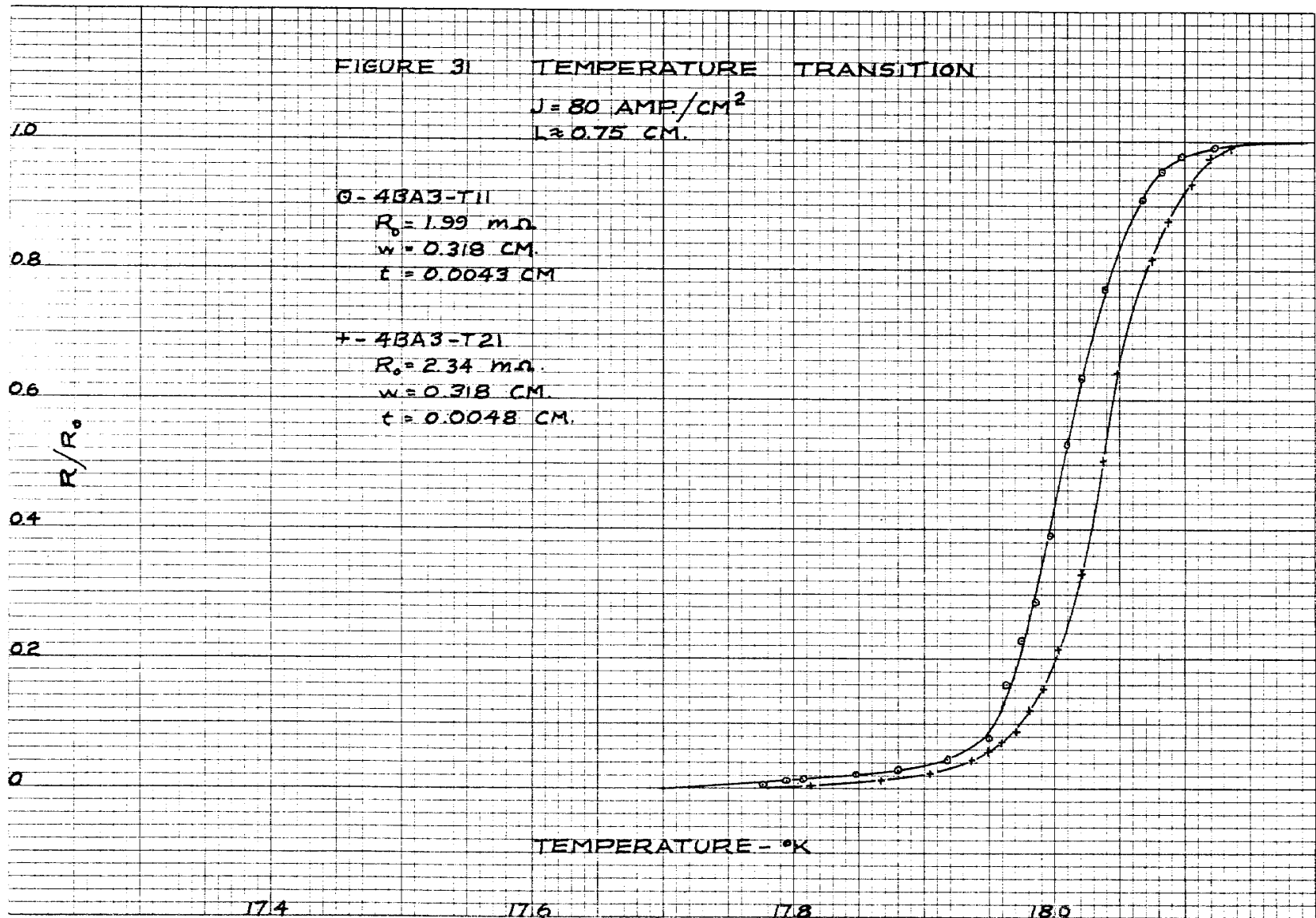


FIGURE 32 TEMPERATURE TRANSITION

$J = 80 \text{ AMP/CM}^2$
 $L = 0.75 \text{ CM.}$

Ø - 4BA7-TII
 $R_0 = 3.74 \text{ m}\Omega$
 $w = 0.159 \text{ CM.}$
 $t = 0.0038 \text{ CM.}$

1.0

0.8

0.6

0.4

0.2

0

R/R_0

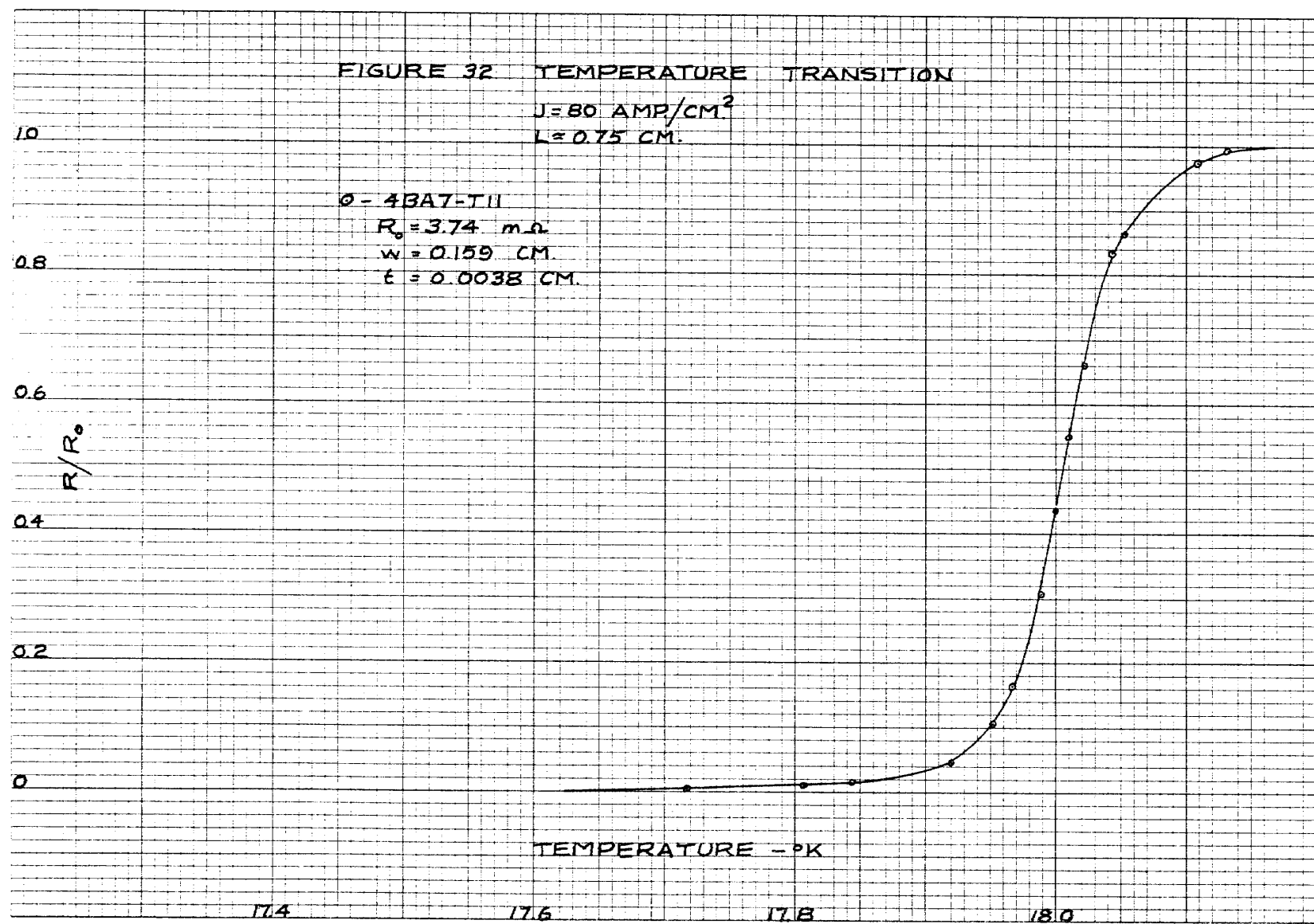
TEMPERATURE - °K

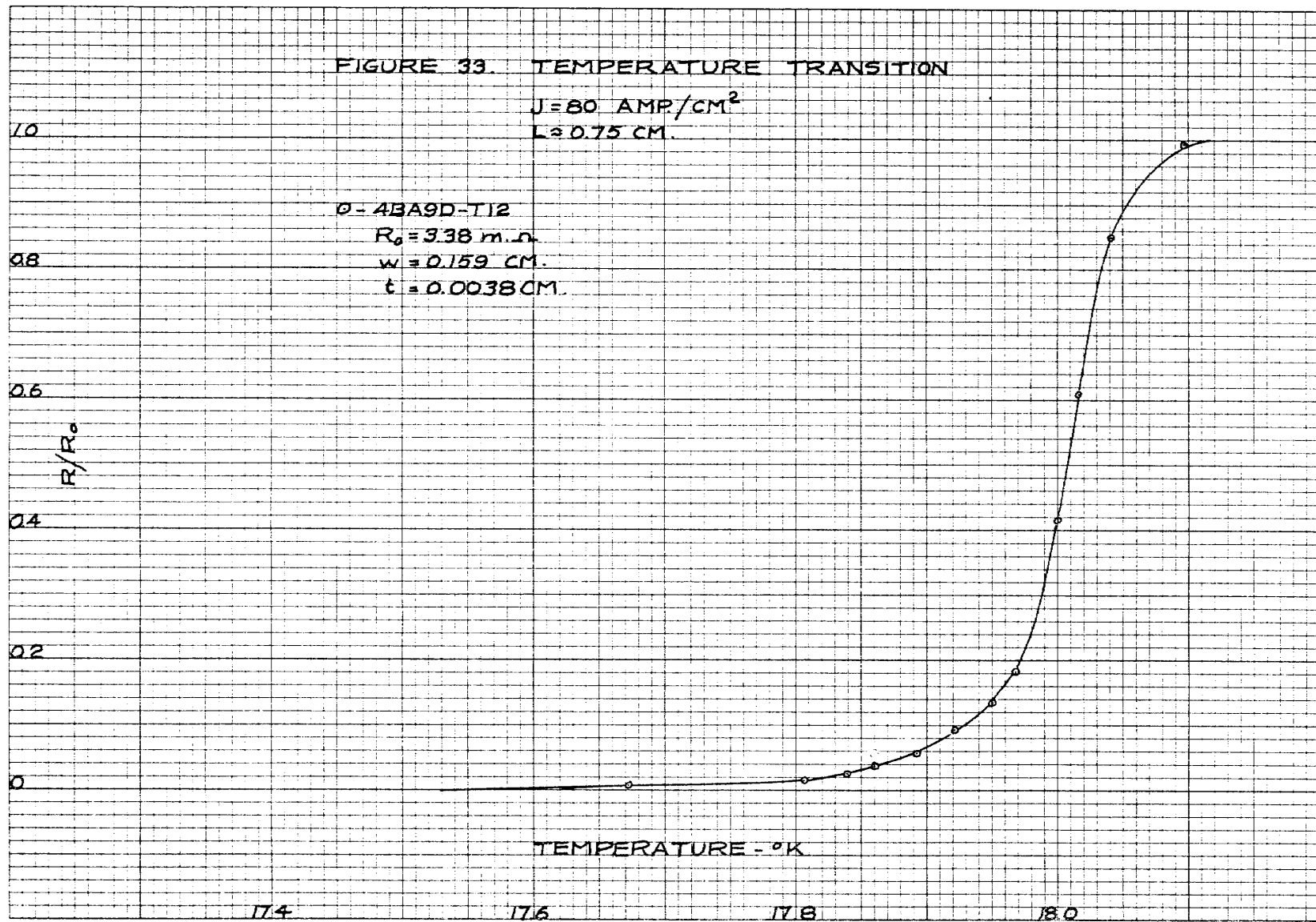
17.4

17.6

17.8

18.0





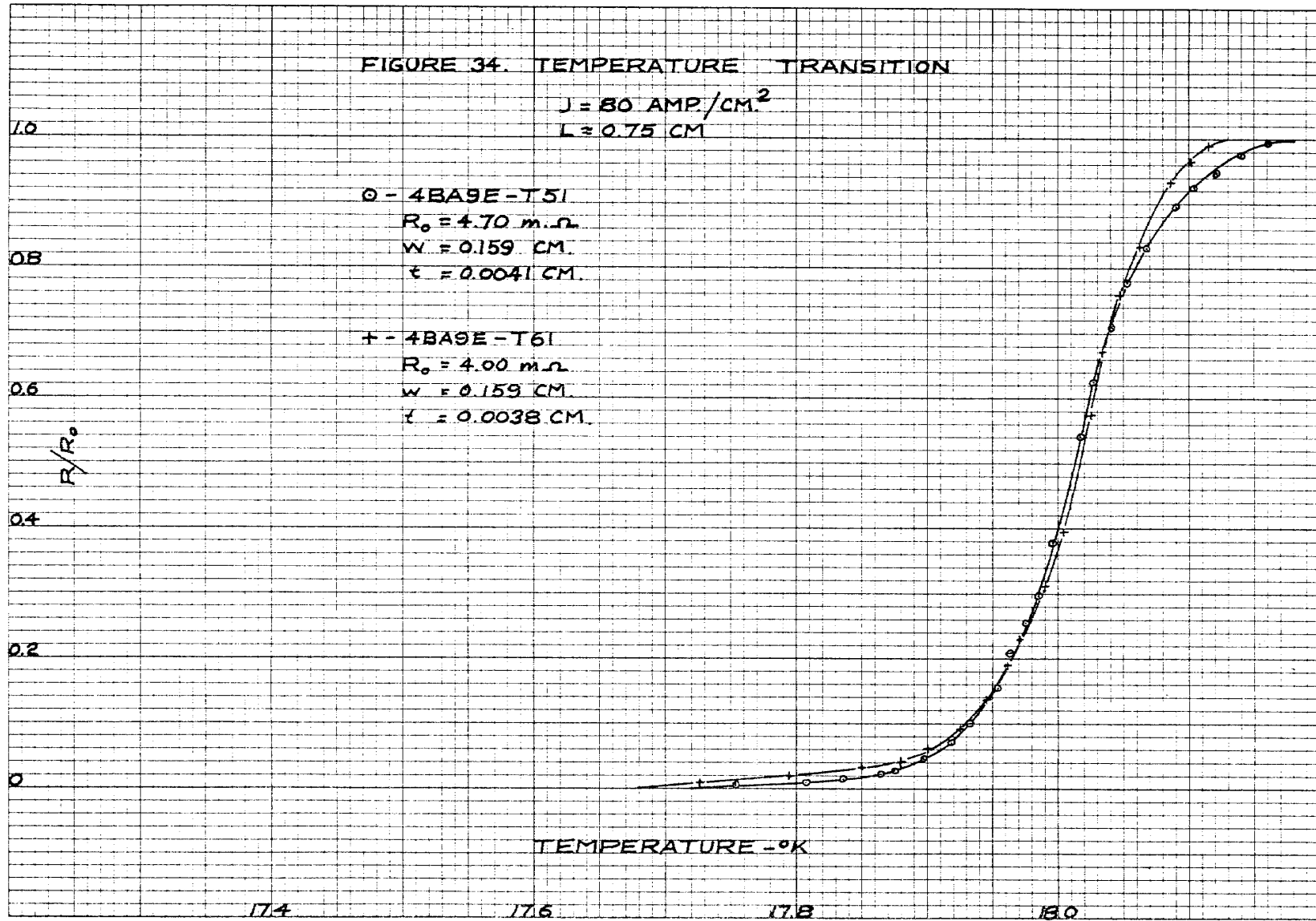


FIGURE 35. TEMPERATURE TRANSITION

$J = 80 \text{ AMP/CM}^2$
 $L \approx 0.75 \text{ CM.}$

○ - 4BA11-T11

$R_0 = 1.86 \text{ m}\Omega$

$w = 0.318 \text{ CM.}$

$t = 0.0041 \text{ CM.}$

+ - 4BA11-T21

$R_0 = 2.12 \text{ m}\Omega$

$w = 0.318 \text{ CM.}$

$t = 0.0036 \text{ CM.}$

R/R_0

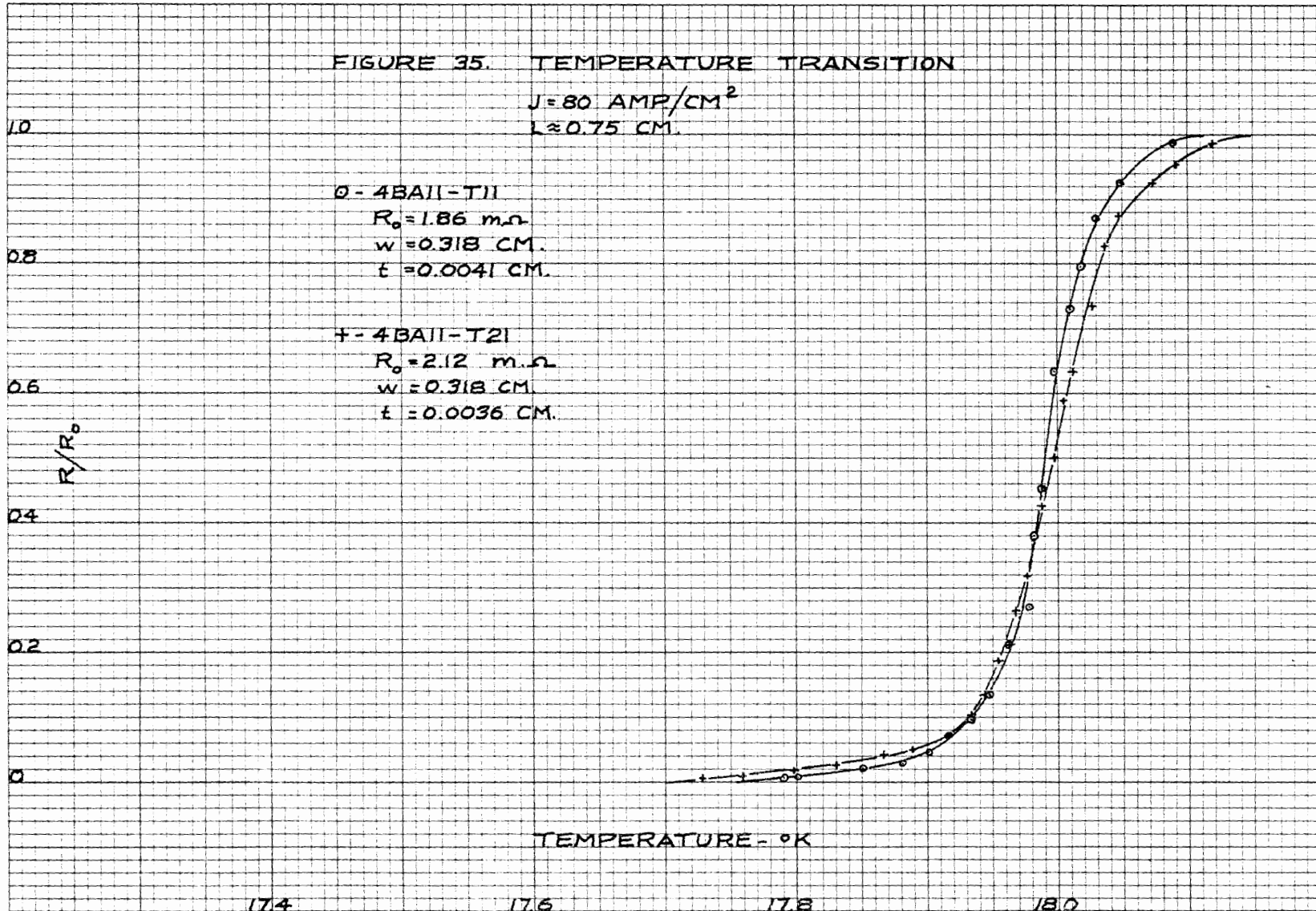
TEMPERATURE - °K

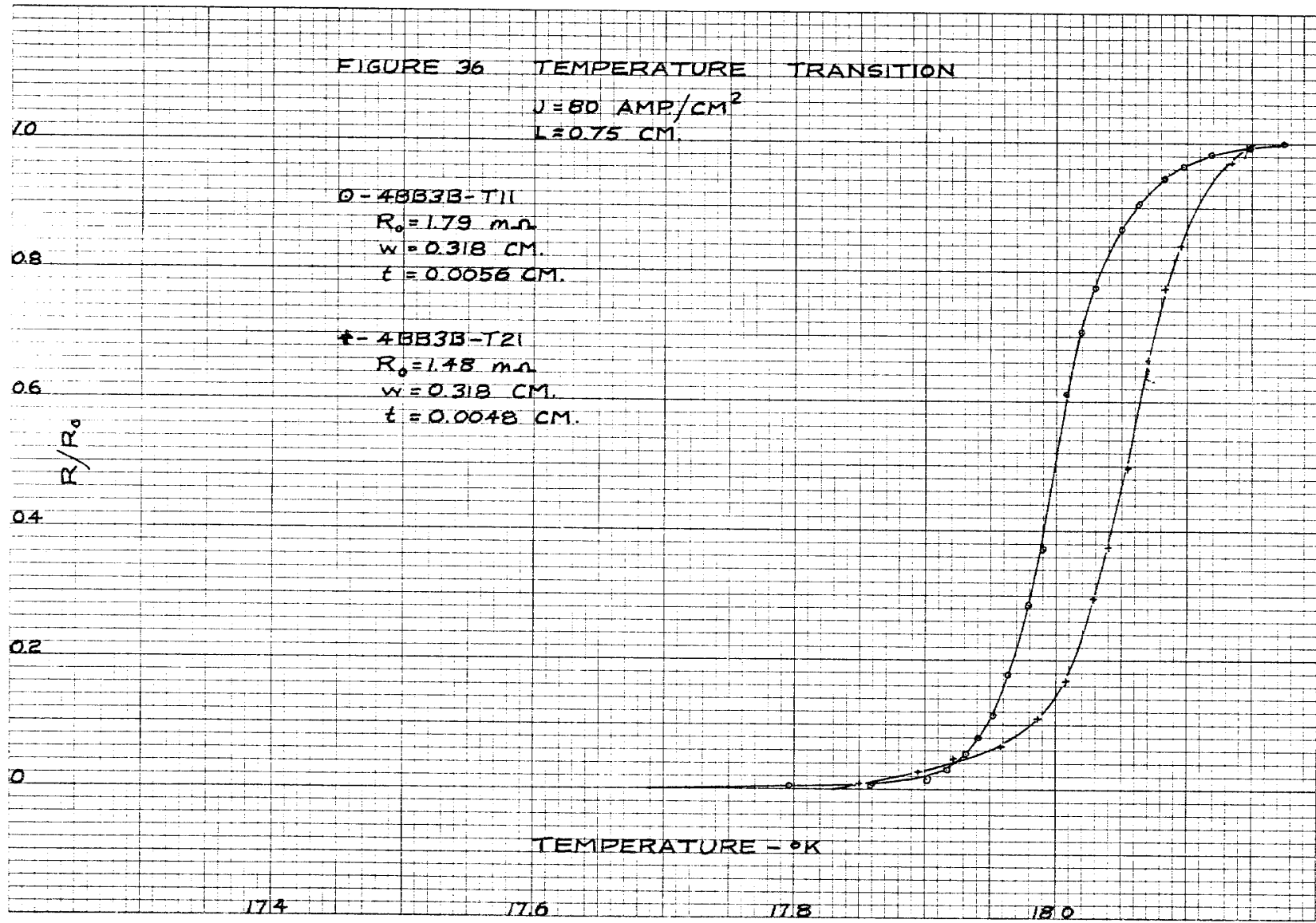
174

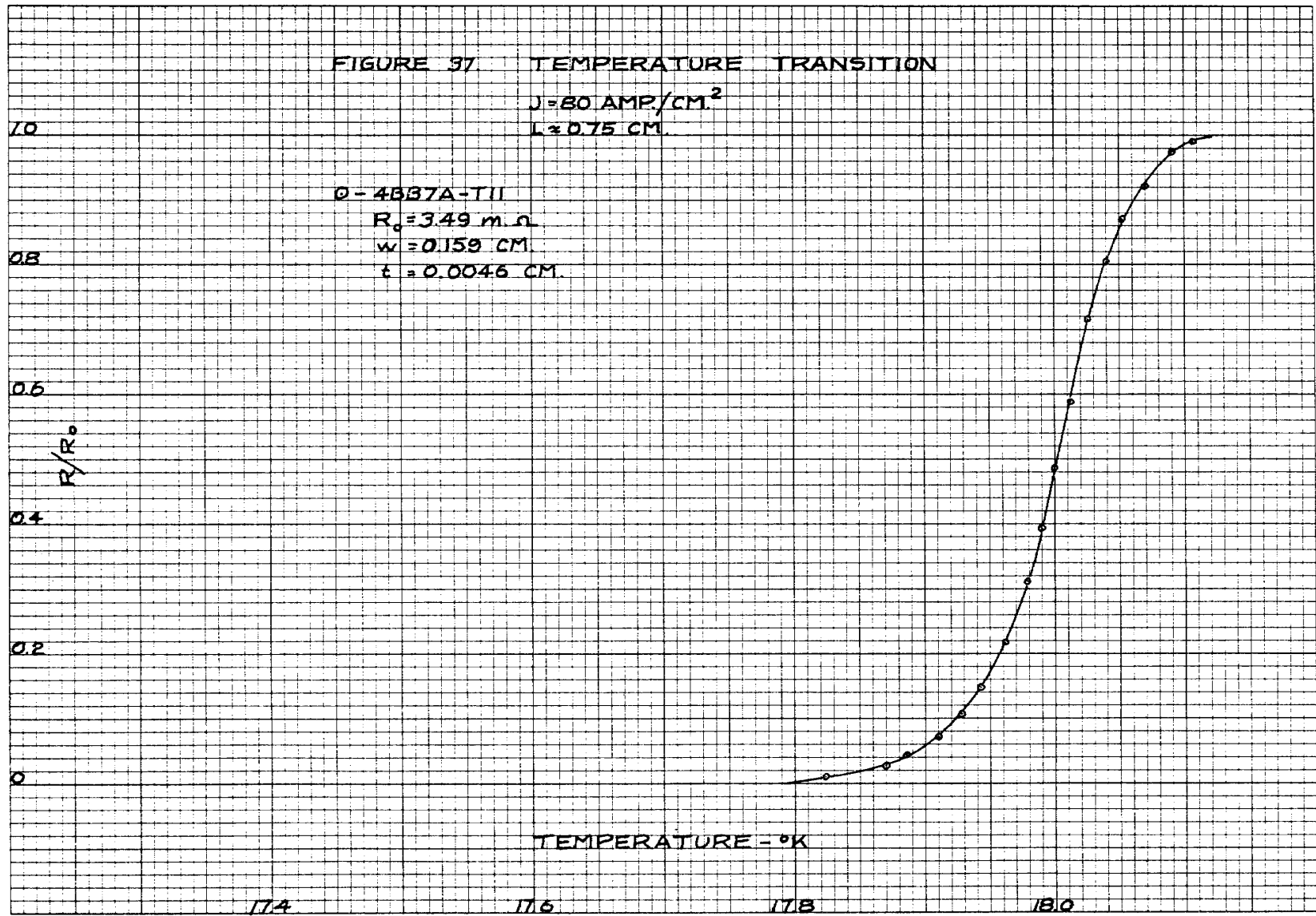
176

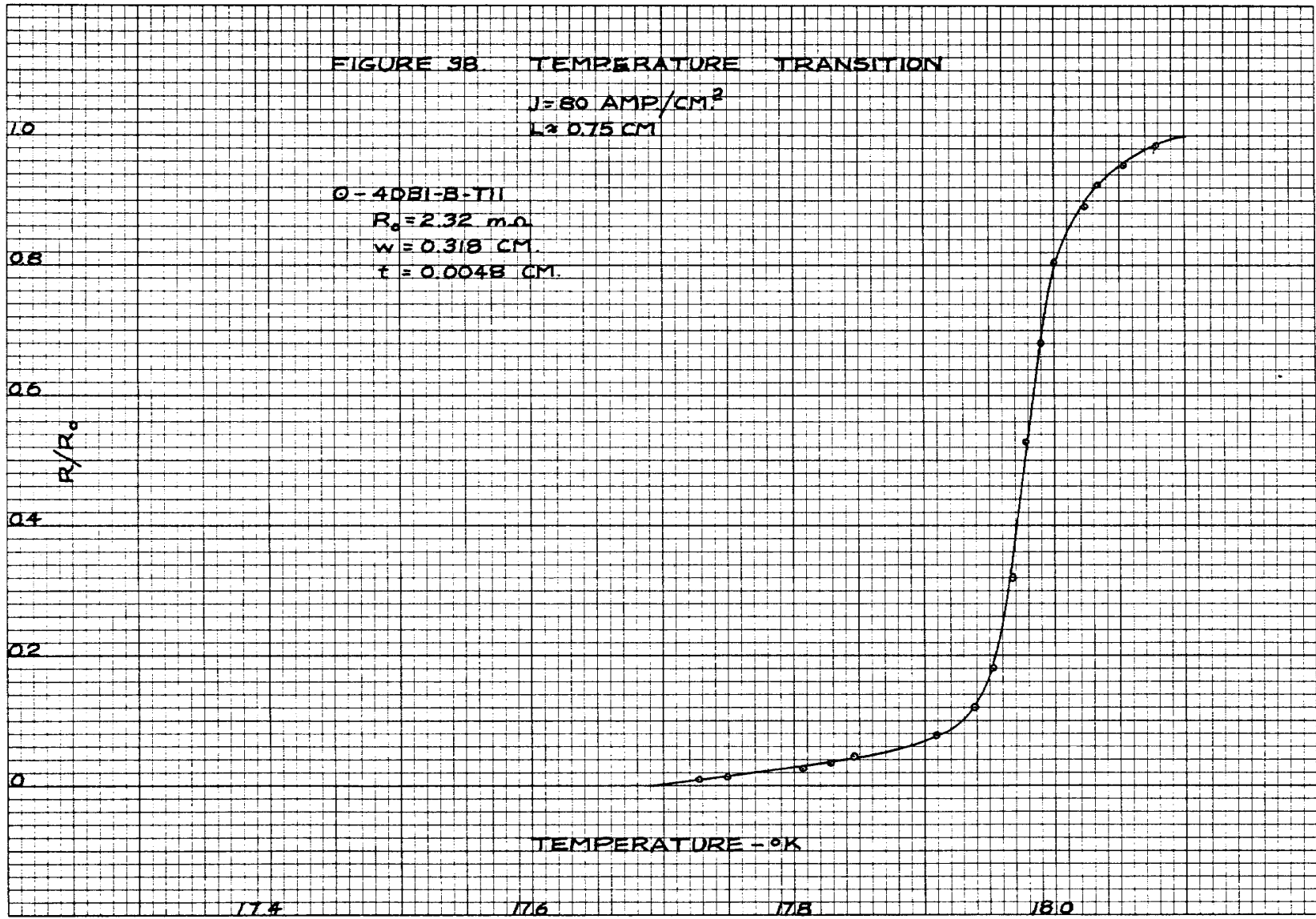
178

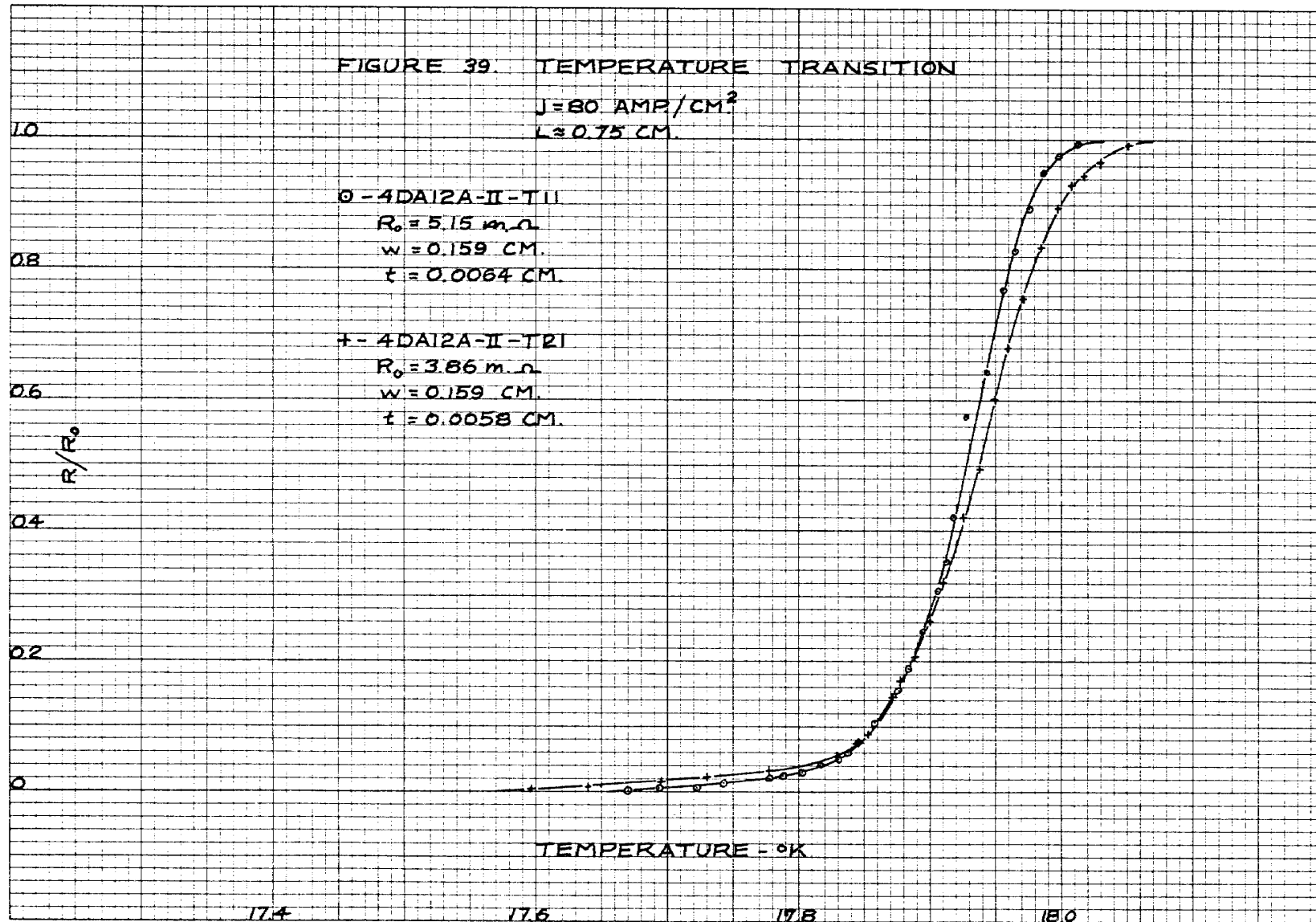
180

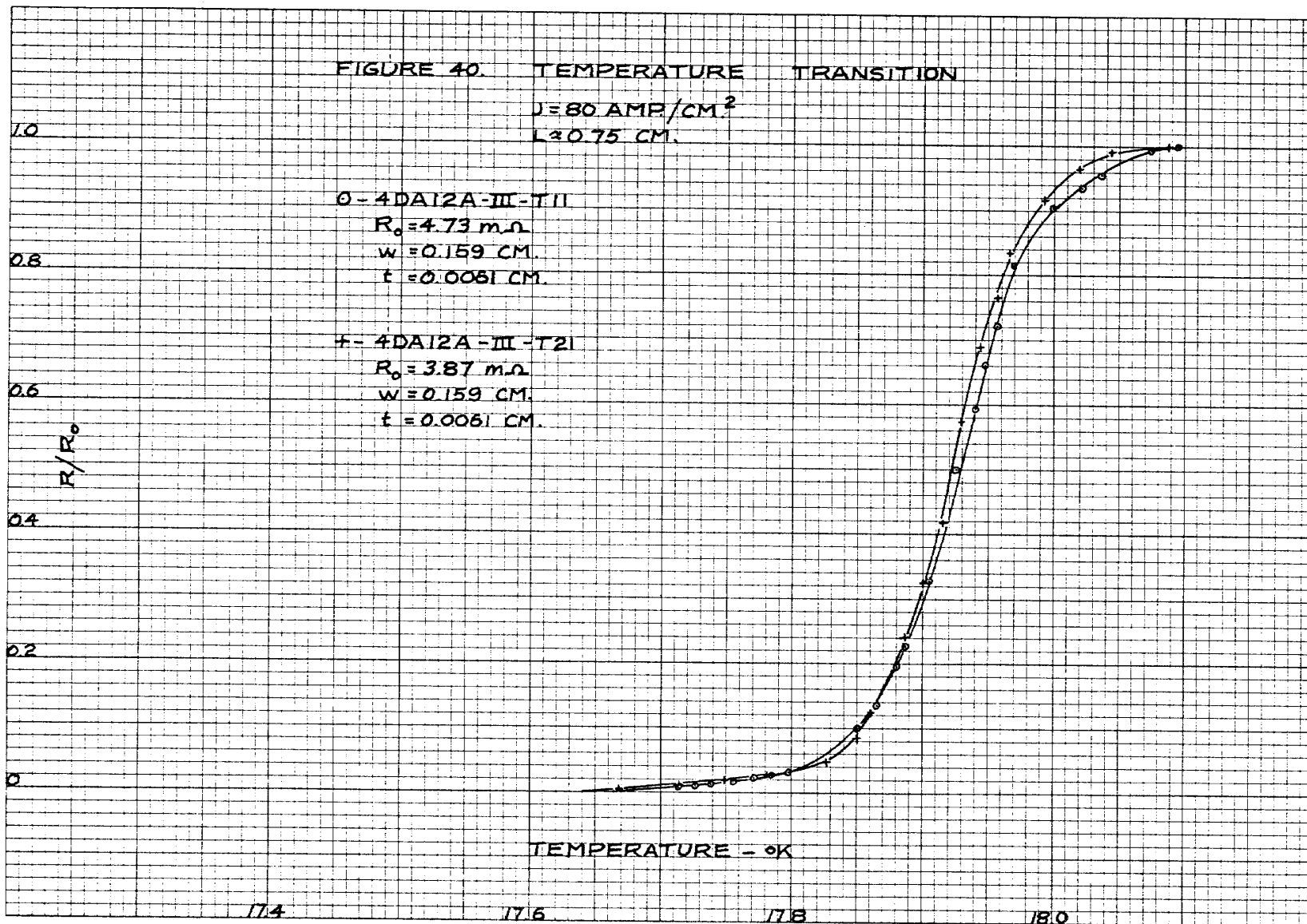


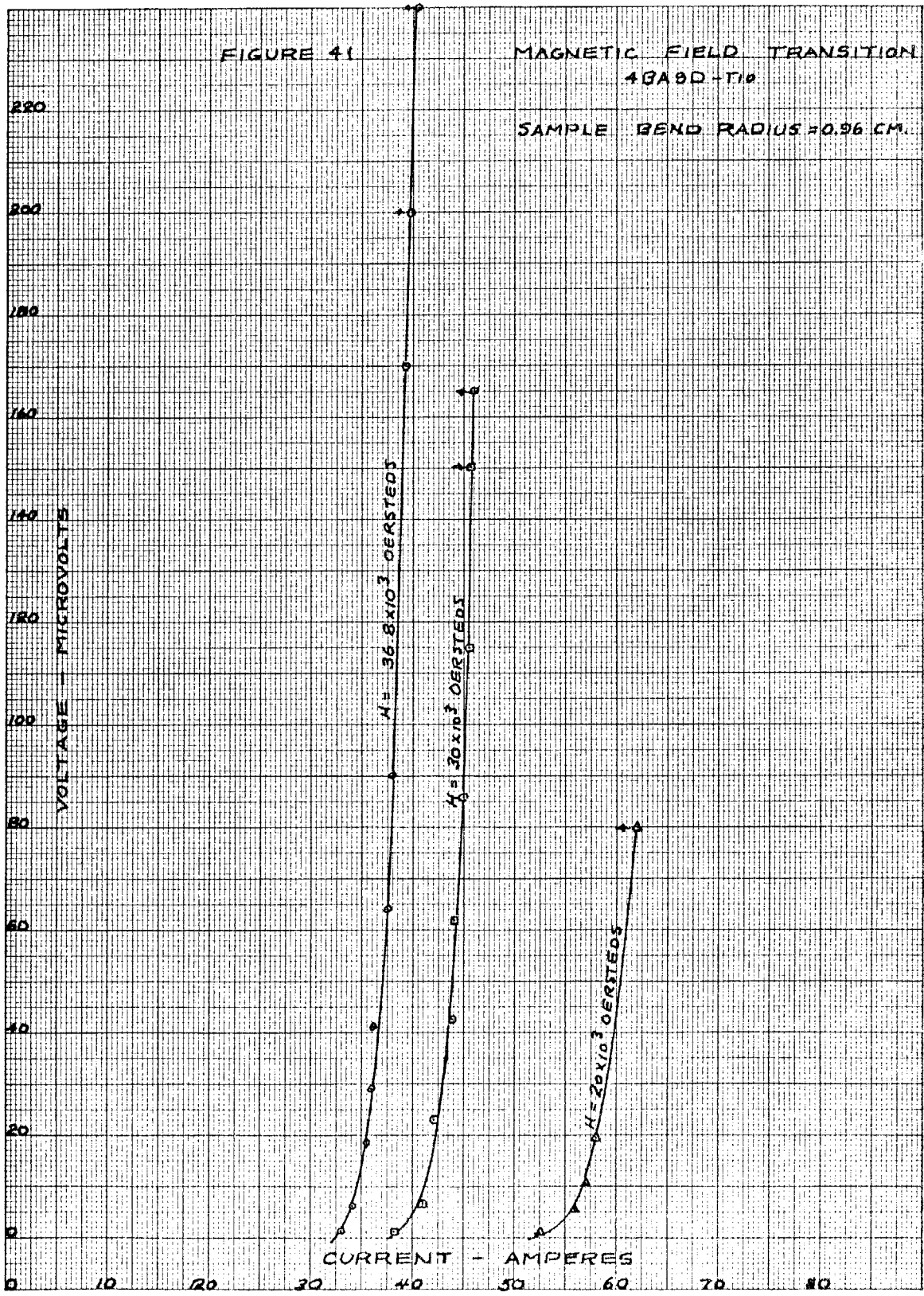












heat transfer coefficient was the same for all samples, the power dissipation criterion implied equal temperatures.

The third criterion chosen was that of full quench of the superconducting phase. Here again a temperature variation was implied because the quenching took place at various power rates in the samples. If one assumes that the heat is converted uniformly from the entire surface of the test sample a power rating of $p/w = .1$ watt/cm corresponds to a temperature rise of 0.16°K in the sample. If one further assumes that the critical current at constant magnetic field has the following temperature dependence;

$$J_c/A = (T_c - T)^2 \quad \text{V-2}$$

one can compute a factor to correct a critical current at $p/w = 0.1$ watt/cm to a value corresponding to $p/w = 0.001$ watt/cm. The resulting factor is

$$\frac{J\left(\frac{p}{w} = 0.001 \frac{\text{W}}{\text{cm}}\right)}{J\left(\frac{p}{w} = 0.1 \frac{\text{W}}{\text{cm}}\right)} = 1.01 \quad \text{V-3}$$

The above factor indicated that the power dissipation errors were within the experimental scatter of the data and in view of the gross assumptions by which it was derived it was felt that the computation involved in applying the correction was not warranted.

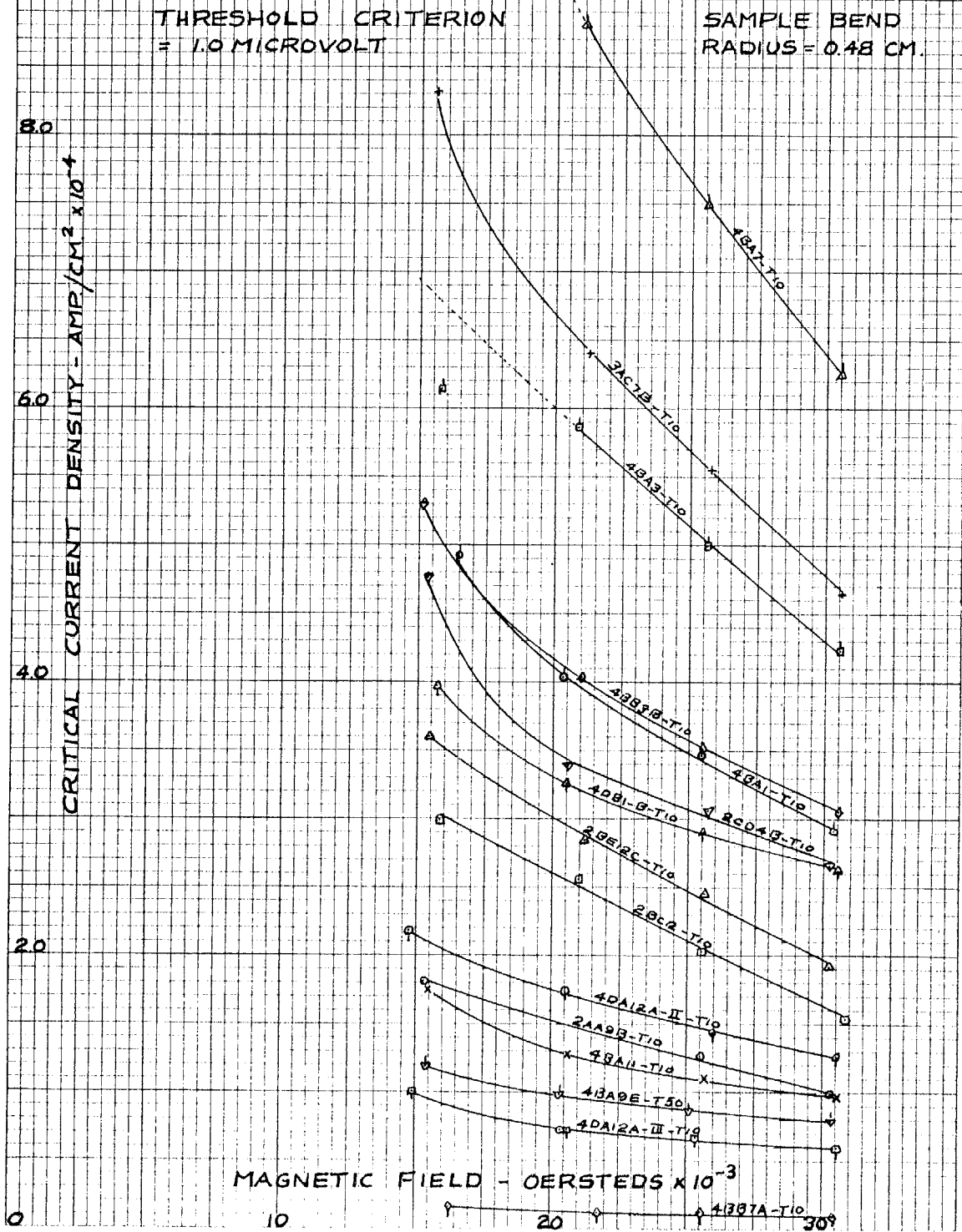
Two sets of data of about fifteen samples each were taken with the two superconducting solenoids. To be accommodated in the 30 kilogauss solenoid the samples had to be

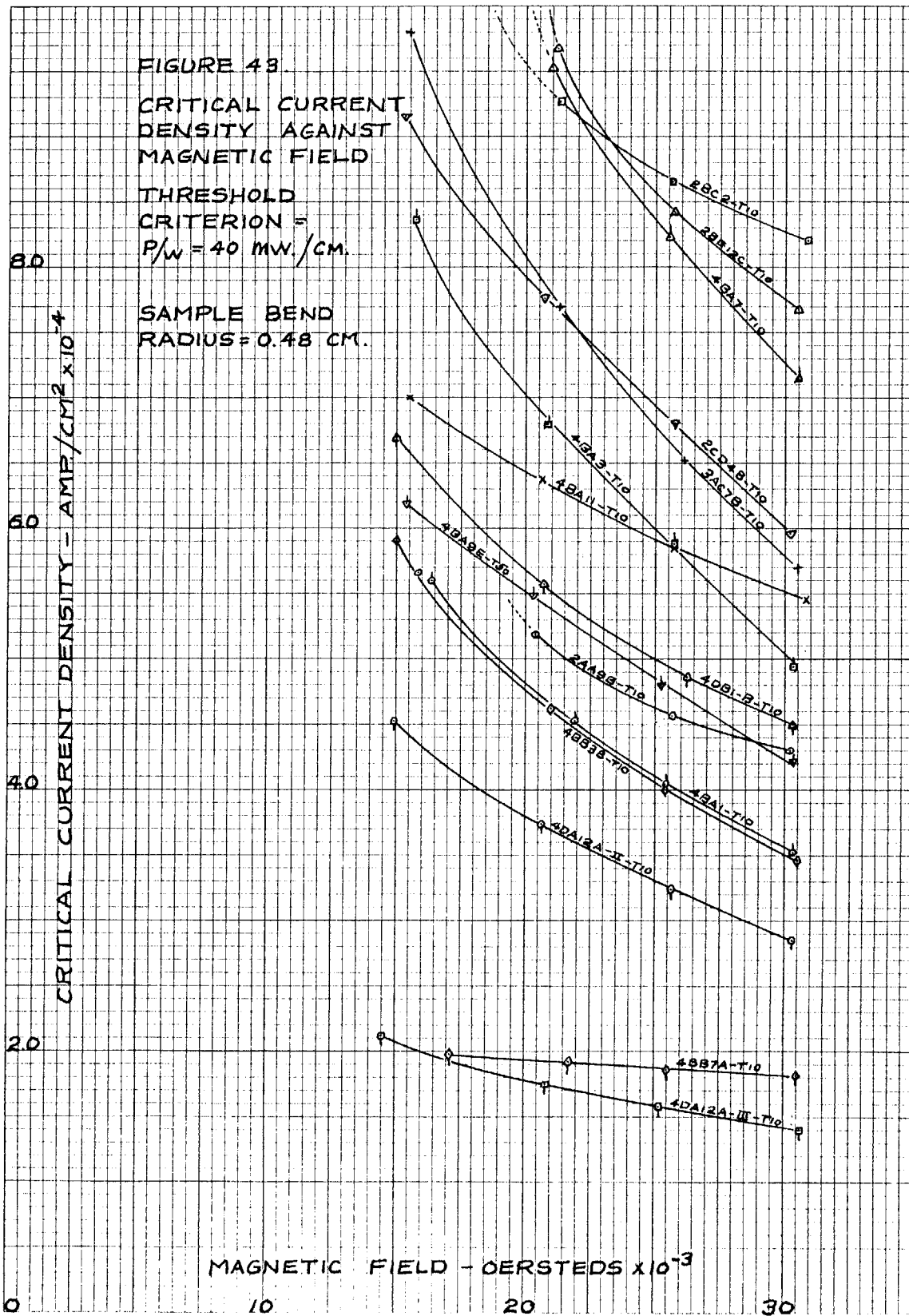
bent on a radius of about 0.48 cm. The 40 kilogauss solenoid required a bend on a radius of 0.96 cm.

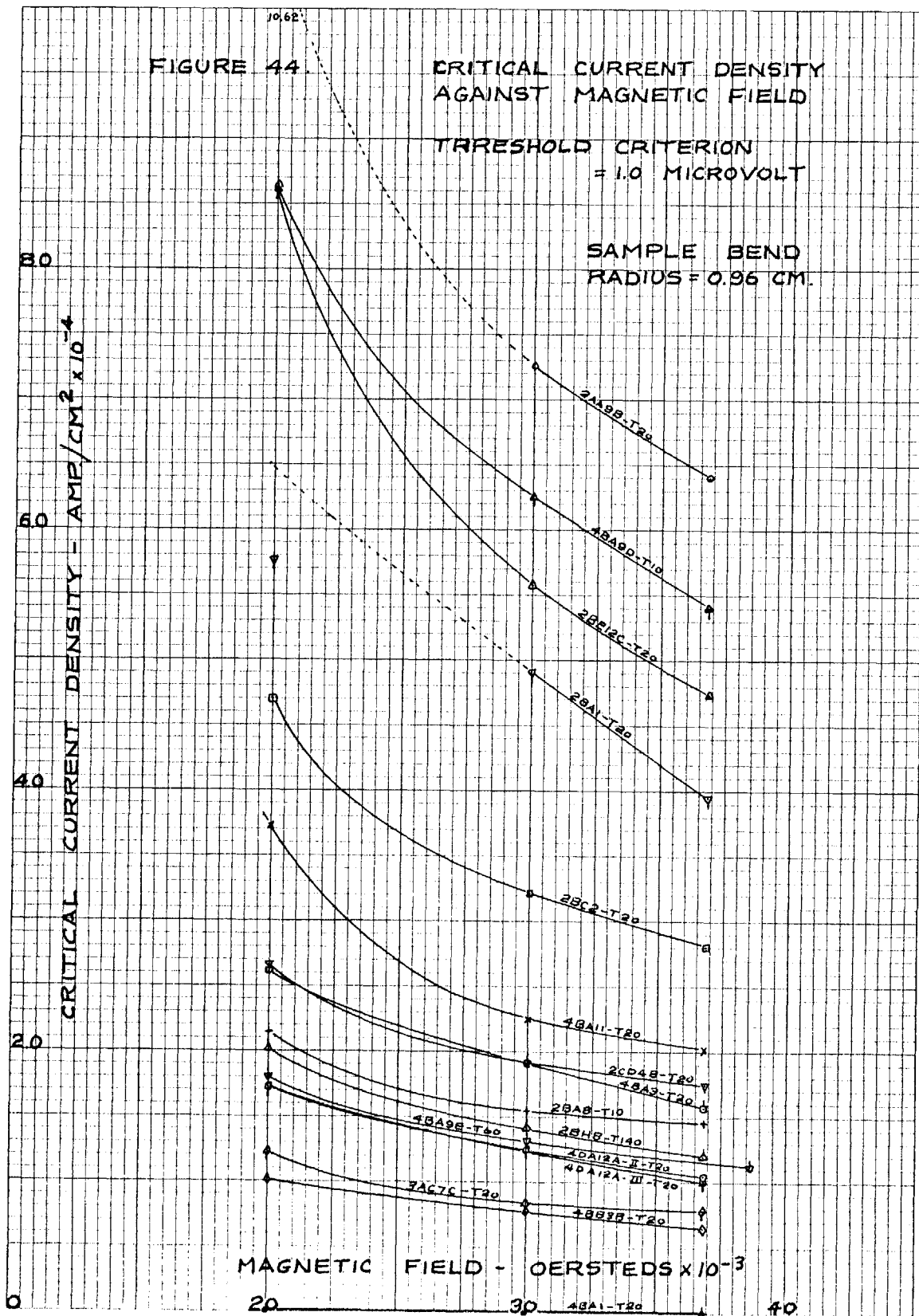
Figure 42 gives critical currents for samples on 0.48 cm radius using 1.0 microvolt as a decision level. Figure 43 shows critical currents for samples on the same radius and with a threshold criterion of $p/w = 0.040$ watt/cm power dissipation factor.

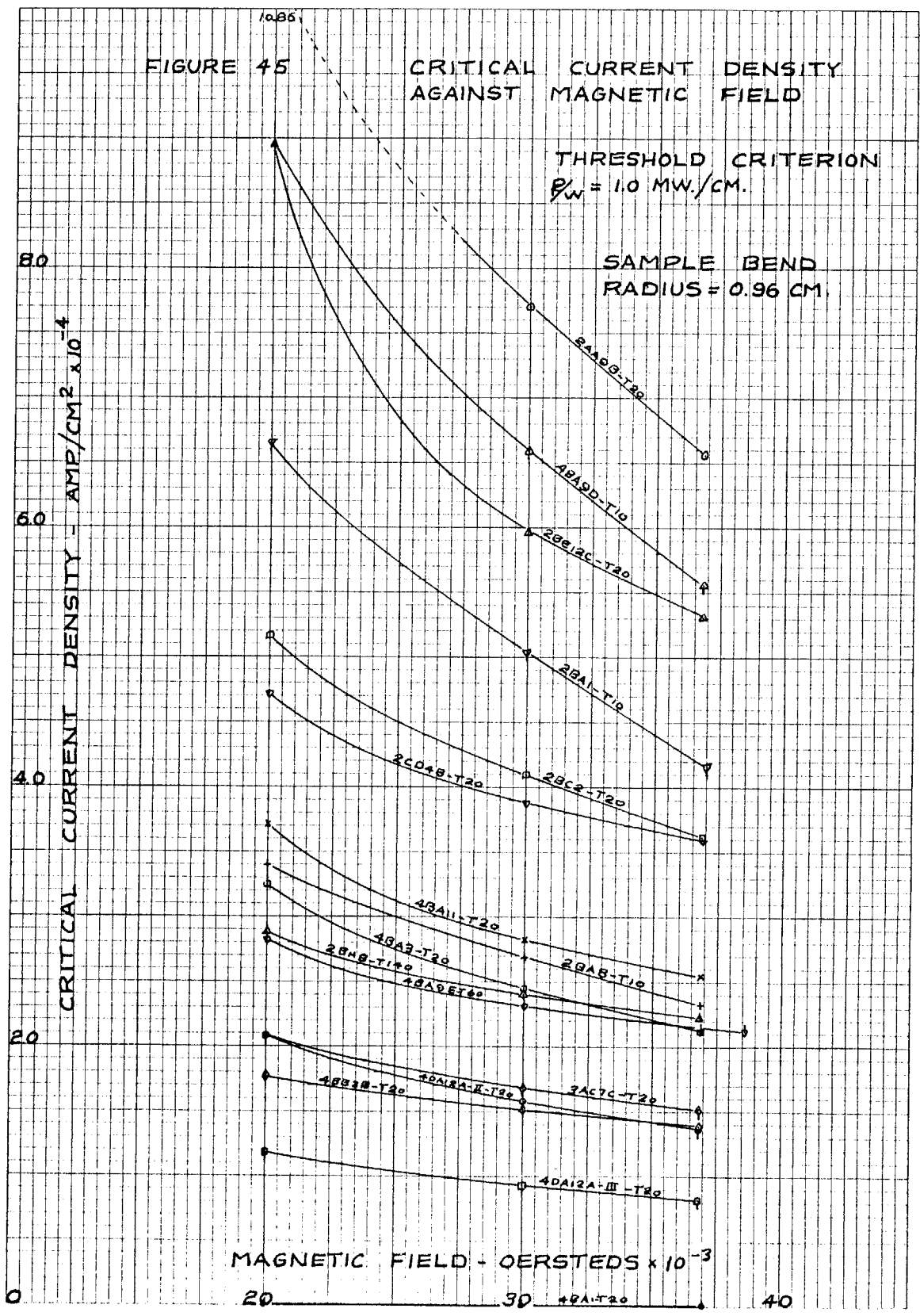
Figures 44, 45, 46 are for samples on a 0.96 cm radius. The threshold criteria are respectively 1.0 microvolt, $p/w = 0.001$ watt/cm and full quench.

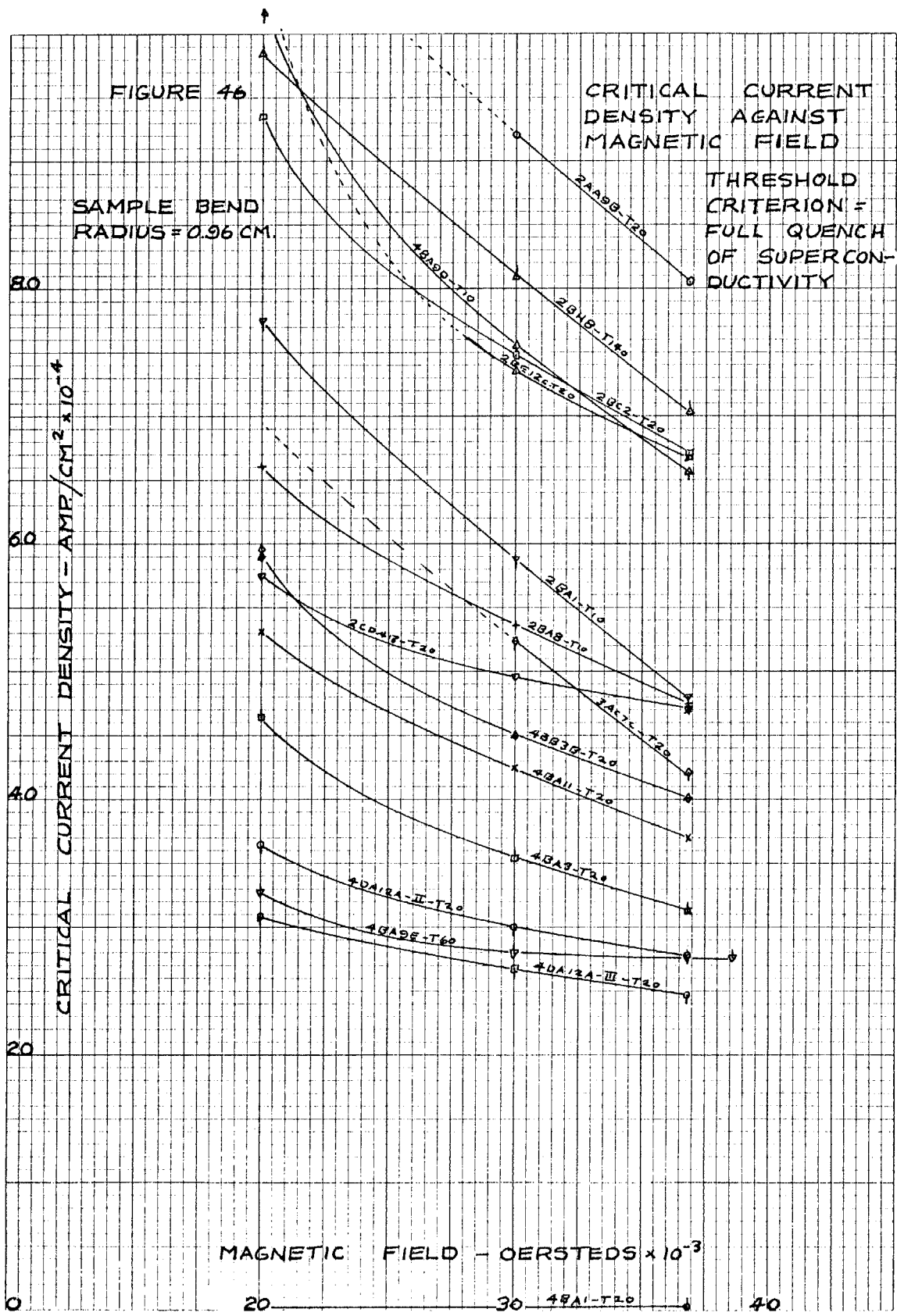
FIGURE 42. CRITICAL CURRENT DENSITY AGAINST MAGNETIC FIELD











VI. CORRELATION AND DISCUSSION

Critical Current Formulation

The first step towards relating the temperature transitions to the critical currents at high magnetic fields was to attempt a formulation of the critical current data. For this purpose equation III-36 was used in the form,

$$J_c (H + H^*) = \alpha \quad \text{VI-1}$$

Taking combinations of two points of the critical current data the parameters α and H^* were computed for the various samples and threshold criteria. For the threshold criterion of 1.0 microvolt voltage rise the computed values of H^* ranged from -1.910×10^3 to 13.95×10^3 with many values near 5×10^3 . It was recalled that Kim, Hempstead and Strnad⁽³¹⁾ obtained their formulation for critical persistent currents in Nb_3Sn by assuming a value of 5×10^3 oersteds for H^* . Assuming this value for H^* the average α was computed for each sample and a reasonably good fit to the critical current curves was obtained. Some typical formulations of the critical current data are shown in Figure 47. The value of 5×10^3 oersteds for H^* turns out to be conveniently the thermodynamic critical field for Nb_3Sn .

To obtain similar formulations for the critical currents of threshold criteria $P/w = 1.0$ milliwatt/cm, $P/w = 40$

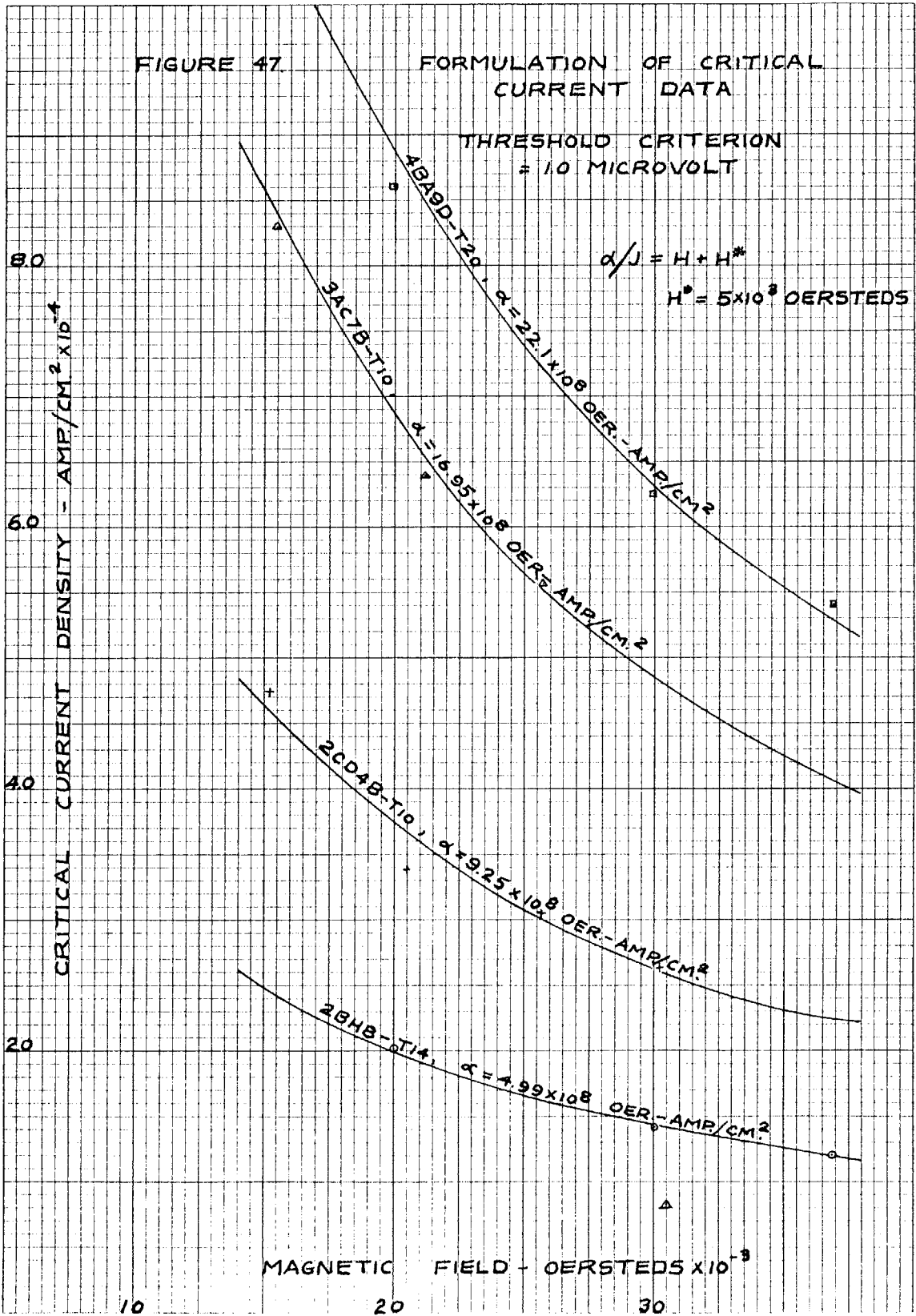
FIGURE 47.

FORMULATION OF CRITICAL CURRENT DATA

THRESHOLD CRITERION
= 10 MICROVOLT

$$\alpha/J = H + H^*$$

$$H^* = 5 \times 10^8 \text{ OERSTEDS}$$



milliwatts/cm and full quench do not lend themselves to this type of formulation.

Referring back to Figures 42-46 it can be seen that the relative qualities of the various samples change with the threshold criterion which decided the critical state. The full quench criterion in particular, is a function of the environment of the sample. Cherry and Gittleman⁽³⁷⁾ have done a detailed analysis of the propagation velocity of a normal-to-superconducting interface in a superconductor carrying a current and find that the initiation of a finite velocity requires that;

$$\frac{I^2}{2\pi^2 ha^3 (\sqrt{K_S/K_N} + 1)\sigma} > T_C - T_B \quad \text{VI-2}$$

The left hand side of inequality VI-2 represents the temperature difference between the conductor and the environment which is necessary to allow dissipation of the power generated in the normal portion. Clearly, the heat conduction from a superconductor in the interior of a coil would be less than that from a sample surrounded by liquid helium and hence the quenching current for the latter would have a nebulous relation to the quenching current for the former.

In terms of coil performance of a superconductor the P/w criteria are probably most valid. However, to use such criteria with confidence would require a knowledge of the magnetic field distribution in the coil upon which T_c depends, as well as the heat transfer parameters.

Thus the conservative threshold criterion of the smallest detectable voltage which in this case is 1.0 microvolt, is probably the most easily useable one for estimating coil performance.

Correlation with Temperature Transitions

The defect density parameter computed previously was compared with various characteristics of the temperature transitions namely the temperature for $R/R_0 = 0.5$, the temperature for initial resistance, the slope of the transition at $R/R_0 = 0.5$, the value of final resistivity based on an assumed sample length of 0.75 cm and the width of the transition on the temperature scale. The only property of the transition which showed an ordered pattern with respect to α was the width of the temperature transition. The correlation results are tabulated in Table II and plotted in Figure 48.

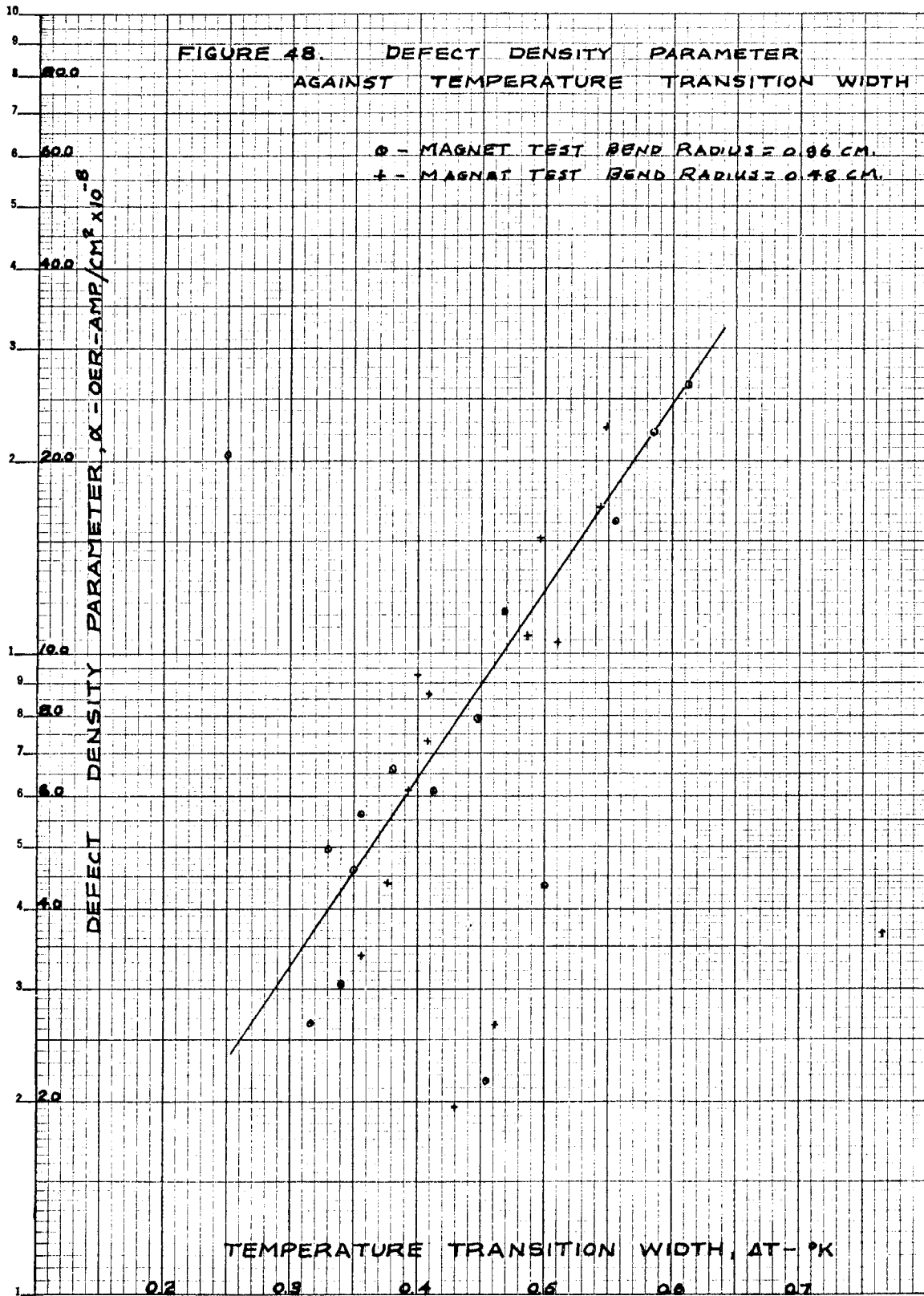
There is enough scatter to the points to allow considerable leeway in drawing the line shown. However, the points indicate that the defect density parameter α is an exponential function of the temperature transition width and the curve shown has been formulated as follows,

$$\alpha \approx 5.0 e^{(12.1 \Delta T - 4.4)}$$

VI-3

Table II
Correlation Results

Sample	ω cm	t cm	ρ_o $\mu\Omega$ -cm	r cm	α oer-Amp $\times 10^8 \text{cm}^2$	ΔT $^{\circ}\text{K}$
2AA9B-T1	0.159	0.0036	6.06	0.48	3.67	0.765
2AA9B-T2	0.159	0.0036	6.37	0.96	26.3	0.612
2BA1-B-T1	0.159	0.0051	10.88	0.96	16.03	0.555
2BA8-T1	0.159	0.0041	4.71	0.96	5.61	0.356
2BC2-T1	0.318	0.0033	4.50	0.48	6.12	0.392
2BC2-T2	0.318	0.0036	4.55	0.96	11.57	0.469
2BE12C-T1	0.159	0.0036	4.66	0.48	7.31	0.408
2BE12C-T2	0.159	0.0036	4.66	0.96	20.5	0.250
2BH8-T14	0.159	0.0036	3.25	0.96	4.99	0.330
2CD4B-T1	0.318	0.0030	7.50	0.48	9.25	0.400
2CD4B-T2	0.318	0.0033	6.87	0.96	6.92	0.412
3AC7B-T1	0.159	0.0036	3.36	0.48	16.95	0.543
3AC7C-T2	0.159	0.0030	3.73	0.96	3.07	0.340
4BA1-T1	0.318	0.0064	5.46	0.48	10.43	0.510
4BA1-T2	0.318	0.0048	3.30	0.96	0.005	2.56
4BA3-T1	0.318	0.0043	3.63	0.48	15.13	0.497
4BA3-T2	0.318	0.0048	4.77	0.96	6.60	0.380
4BA7-T1	0.159	0.0038	3.03	0.48	22.6	0.547
4BA9D-T1	0.159	0.0038	2.68	0.96	22.1	0.585
4BA9E-T5	0.159	0.0041	4.06	0.48	2.64	0.461
4BA9E-T6	0.159	0.0038	3.25	0.96	4.60	0.350
4BA11-T1	0.318	0.0041	3.20	0.48	3.39	0.357
4BA11-T2	0.318	0.0036	3.18	0.96	7.96	0.448
4BB3B-T1	0.318	0.0056	4.39	0.48	10.63	0.487
4BB3B-T2	0.318	0.0048	3.01	0.96	2.66	0.317
4BB7A-T1	0.159	0.0046	3.40	0.48	0.34	0.333
4DA12A-II-T1	0.159	0.0064	7.45	0.48	4.40	0.377
4DA12A-II-T2	0.159	0.0058	4.70	0.96	4.35	0.500
4DA12A-III-T1	0.159	0.0061	4.67	0.48	1.97	0.430
4DA12A-III-T2	0.159	0.0061	3.82	0.96	2.16	0.454
4DB1-B-T1	0.318	0.0048	4.74	0.48	8.66	0.409



The lonely point in the upper left hand side of the plot corresponds to sample 2BE12C-T2 and indicates that the temperature test of this sample was not valid. Possibly the thermal contact between the temperature control body and the sample was poor and the transition was delayed together with the toe being obscured through poor voltage contacts.

The four points in the lower midplot correspond to samples 4BB3B-T2, 4DA12-II-T2, 4DA12A-III-T1, 4DA12A-III-T2 which together with 4BB7A-T1 which is off the plot to the bottom, represent some of the thicker samples. These thicker samples are apparently more susceptible to damage in the transfer from the temperature sample holder to the magnet sample holder due to the brittle nature of the Nb_3Sn compound. The author suspects that the inferior magnet performance of these points is due to such damage in transfer.

The point to the extreme right of the plot corresponds to sample 2AA9B-T1 which together with sample 4BA1-T2 off the plot to the right, represent cases of mechanical defect. The form of the temperature transition for mechanically deformed Nb_3Sn -coated Nb wires has been studied by Saur and Wurm⁽³⁸⁾ and has the same characteristics of extreme width and shallow slope at $R/R_0 = 0.5$ as the transitions of these samples. Apparently, undesirable mechanical defects are so indicated by the transition while desirable chemical defects and small mechanical defects are indicated

by a transition with a relatively steep slope at $R/R_0 = 0.5$ and a long toe. In this case of Nb_3Sn the chemical defects as well as impurities in the components can be intermediate phases $NbSn_2$ and Nb_2Sn_3 which are not superconductive at the temperatures of these tests. Van Ooijen, Van Vucht and Druyvesteyn⁽³⁹⁾ give the critical temperature of $NbSn_2$ at $2.60^\circ K$ while Enstrom, Pearsall and Wulff⁽⁴⁰⁾ give the critical temperature of Nb_2Sn_3 as less than $3.4^\circ K$.

It is significant that there seems to be no width dependence on the performance of the various samples as indicated by the nearly uniform scatter of the results for each width about the line in Figure 48. This result would lead one to assume a uniform current density across the superconductor.

Consideration of the composition of the superconductors under test explains to some extent why only the extremes of either the temperature transitions or magnetic field transitions can be related. The superconductor as described previously consists of two layers of Nb_3Sn on a strata of niobium and may or may not have a superposed layer of unreacted tin. It is only the initiation of resistive inclusions or the final quenching of superconductive inclusions which are entirely dependent on the structure of the Nb_3Sn layers. In the intermediate state the current might be bypassing the resistive Nb_3Sn inclusions through the tin or niobium layers and hence the shape of the transition

would depend in part on the size and condition of these layers. In a homogeneous superconductor one would expect the defect density to be reflected by the normal state resistivity. Reference to Table II confirms that there was no systematic correspondence between α and ρ_0 for the superconductors under test.

As an engineering tool the relationship described by equation VI-3 and shown in Figure 48 is somewhat of a disappointment. If one were to measure the temperature transition of a long length of a similar superconductor the width of the transition would be a measure of the best performance of the total length rather than the worst performance which one would wish to know to set a lower performance limit on the length. If one could run the long length through a controlled temperature zone while carrying a small current, a pair of closely spaced voltage contacts could detect a loss of resistance at a temperature where a limiting performance criterion would dictate that the toe of the transition should exist. Such a scheme would have the advantage over a magnetic field scanner in that Lorentz forces would be avoided. Also, to use low test currents a magnetic field scanner would require quite high magnetic fields.

Conclusions

The formulation of the magnetic field test data by use of equation VI-1 confirms that high current densities

at high magnetic fields in non-ideal superconductors are dependent on the ability of structural defects to stabilize the current against the Lorentz force.

The density and/or intensity of the structural defects can be measured in terms of the width on the temperature scale of the resistive transition at low current density in the earth's magnetic field and near the critical temperature. The high field performance at 4.2°K is found to vary exponentially with this transition width with the qualification that the transition width must not exceed a limit of about 0.65°K . Transition widths in excess of this limit are liable to indicate mechanical damage and impaired performance at high magnetic fields.

VII. FUTURE WORK

In order to refine the relationship indicated in this thesis the author would suggest two efforts which are both dependent on improved sensitivity of voltage measurements.

First, the fit of the critical current curves can probably be improved by both increased voltage sensitivity and an increase of data per sample.

Second, precision in measuring the toe of the resistive transitions could be improved with increased voltage sensitivity. Alternatively, the precision in measuring the resistive transition toe might be improved through investigating the effect of various test current densities.

In addition, the author would suggest that the sample holders be designed for use in both temperature and magnetic field tests so that the risk of damage through demounting and remounting between tests would be avoided.

VIII. REFERENCE

1. Kamerlingh Onnes, H (1911) Leiden Comm. 122b 124c.
2. Quinn, D. J. and Ittner, W. B. (1962) J. Appl. Phys. 33, p 748.
3. Kammerlingh Onnes, H (1913) Leiden Comm. Supp. 35.
4. Silsbee, F. B. (1917) Bull. Bur. of Stds. 14, p 301.
5. Matthias, B. T., Geballe, T. H., Geller, S., Corenzwit, E. (1954) Phys. Rev. 95, p 1435.
6. Kunzler, J. E., Buehler, E., Hsu, F. S. L. and Wernick, J. H. (1961) Phy. Rev. Lett. 6, p 89.
7. Berlincourt, J. G., Hake, R. R., and Leslie, D. H. (1961) Phys. Rev. Lett. 6, p 671.
8. Autler, S. H., (1959) Bull. Am. Phys. Soc., 4, p 413.
9. Autler, S. H. (1961) Proc. Int. Conf. on High Magnetic Fields, p 344, M.I.T. Press - Wiley.
10. Meissner, W. and Ochsenfeld, R. (1933) Naturwissenschaften, 21, p 787.
11. Kunzler, J. E., (1961) Rev. Mod. Phys. 33, p 501.
12. Logue, H. L., (1961) Proc. Int. Conf. on High Mag. Fields p 156, M.I.T. Press - Wiley.
13. Kneip, G. D, Jr., Betterton, J. O., Jr., Easton, D. S. and Scarbrough, J. O., (1962) J. App. Phys. 33 p 754.
14. Arp, V. D., Kropschot, R. H., Wilson, J. H., Love, W. F. and Phelan, R., (1961) Phys. Rev. Lett., 6, p 452.
15. Aron, P. R., and Hitchcock, H. C., (1962) J. App. Phys. 33, p 2242.
16. Fink, H. J. (1959) Can. J. Phys. 37, p 485.
17. Rinderer, L. (1956) Helv. Phys. Acta 29, p 339.

18. Desorbo, W. (1963) Phys. Rev. 132, p 107.
19. Seraphim, D. P., Novick, D. T., and Budnick, J. I. (1961) Acta Metall. 9, p 446.
20. Simmons, W. A. and Douglass, D. H. (1962) Phys. Rev. Lett. 9, p 153.
21. Muller, C., and Saur, E. (1962) Z. Phys. 170, p 154.
22. Kneip, G. D. Jr., Betterton, J. D., Jr., Easton, D. S. and Scarbrough, J. O. (1961) Proc. Int. Conf. on High Magnetic Fields, p 603, M.I.T. Press - Wiley.
23. London, Fritz, (1961) Superfluids Vol. I Macroscopic Theory of Superconductivity, Dover Publications.
24. Shoenberg, D. (1952) Superconductivity, Cambridge University Press.
25. Lynton, Ernest A. (1962) Superconductivity, Methuen and Co. Ltd.
26. Scott, R. B. (1948) J. Res. Nat. Bur. Stds. 41, p 581.
27. Bean, C. P., Doyle M. V., and Pineus, A. G., (1962) Phys. Rev. Lett. 9, p 94.
28. Kamper, R. A., (1963) Phys. Lett. 5, p 9.
29. Heaton, J. W. and Rose-Innes, A. C. (1964) Cryogenics, 4, p 85.
30. Bean, C. P. (1962) Phys. Rev. Lett. 8, p 250.
31. Kim, Y. B., Hempstead C. F., and Strnad, A. R. (1962) Phys. Rev. Lett., 9, p 306.
32. Kim, Y. B., Hempstead, C. F., and Strnad, A. R. (1963) Phys. Rev., 129, p 528.
33. LeBlanc, M. A. R. (1963) Phys. Rev. Lett. 11, p 149.
34. Budnick, T. J. (1960) Phys. Rev., 119, p 1278.
35. White, G. K. (1959) Experimental Techniques in Low-Temperature Physics, Clarendon Press.
36. Scott, R. B. (1959) Cryogenic Engineering, D. Van Nostrand and Company.

37. Cherry, W. H. and Gittleman, J. I. (1960) Solid State Electronics, 1, p 287.
38. Saur, E. J. and Wurm, J. P. (1961) Proc. Int. Conf. on High Magnetic Fields, p 589, M.I.T. Press - Wiley.
39. Van Ooijen, D. J., Van Vucht, J. H. N. and Druyvesteyn, W. T. (1962) Phys. Lett. 3, p 128.
40. Enstrom, R. E., Pearsall, G. W. and Wulff, J. (1963) Appl. Phys. Lett., 3, p 81.
41. Autler, S. H., Several discussions which formed a general reference and initiation of the author to the field of superconductivity and took place when Dr. Autler was at the M.I.T. Lincoln Laboratory.

APPENDIX A

Process for Copper Plating Niobium-Tin Ribbon

Solutions: (a) Cleaning

Sodium Hydroxide 300 grams

Water 400 grams

Use at $95 \pm 5^{\circ}\text{C}$

(b) Plating

Copper cyanide 26 grams/liter

Sodium cyanide 35 grams/liter

Sodium carbonate 30 grams/liter

Rochelle salts 45 grams/liter

pH 12-12.6 (adjust with NaOH if necessary)

Use at $65 \pm 5^{\circ}\text{C}$

Procedure: Clean ribbon in acetone to remove grease.

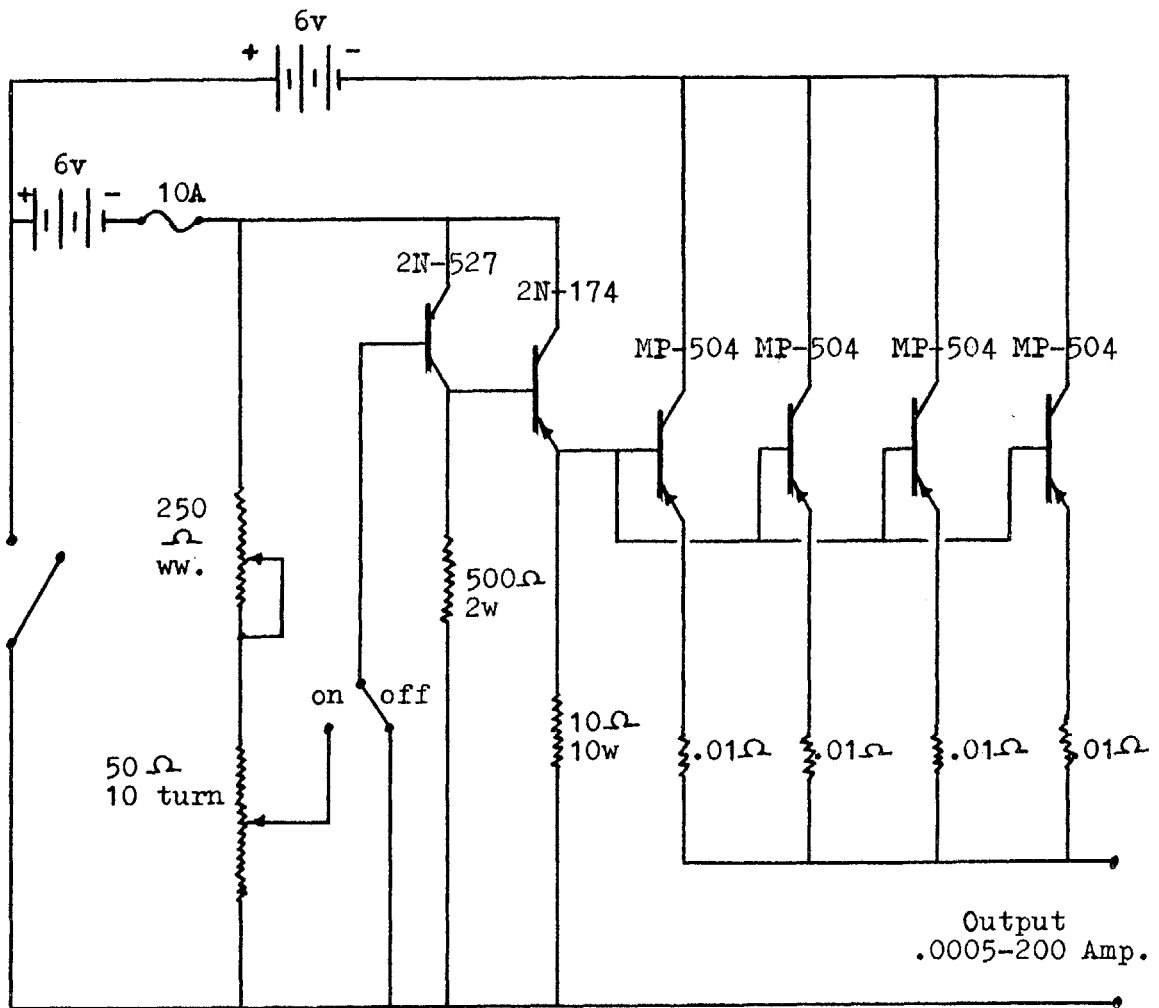
Clean in caustic for two minutes using a platinum wire as anode and applying a surface current density of 160 Ma/in^2 . Rinse in clean water when this step is completed and avoid prolonged exposure to air when transferring to the plating bath.

Plate for five minutes using copper as anode and applying a surface current density of 320 Ma/in^2 . Rinse in clean water and dry.

Results: This procedure results in a uniform layer of copper about 0.00015 in thick over the surface of the Nb₃Sn ribbon. The copper plated ribbon may be soldered with lead-tin solder using a mild rosin flux.

Appendix B

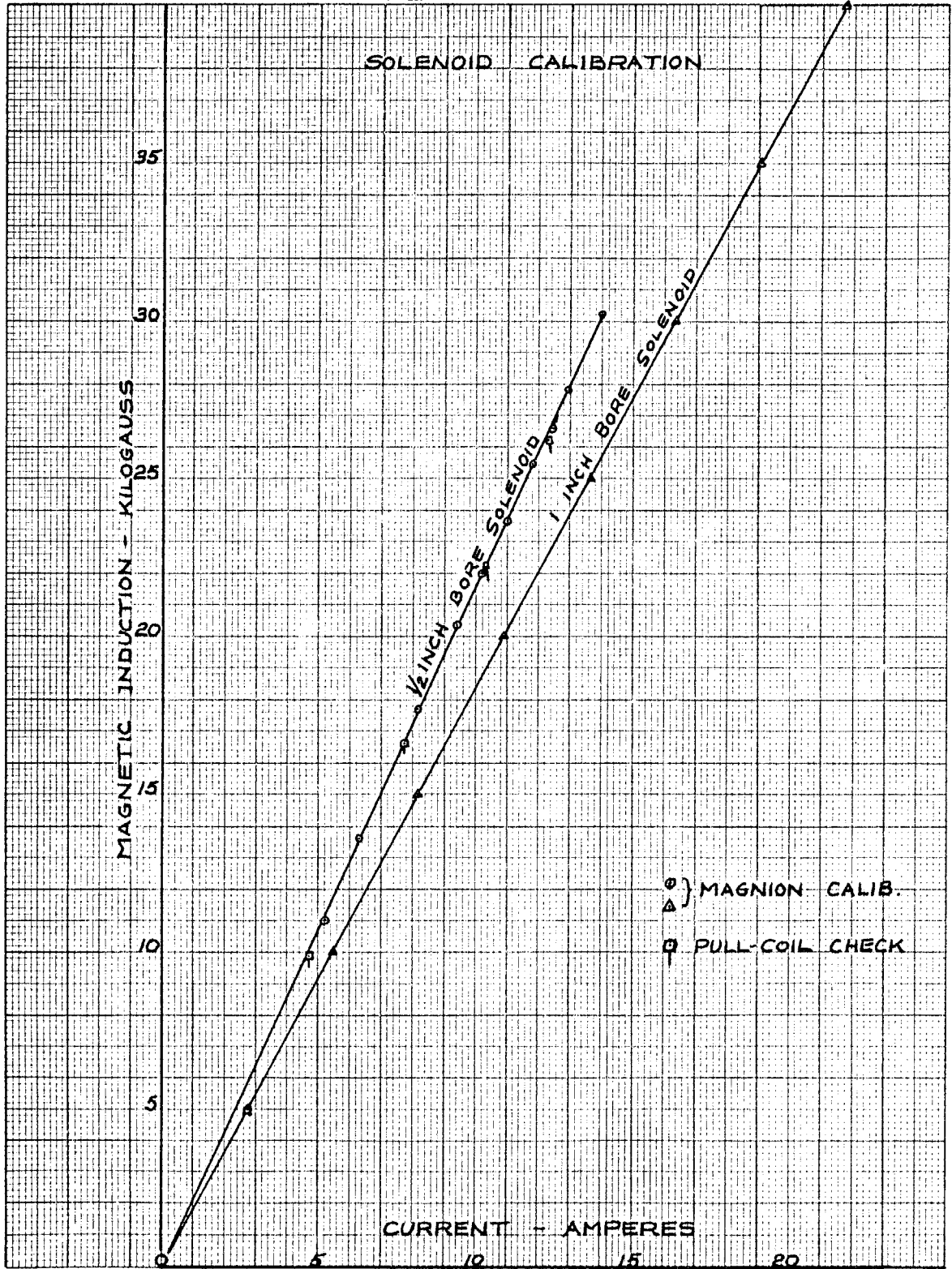
Current Control Circuit Diagram



APPENDIX C

Superconducting Solenoid Calibrations

(C2)



APPENDIX D

Tabulation of Temperatures for Normal
Hydrogen Vapor Pressures

Equation from Scott⁽³⁶⁾ page 298

$$\log_{10} p_{\text{MM Hg}} = 4.66687 - \frac{44.9569}{T} + 0.020537T$$

(D2)

T(DEGREES K)	LOG(10)(P(MM-HG))	P(MM-HG)
1.300000E 01	1.4756279E 00	2.9897020E 01
1.305000E 01	1.4899047E 00	3.0896174E 01
1.310000E 01	1.5040803E 00	3.1921280E 01
1.315000E 01	1.5181559E 00	3.2972805E 01
1.320000E 01	1.5321326E 00	3.4051214E 01
1.325000E 01	1.5460117E 00	3.5156991E 01
1.330000E 01	1.5597941E 00	3.6290596E 01
1.335000E 01	1.5734809E 00	3.7452507E 01
1.340000E 01	1.5870733E 00	3.8643219E 01
1.345000E 01	1.6005722E 00	3.9863204E 01
1.350000E 01	1.6139788E 00	4.1112965E 01
1.355000E 01	1.6272940E 00	4.2392985E 01
1.360000E 01	1.6405188E 00	4.3703760E 01
1.365000E 01	1.6536543E 00	4.5045800E 01
1.370000E 01	1.6667014E 00	4.6419601E 01
1.375000E 01	1.6796610E 00	4.7825663E 01
1.380000E 01	1.6925342E 00	4.9264514E 01
1.385000E 01	1.7053219E 00	5.0736663E 01
1.390000E 01	1.7180249E 00	5.2242614E 01
1.395000E 01	1.7306443E 00	5.3782910E 01
1.400000E 01	1.7431809E 00	5.5358065E 01
1.405000E 01	1.7556355E 00	5.6968594E 01
1.410000E 01	1.7680091E 00	5.8615045E 01
1.415000E 01	1.7803025E 00	6.0297943E 01
1.420000E 01	1.7925165E 00	6.2017820E 01
1.425000E 01	1.8046521E 00	6.3775240E 01
1.430000E 01	1.8167099E 00	6.5570712E 01
1.435000E 01	1.8286909E 00	6.7404812E 01
1.440000E 01	1.8405959E 00	6.9278089E 01
1.445000E 01	1.8524255E 00	7.1191067E 01
1.450000E 01	1.8641806E 00	7.3144319E 01
1.455000E 01	1.8758620E 00	7.5138410E 01
1.460000E 01	1.8874705E 00	7.7173909E 01
1.465000E 01	1.8990067E 00	7.9251356E 01
1.470000E 01	1.9104714E 00	8.1371327E 01
1.475000E 01	1.9218653E 00	8.3534389E 01
1.480000E 01	1.9331892E 00	8.5741129E 01
1.485000E 01	1.9444438E 00	8.7992124E 01
1.490000E 01	1.9556297E 00	9.0287931E 01
1.495000E 01	1.9667476E 00	9.2629133E 01
1.500000E 01	1.9777983E 00	9.5016340E 01
1.505000E 01	1.9887824E 00	9.7450125E 01
1.510000E 01	1.9997006E 00	9.9931084E 01
1.515000E 01	2.0105534E 00	1.0245978E 02
1.520000E 01	2.0213416E 00	1.0503683E 02 ✓
1.525000E 01	2.0320658E 00	1.0766283E 02
1.530000E 01	2.0427266E 00	1.1033838E 02
1.535000E 01	2.0533247E 00	1.1306409E 02
1.540000E 01	2.0638606E 00	1.1584055E 02 ✓
1.545000E 01	2.0743349E 00	1.1866835E 02

(D3)

T(DEGREES K)	LOG(10)(P(MM-HG))	P(MM-HG)
1.550000E 01	2.0847483E 00	1.2154814E 02
1.555000E 01	2.0951014E 00	1.2448052E 02
1.560000E 01	2.1053946E 00	1.2746607E 02 ✓
1.565000E 01	2.1156287E 00	1.3050547E 02
1.570000E 01	2.1258041E 00	1.3359927E 02
1.575000E 01	2.1359214E 00	1.3674813E 02
1.580000E 01	2.1459812E 00	1.3995267E 02 ✓
1.585000E 01	2.1559840E 00	1.4321351E 02
1.590000E 01	2.1659303E 00	1.4653127E 02
1.595000E 01	2.1758207E 00	1.4990658E 02 ✓
1.600000E 01	2.1856558E 00	1.5334012E 02
1.605000E 01	2.1954359E 00	1.5683244E 02
1.610000E 01	2.2051617E 00	1.6038424E 02
1.615000E 01	2.2148336E 00	1.6399613E 02
1.620000E 01	2.2244521E 00	1.6766874E 02 ✓
1.625000E 01	2.2340178E 00	1.7140276E 02
1.630000E 01	2.2435311E 00	1.7519879E 02
1.635000E 01	2.2529925E 00	1.7905749E 02
1.640000E 01	2.2624024E 00	1.8297948E 02
1.645000E 01	2.2717614E 00	1.8696547E 02
1.650000E 01	2.2810699E 00	1.9101607E 02
1.655000E 01	2.2903283E 00	1.9513191E 02
1.660000E 01	2.2995372E 00	1.9931372E 02
1.665000E 01	2.3086969E 00	2.0356209E 02
1.670000E 01	2.3178080E 00	2.0787775E 02
1.675000E 01	2.3268707E 00	2.1226124E 02
1.680000E 01	2.3358856E 00	2.1671332E 02 ✓
1.685000E 01	2.3448532E 00	2.2123468E 02
1.690000E 01	2.3537737E 00	2.2582587E 02
1.695000E 01	2.3626477E 00	2.3048767E 02
1.700000E 01	2.3714755E 00	2.3522068E 02 ✓
1.705000E 01	2.3802575E 00	2.4002556E 02
1.710000E 01	2.3889942E 00	2.4490305E 02
1.715000E 01	2.3976860E 00	2.4985382E 02
1.720000E 01	2.4063331E 00	2.5487844E 02 ✓
1.725000E 01	2.4149361E 00	2.5997770E 02
1.730000E 01	2.4234954E 00	2.6515230E 02
1.735000E 01	2.4320112E 00	2.7040281E 02
1.740000E 01	2.4404839E 00	2.7572992E 02 ✓
1.745000E 01	2.4489140E 00	2.8113441E 02
1.750000E 01	2.4573018E 00	2.8661690E 02
1.755000E 01	2.4656476E 00	2.9217806E 02
1.760000E 01	2.4739519E 00	2.9781866E 02 ✓
1.765000E 01	2.4822149E 00	3.0353928E 02
1.770000E 01	2.4904370E 00	3.0934065E 02
1.775000E 01	2.4986187E 00	3.1522358E 02
1.780000E 01	2.5067601E 00	3.2118858E 02 ✓
1.785000E 01	2.5148616E 00	3.2723639E 02
1.790000E 01	2.5229236E 00	3.3336776E 02
1.795000E 01	2.5309465E 00	3.3958344E 02

(D4)

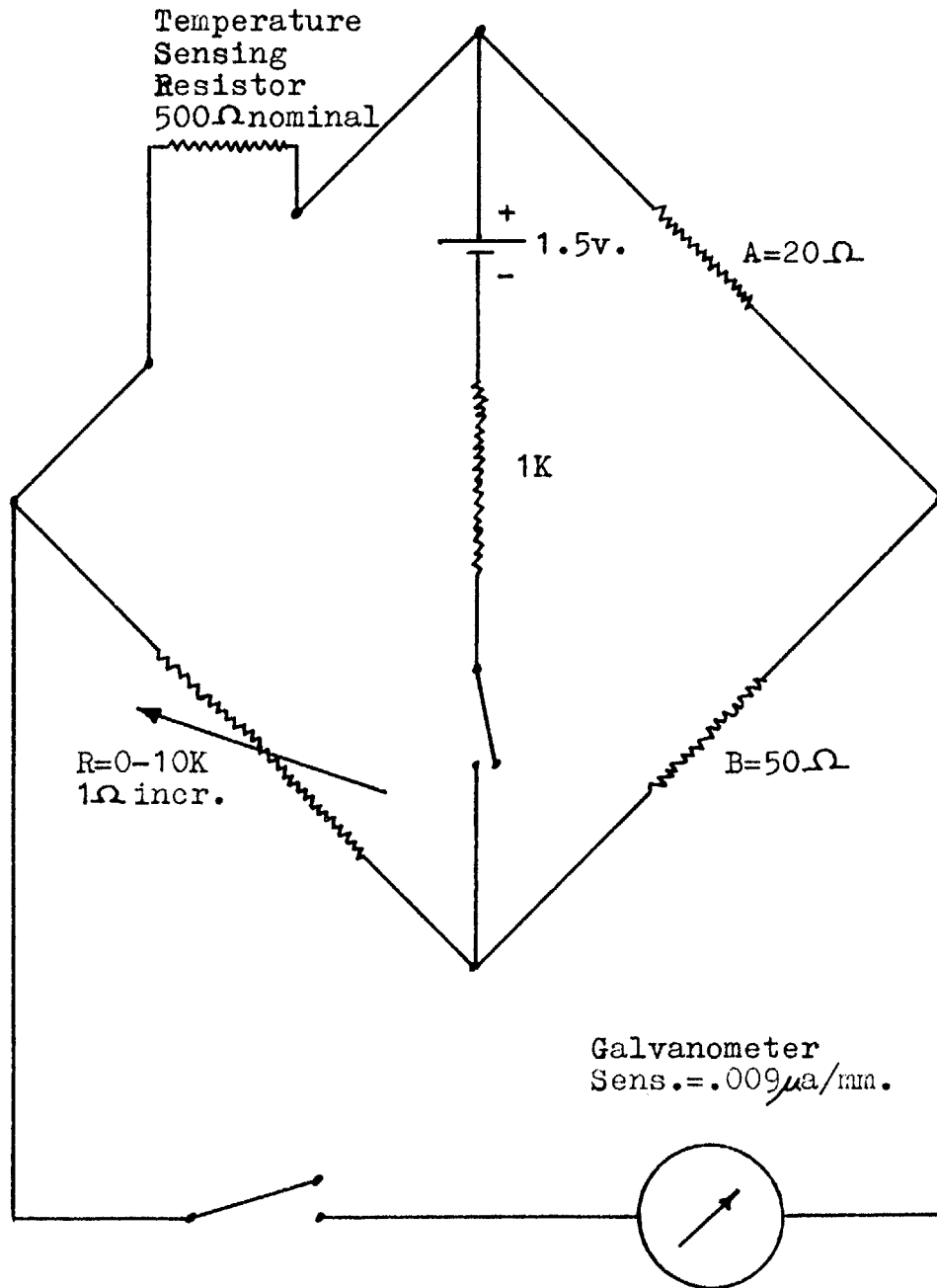
T(DEGREES K)	LOG(10)(P(MM-HG))	P(MM-HG)
1.800000E 01	2.5389304E 00	3.4588394E 02 ✓
1.805000E 01	2.5468759E 00	3.5227019E 02
1.810000E 01	2.5547831E 00	3.5874272E 02
1.815000E 01	2.5626524E 00	3.6530229E 02
1.820000E 01	2.5704841E 00	3.7194960E 02 ✓
1.825000E 01	2.5782785E 00	3.7868535E 02
1.830000E 01	2.5860359E 00	3.8551022E 02
1.835000E 01	2.5937566E 00	3.9242494E 02
1.840000E 01	2.6014410E 00	3.9943029E 02 ✓
1.845000E 01	2.6090893E 00	4.0652691E 02
1.850000E 01	2.6167018E 00	4.1371551E 02
1.855000E 01	2.6242788E 00	4.2099680E 02
1.860000E 01	2.6318206E 00	4.2837153E 02 ✓
1.865000E 01	2.6393274E 00	4.3584031E 02
1.870000E 01	2.6467996E 00	4.4340399E 02
1.875000E 01	2.6542374E 00	4.5106320E 02
1.880000E 01	2.6616411E 00	4.5881869E 02 ✓
1.885000E 01	2.6690110E 00	4.6667120E 02
1.890000E 01	2.6763473E 00	4.7462138E 02
1.895000E 01	2.6836504E 00	4.8267010E 02
1.900000E 01	2.6909204E 00	4.9081791E 02 ✓
1.905000E 01	2.6981576E 00	4.9906556E 02 ✓
1.910000E 01	2.7053623E 00	5.0741383E 02
1.915000E 01	2.7125348E 00	5.1586350E 02
1.920000E 01	2.7196752E 00	5.2441511E 02 ✓
1.925000E 01	2.7267839E 00	5.3306958E 02
1.930000E 01	2.7338610E 00	5.4182745E 02
1.935000E 01	2.7409069E 00	5.5068963E 02
1.940000E 01	2.7479218E 00	5.5965682E 02 ✓
1.945000E 01	2.7549059E 00	5.6872969E 02
1.950000E 01	2.7618594E 00	5.7790892E 02
1.955000E 01	2.7687827E 00	5.8719547E 02
1.960000E 01	2.7756758E 00	5.9658977E 02 ✓
1.965000E 01	2.7825391E 00	6.0609276E 02
1.970000E 01	2.7893728E 00	6.1570517E 02
1.975000E 01	2.7961770E 00	6.2542754E 02
1.980000E 01	2.8029521E 00	6.3526086E 02 ✓
1.985000E 01	2.8096982E 00	6.4520571E 02
1.990000E 01	2.8164156E 00	6.5526293E 02
1.995000E 01	2.8231045E 00	6.6543325E 02
2.000000E 01	2.8297650E 00	6.7571724E 02 ✓ ✓
2.005000E 01	2.8363974E 00	6.8611577E 02
2.010000E 01	2.8430020E 00	6.9662972E 02
2.015000E 01	2.8495789E 00	7.0725968E 02
2.020000E 01	2.8561283E 00	7.1800637E 02 ✓
2.025000E 01	2.8626504E 00	7.2887054E 02
2.030000E 01	2.8691455E 00	7.3985310E 02
2.035000E 01	2.8756137E 00	7.5095463E 02
2.040000E 01	2.8820552E 00	7.6217588E 02 ✓
2.045000E 01	2.8884702E 00	7.7351760E 02

(D5)

T (DEGREES K)	LOG(10) (P (MM-HG))	P (MM-HG)
2.050000E 01	2.8948590E 00	7.8498074E 02
2.055000E 01	2.9012217E 00	7.9656588E 02
2.060000E 01	2.9075584E 00	8.0827361E 02
2.065000E 01	2.9138695E 00	8.2010507E 02
2.070000E 01	2.9201550E 00	8.3206068E 02
2.075000E 01	2.9264152E 00	8.4414140E 02
2.080000E 01	2.9326502E 00	8.5634783E 02
2.085000E 01	2.9388602E 00	8.6868075E 02
2.090000E 01	2.9450455E 00	8.8114118E 02
2.095000E 01	2.9512061E 00	8.9372951E 02
2.100000E 01	2.9573422E 00	9.0644655E 02 ✓
2.105000E 01	2.9634541E 00	9.1929331E 02
2.110000E 01	2.9695419E 00	9.3227041E 02
2.115000E 01	2.9756058E 00	9.4537867E 02
2.120000E 01	2.9816459E 00	9.5861871E 02
2.125000E 01	2.9876624E 00	9.7199135E 02
2.130000E 01	2.9936555E 00	9.8549744E 02
2.135000E 01	2.9996253E 00	9.9913759E 02
2.140000E 01	3.0055721E 00	1.0129129E 03
2.145000E 01	3.0114959E 00	1.0268237E 03
2.150000E 01	3.0173959E 00	1.0408710E 03
2.155000E 01	3.0232753E 00	1.0550555E 03
2.160000E 01	3.0291312E 00	1.0693779E 03
2.165000E 01	3.0349649E 00	1.0838393E 03
2.170000E 01	3.0407764E 00	1.0984402E 03
2.175000E 01	3.0465658E 00	1.1131810E 03
2.180000E 01	3.0523335E 00	1.1280634E 03
2.185000E 01	3.0580794E 00	1.1430873E 03
2.190000E 01	3.0638038E 00	1.1582540E 03
2.195000E 01	3.0695068E 00	1.1735641E 03
2.200000E 01	3.0751885E 00	1.1890182E 03 ✓
2.205000E 01	3.0808492E 00	1.2046176E 03
2.210000E 01	3.0864888E 00	1.2203623E 03
2.215000E 01	3.0921077E 00	1.2362540E 03
2.220000E 01	3.0977058E 00	1.2522926E 03
2.225000E 01	3.1032834E 00	1.2684793E 03
2.230000E 01	3.1088406E 00	1.2848150E 03
2.235000E 01	3.1143775E 00	1.3013002E 03
2.240000E 01	3.1198943E 00	1.3179359E 03
2.245000E 01	3.1253911E 00	1.3347229E 03
2.250000E 01	3.1308681E 00	1.3516620E 03
2.255000E 01	3.1363252E 00	1.3687534E 03
2.260000E 01	3.1417628E 00	1.3859986E 03
2.265000E 01	3.1471810E 00	1.4033985E 03
2.270000E 01	3.1525797E 00	1.4209530E 03
2.275000E 01	3.1579593E 00	1.4386637E 03
2.280000E 01	3.1633197E 00	1.4565309E 03
2.285000E 01	3.1686612E 00	1.4745558E 03
2.290000E 01	3.1739839E 00	1.4927391E 03
2.295000E 01	3.1792878E 00	1.5110812E 03 ✓

Appendix E

Wheatstone Bridge Circuit



BIOGRAPHICAL NOTE

John Douglas Bannister was born in Toronto, Canada on June 1, 1928. He married Elizabeth Anne Craddock and has a thriving daughter Catherine, age ten.

He attended elementary school in Lambton, Ontario and matriculated from Etobicoke High School in 1947. From 1948 to 1955 he was employed by International Harvester Company of Canada in Toronto where he started as a shipping room helper and subsequently became central Ontario parts merchandiser, parts department foreman and purchaser. Leaving International Harvester, he attended University of Toronto where he graduated third in a class of 105 mechanical engineers in 1959. In the third year at University of Toronto he won the Boiler Inspection and Insurance Company Scholarship for the best academic performance by a mechanical engineer.

While an undergraduate he benefitted greatly by being a Summer Student at the National Research Council in Ottawa where he participated in various gas turbine research programs. Much of the gas turbine research was on propulsion systems for vertical take-off aircraft and led him to do an undergraduate thesis study of various gas turbine cycles in conjunction with propulsion configurations for vertical take-off.

In 1959-60 he was a Walter P. Murphy fellow at Northwestern University. His master's degree thesis there was a theoretical and experimental study of the mechanism of sublimation drying of frozen foodstuffs.

In 1960 he entered M.I.T. and was supported for a year by a research assistantship under Professor Joseph Keenan. During the summer of 1961 he worked at the Cambridge Electron Accelerator and became interested in Cryogenics while designing a refrigeration unit for a liquid hydrogen target. He was subsequently taken into the Cryogenic Laboratory as a research assistant by Professor Collins.